THESIS

LNAPL LONGEVITY AS A FUNCTION OF REMEDIAL ACTIONS:

TOOLS FOR EVALUATING LNAPL REMEDIES

Submitted by

Anna Meryle Skinner

Department of Civil and Environmental Engineering

In partial fulfillment of the requirements

For the Degree of Master of Science

Colorado State University

Fort Collins, Colorado

Fall 2013

Master's Committee:

Advisor: Tom Sale

Michael Ronayne
Charles Shackelford

ABSTRACT

LNAPL LONGEVITY AS A FUNCTION OF REMEDIAL ACTIONS:

TOOLS FOR EVALUATING LNAPL REMEDIES

The impacts of remedial measures on the longevity of light non-aqueous phase liquid [LNAPL] releases are rarely quantified at sites where active remediation of LNAPL bodies has been carried out. Without an understanding of LNAPL longevity, decisions regarding the appropriateness of remediation strategies and their scheduling in the life cycle of an LNAPL release could be regarded as arbitrary in some respects. Because LNAPL bodies are continually evolving with respect to composition, internal and external transport, distribution, and lateral and longitudinal mobility, it appears that a necessary part of any site conceptual model guiding remediation decisions should include an understanding of LNAPL evolution over time in terms of mass remaining. Understanding LNAPL remaining versus time would enable decision makers to estimate and compare the effects of various treatment remedies, combinations thereof, and different scheduling of treatment remedies within the remedial time frame.

This thesis presents work done to develop a novel LNAPL longevity predictive model [LLPM]. A series of laboratory sand tank experiments were conducted to gain an improved understanding of the effects of natural losses and remedial measures on LNAPL longevity as well as provide laboratory-scale input parameters for the development of the LLPM. Results from the laboratory studies were then used as a basis for developing and testing the LLPM.

The laboratory work consisted of four sand tank experiments in which a known mass of LNAPL was introduced to the system. Measurements were taken throughout the expansion and depletion of the LNAPL pool to track remaining LNAPL. These measurements were used to describe the

evolution of the LNAPL releases over the experimental time frame. Different remediation approaches were applied to each experiment to determine their effects on LNAPL release evolution and overall longevity. The two treatment remedies that were applied were LNAPL recovery via well skimming and water table fluctuations. A base scenario was established by not applying either remedy. Next, one experiment was conducted where each of the treatment remedies was applied singly. The final experiment was conducted by applying both treatment remedies.

Methyl-tert-butyl ether [MTBE] was the LNAPL used in the laboratory experiments. The experimental data showed that LNAPL recovery decreased the longevity of the MTBE release, while water table fluctuations acted to increase longevity. The increase caused by water table fluctuations was smaller than the decrease caused by LNAPL recovery. Mass balance measurements from laboratory experimentation were used to develop a version of the model that could be tested with laboratory-scale data. A key result was that LNAPL can be fully depleted over time by natural and/or engineered processes.

The LLPM was then developed by applying numerical methods to combinations of zero and first order ordinary differential equations used to simulate LNAPL depletion processes. Laboratory-scale input parameters were used to test the LLPM against data from the laboratory experiments. A field-scale application and sensitivity analysis of the LLPM were completed to demonstrate the field-scale capabilities of the model and examine which governing processes had the greatest effects on LNAPL longevity and evolution. One significant difference was recognized between the laboratory-scale and field-scale input. In the laboratory experiments, the dominant loss mechanism was volatilization, while in the field, biological degradation is thought to be most significant.

First, the model was developed by combining numerical solutions for zero and first order reaction rate differential equations. First order loss rates change as the mass in the system changes, whereas zero order loss rates are constant regardless of how much mass remains in the system. Based on available literature, volatilization, dissolution, and biological degradation were modeled as zero order processes, while active remedies such as LNAPL/hydraulic recovery and Soil Vapor Extraction were modeled as first order processes. Loss mechanisms were applied to the LNAPL release according to the distribution of mass between two compartments: one containing the continuous fraction of LNAPL and the other containing the discontinuous fraction. Another important parameter that became apparent through the literature review was subsurface temperature. The rate at which biological degradation occurs was found to be related to temperature; therefore, fluctuations in temperature can produce corresponding fluctuations in the overall depletion rate of LNAPL.

Next, the accuracy of the model was tested using mass balance data from the laboratory experiments. Simulations of the sand tank experiments with laboratory-scale data achieved a favorable fit between the model and experimental data. This signaled that the model was ready to be applied to a field-scale scenario.

Field-scale input parameters were used to demonstrate the field-scale application and conduct a sensitivity analysis of the LLPM. The sensitivity analysis examined the relative effects of two treatment remedies: hydraulic recovery and thermal enhancement of biological degradation. This analysis showed that the mass distribution of LNAPL between the two designated fractions plays an important role in the evolution of the LNAPL release and the effectiveness of remediation technologies.

It was also concluded that all parameters related to hydraulic recovery had a significant impact on the LNAPL longevity and evolution. For example, the effectiveness of hydraulic recovery to reduce LNAPL longevity was reduced as hydraulic recovery was scheduled later in the release time frame. Therefore, the life cycle stage of a LNAPL release may play a role in the effectiveness and appropriateness of various treatment remedies. The results of the laboratory sand tank experiments also support this idea. This suggests the evaluation of the interactions of multiple remedies and natural losses will be necessary to develop an accurate analysis of LNAPL longevity and evolution as LNAPL releases pass through different life cycle stages.

The effects of water table fluctuations on LNAPL mass distribution, longevity, and evolution were examined. Because different loss mechanisms affect LNAPL in the different fraction compartments, the effects of water table fluctuations were thought to be important. Water table fluctuations act to distribute LNAPL mass vertically throughout a smear zone. This may produce averaging effects that support the designation of biological degradation as a zero order process.

The beta version of the LLPM developed herein has specific limitations and challenges. One of the most significant challenges of this work is a lack of field-scale LNAPL longevity and evolution data to compare to the results of the LLPM. Suggestions for future work to address these limitations and challenges are given. One example is that of conducting multi-component LNAPL laboratory sand tank studies. These types of studies would further develop the conceptual model of LNAPL releases and increase the field applicability of the LLPM to real world sites where multi-component contaminants are often present. Future work should be done to make the model more robust and derive next generation versions of the LLPM. Through

future work it is anticipated that a version of the LLPM will be developed that practitioners can use to guide sustainable remediation planning for LNAPL sites.

ACKNOWLEDGEMENTS

I would like to acknowledge the following groups and individuals for their part in supporting the work of this thesis:

- Shell Oil for the funding for this project
- Sanjay Garg for the guidance and insight he provided
- Dr. Tom Sale for his advisement and providing me with a project and therefore a means to attain this master's degree
- Dr. Michael Ronayne and Dr. Charles Shackelford as members of my committee
- Dr. Art Corey for the assistance his scholarship and advice provided
- Dr. Julio Zimbron, Dr. Jens Blotevogel, Mitch Olson, Gary Dick, Alison Hawkins, Wes Tulli, Adam Byrne, Scott Williams, Maria Renno, Daria Akhbari, and Jennifer Wahlberg at the Center for Contaminant Hydrology for their help running experiments and general advice and encouragement as it relates to various parts of this work
- My family, especially my husband, Coulter, for their support and dedication to me during this part of my life

TABLE OF CONTENTS

LIST OF TABLES

LIST OF FIGURES

1. INTRODUCTION

In recent years, it has been recognized that many subsurface releases of light non-aqueous phase liquids [LNAPLs] are stable or shrinking (Mahler et al. 2012). In large part this can be attributed to the effects of natural losses through volatilization, dissolution, and biological degradation. A conceptual model matching this idea is shown in Figure 1. In Figure 1, the early stage is characterized by LNAPL pool expansion, the middle stage by stability, and the late stage by contraction all due to different net fluxes at the different stages.

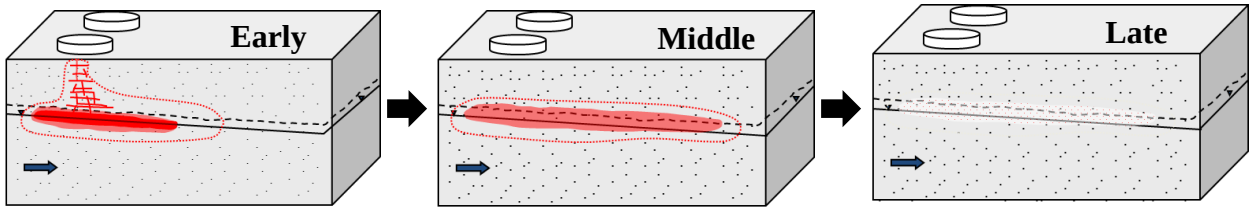

Figure 1 – Conceptual model of life cycle stages for LNAPL evolution proceeding from left to right, the small blue arrows indicate the direction of groundwater flow

Following McCoy 2012, natural losses of LNAPLs on the order of hundreds to thousands of gal/acre/year have been observed. The implications of losses of this magnitude are numerous. Relative to this thesis, key implications include: LNAPL releases evolve over time and eventually disappear, it is difficult to ascertain the appropriate timing and combinations of treatment remedies (both active and passive) without including the effects of natural losses, and tools are needed that incorporate time variant loss mechanisms to produce dynamic site conceptual models. Dynamic site conceptual models have the potential to facilitate sustainable remediation planning.

Herein this need is met through laboratory experimentation and the development of an LNAPL longevity predictive model [LLPM]. LNAPL longevity is a function of multiple factors including hydrogeologic conditions, release characteristics, active remedies, and natural losses. This effort is novel. Consequentially, not all aspects of these factors have been rigorously developed; nevertheless, the procedures and efforts outlined within form a foundation for this type of work.

1.1 Objectives and Assumptions

The overarching objective of the research described in this thesis is to develop a "first edition" or beta version tool that anticipates the benefits of investments associated with remedial actions at LNAPL sites. This in turn will support development of sustainable remedies for LNAPL sites. The primary output needed to achieve this objective is an LNAPL mass balance for the lifetime of a release (i.e. the LNAPL evolution) ultimately resulting in an estimate of LNAPL longevity.

The author offers the perspective that this is a preliminary/pioneering effort for this type of model. A primary advancement is determining the components that are necessary to produce an LNAPL longevity model and establishing methods for the development of this and future versions of the model. There are significant challenges – and assumptions – associated with this work; therefore, future projects and research efforts will be required before a version suitable for use by practitioners is available. The most significant challenge to the development of this model is a lack of field data documenting LNAPL longevity and evolution to compare the model to.

Assumptions central to this research effort include:

- Dissolution, volatilization, and biological degradation act on LNAPL releases as zero order processes. A key implication of this is that these processes will eventually lead to complete depletion of LNAPL.

- Hydraulic recovery and soil vapor extraction [SVE] – referred to as active remedies – act on LNAPL releases as first order processes. A key implication of this is that the effectiveness of these remedies will decay over time. These processes alone cannot lead to complete depletion of LNAPL.

- It is necessary to partition LNAPL into continuous and discontinuous fractions. Where volatilization and hydraulic recovery act on the continuous fraction, dissolution acts on the discontinuous fraction, and both fractions are acted upon by biological degradation.

- Water table fluctuations lead to time variant fractions of continuous and discontinuous LNAPL.

- Temperature fluctuations lead to time variant rates of biological degradation of LNAPL.

- A series of laboratory sand tank experiments for which an LNAPL mass balance is performed can be used to validate a mass balance model for LNAPL longevity

1.2 Organization and Content

Chapter 2 provides a review of previous work that is relevant to this thesis. This review introduces themes that reappear throughout the document. Chapter 3 describes a laboratory study addressing LNAPL longevity. Methods for conducting a series of laboratory sand tank

experiments, as well as analyzing samples obtained from those experiments, are outlined in detail. Results of these experiments are also presented. The development of the LLPM is described in Chapter 4. Modeling assumptions and methods are introduced and described. The necessary model inputs and resulting outputs are introduced. Also, the results of the application of the model to the laboratory experiments are included in Chapter 4. Chapter 5 presents a field-scale application and parameter sensitivity analysis of the model. This chapter includes a description of the methods used to complete the field-scale application and sensitivity analysis and the results thereof. Limitations of the model are also included in Chapter 5. Finally, Chapter 6 gives a summary of this thesis including key ideas, themes, results, and possibilities for future work. Complimentary information, not covered in the main chapters, is included in the appendices.

2. LITERATURE REVIEW

This chapter introduces key concepts that pertain to this thesis. The concepts described in this chapter are expanded on throughout the remainder of the thesis. Specifically, the design of the laboratory study of LNAPL longevity and the LLPM was built upon the foundation set forth in the following review. First, the concept that natural losses play an important role in the evolution of LNAPL bodies is considered. Second, quantification methods for natural losses are briefly introduced. Next, functionalities that were necessary to include in the LLPM are discussed such as to establish the effects of temperature fluctuations on biological degradation, application of subsurface heating to stimulate biological degradation, and distribution of mass between continuous fraction and discontinuous fraction compartments,. Finally, previous modeling efforts are presented including methods of parameter determination that are appropriate for the model developed herein along with possible limitations of active remedies.

2.1 Significance of Natural Losses

LNAPL stability as a function of fluxes acting on and within the LNAPL system was evaluated in Mahler et al. 2012. It was recognized that LNAPL bodies can be stable even while active releases of LNAPL are occurring and/or where there are non-zero LNAPL fluxes within LNAPL bodies. The authors suggested that this conceptual discrepancy could be addressed by the hypothesis that natural losses are acting on these observed stable LNAPL bodies in a way that balances the non-zero internal fluxes.

Development of analytical models to examine these processes showed that the stability of the theoretical LNAPL pool was directly dependent on natural losses of LNAPL. For certain applications, LNAPL pool stability was more sensitive to changes in the natural loss rate than

changes to the rate of LNAPL inflow into the system. In addition to affecting the stability of LNAPL bodies, natural losses were also suggested to impact LNAPL longevity according to experimental data presented in Mahler 2010.

2.2 Quantification of Natural Losses

Based on the above observations, the model developed in Chapter 4 of this work requires quantitative estimates of natural loss rates for LNAPL bodies under field conditions. Methods for estimating natural losses include the gradient method (Johnson et al. 2006), Licor Trap Method (Amos et al. 2005), a mass balance method (Mahler et al. 2012), and CO_2 Trap Method (Zimbron et al. 2013).

Johnson et al. 2006 addresses four questions relevant to quantification of natural losses of LNAPLs. Methods of answering these questions are given including a method for determining current rates of mass removal due to natural losses. The method suggests what type of data to collect and how to analyze that data in order to arrive at an estimate for the current rates of natural losses at a hydrocarbon release site.

The importance of methanogenesis as a long-term degradation pathway for petroleum hydrocarbon releases is highlighted in Amos et al. 2005. Methods for capturing and quantifying Argon and Nitrogen gases and their correlation to methanogenesis are given. This work recognized the difficulty associated with making source longevity predictions and subsequently the lack of reliable estimates of such.

In a laboratory sand tank experiment, Mahler et al. 2012 conducted a mass balance on a LNAPL release that included a known injection rate, measured dissolution rate, and estimated

volatilization rate. Overall natural loss rates, including dissolution and volatilization, of between 17,962 and 47,908 m^3/ha/yr (1,920,260 and 5,121,690 gal/acre/yr) were observed for various injection rates. These rates are orders of magnitude higher than those observed using the Zimbron et al. CO_2 trap method. This discrepancy is understandable because in Mahler et al. 2012, a single component LNAPL – Methyl-tert-butyl ether [MTBE] – was used. MTBE has a higher vapor pressure and solubility which contributed to the observed high natural loss rates. Also, a thinner vadose zone was simulated in the laboratory study of Mahler et al. 2012 than was present at field locations where CO_2 traps of Zimbron et al. 2013 have obtained measurements.

Zimbron et al. 2013 contains a description of a device to measure passive CO_2 gas flux from the subsurface. Building on CO_2 data presented in McCoy 2012, data from two hundred measurements indicate a range of natural loss rates from 7.48 to 112 m^3/hectare/yr (800 to 12,000 gal/acre/yr) with a median value of 32.7 m^3/hectare/yr (3,500 gal/acre/yr). These values were determined by correcting all measurements for background levels of CO_2 flux from traps believed not to be currently underlain by LNAPL. Data from McCoy 2012 was used in the field-scale application and sensitivity analysis of the LLPM developed as part of this thesis work.

2.3 Effect of Temperature

Another parameter that may affect natural loss rates at a site is the temperature in the subsurface. Zeman 2012 introduced the idea that biological LNAPL degradation could be enhanced by maintaining a certain temperature within the subsurface. Irianni Renno 2013 and Akhbari 2013 have further developed the hypothesis that thermally enhanced biological degradation, with minimal energy requirements, could be a sustainable remediation alternative for LNAPL sites.

As part of Zeman 2012, a thermal microcosm study was conducted that monitored soil microbiology and contaminant degradation at six different temperatures: 4°C, 9°C, 22°C, 30°C, 35°C, and 40°C. Higher levels of biogas production and contaminant degradation were observed in the microcosms at 22°C and 30°C; thus, it was concluded that temperature can have a large impact on the rate of LNAPL degradation in the subsurface.

From evaluation of these works it was concluded that models addressing LNAPL longevity need to incorporate the effects of temperature fluctuations on the rate of biological degradation. Also, functionality to include thermally enhanced biological degradation would be an important component of such a model.

2.4 Significance of LNAPL Fractionation

A key aspect of understanding losses of LNAPL, from natural mechanisms or active remedies, is whether they act on LNAPL that occurs as a part of the continuous or discontinuous fraction. An example of LNAPL distribution demonstrating both fractions is shown in Figure 2 (a photograph from the laboratory sank tank studies described in Chapter 3 of this thesis). Numerous works have stated that a series of connected pore spaces of any fluid occupying a porous media is needed in order for that fluid to flow. Brooks and Corey 1964 is one of these. This work presented ways to estimate relative fluid saturations and effective permeabilities in porous media when two fluids are interacting based on a force balance of pressures. Based on this, fluids can be labeled as mobile or immobile; mobile being synonymous with continuous fraction and immobile being synonymous with discontinuous fraction. Immobile LNAPL will exist when LNAPL relative saturation is equal to or less than residual saturation because this is the point when effective permeability of the LNAPL will be zero. Another way of describing this is

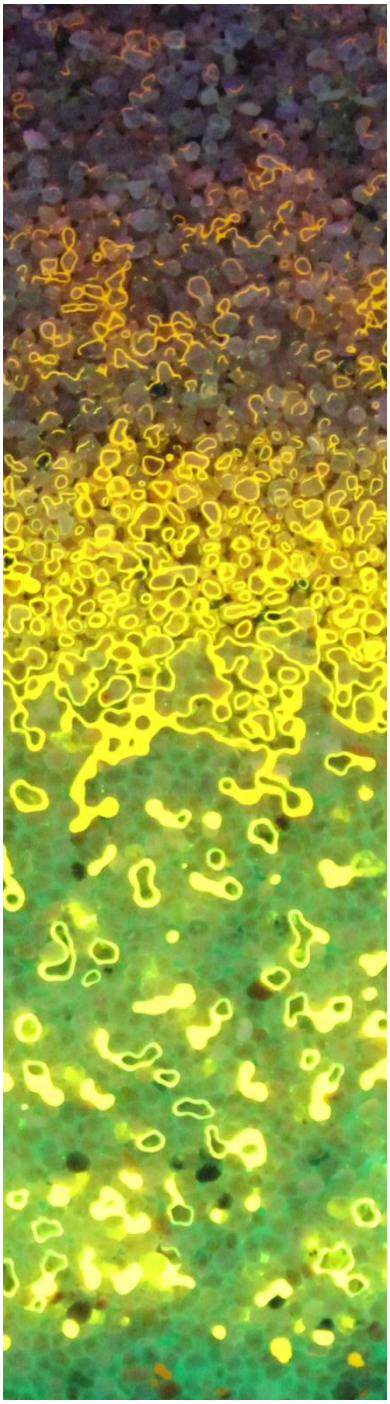

Figure 2 – Distribution of LNAPL (yellow colored) during the Base Case experiment showing mass in the discontinuous fraction below the water (green colored) table and the continuous fraction at and above the water table

LNAPL is discontinuous when the capillary pressure is less than the displacement pressure necessary to enter a pore.

It can then be assumed that different loss mechanisms will affect different components of LNAPL mass according to what fraction exists as continuous and discontinuous fractions. See Table 1 for a list of loss mechanisms and the LNAPL fraction compartment they are thought to affect. For example, hydraulic recovery can only be beneficial when LNAPL exists as a pool of hydraulically connected pore spaces; therefore, continuous fraction LNAPL must be present for hydraulic recovery to recover mass from any subsurface system. Similarly, SVE draws continuous LNAPL up into the vadose zone via capillary action. As the LNAPL is depleted, the continuous fraction declines and ultimately the remaining LNAPL becomes discontinuous and largely unavailable for depletion via SVE.

2.5 Effect of Water Table Fluctuations

Another important component of the LLPM that goes along with the idea of the partitioning of LNAPL mass within porous media is functionality to incorporate the effects of water table fluctuations. Hawkins 2013 notes that a maximum continuous fraction of LNAPL

occurs at low water levels. At high water levels, most of the LNAPL is present as a discontinuous fraction. The water table fluctuations examined in the laboratory experimentation of Hawkins 2013 were categorized as tidal, twice daily cyclical, variations in water level.

Table 1 – List of various loss mechanisms and the LNAPL fraction compartment they are thought to affect.

Loss Mechanism	LNAPL Fraction Compartment Effected
volatilization	continuous
dissolution	discontinuous
biological degradation	both
hydraulic recovery	continuous
SVE	continuous

In Davis and DeWiest 1966, it is explained that under field conditions, variations in the height of the water table may occur for several reasons: changes in groundwater storage, fluctuations in atmospheric pressure, aquifer deformation, and/or well disturbances. The first two of this list can be related to weather conditions. The amount of precipitation, or lack thereof, over an area will affect the amount of groundwater storage during different seasons, and weather conditions cause daily fluctuations in atmospheric pressure. Water table fluctuations due to daily changes in atmospheric pressure can be considered negligible when compared to annual fluctuations due to changes in aquifer storage during different seasons.

Extreme weather conditions, such as flooding and drought, likely set the extremes of the vertical distribution of LNAPL within the subsurface. For example, flood conditions may distribute LNAPL into the discontinuous fraction above the average water table; therefore, making it unavailable for redistribution into the continuous fraction within the average annual water table range for the aquifer. Also, drought may act to maximize the distribution of LNAPL into the

continuous fraction by lowering the water table to a point to allow drainage of LNAPL previously locked as discontinuous fraction below the average annual water table range.

For this work it was important to track the distribution of LNAPL over time as a function of water table fluctuations because different loss mechanisms affect LNAPL in the different fraction compartments. Perhaps one of the most interesting aspects of water table fluctuations is that LNAPL tends to persist over a fixed vertical height (i.e. the smear zone) through time even as LNAPL is being depleted. This provides a basis for the argument that biological degradation of LNAPL can be represented as a zero order process because of the averaging effects water table fluctuations would have in this regard.

2.6 Previous Modeling Efforts

Models have been constructed to predict contaminant fate and transport so as to determine vapor and aqueous phase concentration associated risks at LNAPL sites. For example, Huntley and Beckett 2002 examined the effects that LNAPL removal from source zones could have on risk reduction at LNAPL sites. The authors suggested that complete recovery of LNAPL is generally not feasible; therefore, concentration associated risk is still present at LNAPL sites with residual LNAPL saturation. This residual saturation can be enhanced by the effect of the relative permeabilities acting in multiphase flow. In relation to this and other multiphase flow theories, the limitations of hydraulic recovery of free product (or continuous LNAPL) are introduced along with arbitrary regulatory definitions of cleanup goals for hydraulic recovery based on LNAPL well thicknesses. Quantitative theory is introduced that relates the evolution of aqueous and vapor phase exposure pathways to various remediation strategies thus evaluating the relative risk reduction potential of the various strategies.

Results of the study conducted by Huntley and Beckett indicated that hydraulic recovery only provides risk reduction for a specific sub-set of conditions. For example, hydraulic recovery may provide significant risk reduction for a relatively new release in a soil with low heterogeneity and fairly high permeability. Risk longevity reduction, referring to a reduction in the time period for which risks associated with LNAPL contamination exists, can also be achieved only under favorable conditions. However, hydraulic recovery is often performed, for at least some period of time, at most LNAPL sites. If hydraulic recovery of LNAPL is only an appropriate treatment remedy for a limited range of favorable conditions, different remediation approaches are needed for sites where hydraulic recovery was never an appropriate remedy or sites where hydraulic recovery has reached its endpoint of effectiveness.

2.7 Limitations of Active Remedies

Another document that supports the idea that the benefits of active remedies have limitations is Sale 2001. It has been observed that as LNAPL mass is removed from a system by certain processes, the mass recovery rates of those processes decrease due to the decrease in relative transmissivity to LNAPL. By way of decline curve analysis, it was concluded that active treatment remedies such as surfactant flushing, SVE, and hydraulic recovery operate as first order decay equations. Methods of producing first order decay rates – and therefore half-lives of LNAPL being acted upon by first order processes – and the maximum potential recoverable mass from recovery rate and cumulative production data were given. These methods were used to establish reasonable estimates for the hydraulic recovery model parameters used in the field-scale application and sensitivity analysis comprising Chapter 5. The potential limitations of active treatment remedies make it possible that passive treatment remedies can have more

substantial effects on LNAPL longevity throughout the lifetime on an LNAPL release while being less resource intensive.

2.8 Summary

This brief synopsis of previous work by others introduces the motivation for the development of a LNAPL longevity predictive tool. Longevity calculations that provide a mass balance over the lifetime of an LNAPL release would be beneficial in terms of sustainable remediation design and planning. From this, the questions develop of how can LNAPL longevity at a site be predicted in a beneficial way for practitioners and what pieces are necessary to make those predictions. The remainder of this thesis will focus on broadly approaching answers to these questions.

3. LABORATORY STUDY OF LNAPL LONGEVITY

The purpose of this chapter is to describe the series of laboratory sand tank experiments that evaluate LNAPL longevity as a function remedial measures. Building on principles introduced in Chapter 2, the effects of two treatment remedies – LNAPL recovery and water table fluctuations – were examined. First, the objectives of the laboratory sand tank experiments are described. Next, the methods used to conduct the experiments are outlined. Finally, the results of the laboratory study of LNAPL longevity are given.

3.1 Experimental Objectives

The objectives of the series of laboratory sank tank experiments described within were threefold. First, because the fact that LNAPLs have a finite longevity is not widely appreciated, the authors wanted to produce a simple visual demonstration that LNAPL can be fully depleted with time. This would demonstrate that depletion occurs by both naturally occurring and imposed conditions. Second, the authors wanted to study processes that control LNAPL longevity including evaporation, dissolution, LNAPL recovery, and water table fluctuations. Insight gained from these experiments form a conceptual basis for the model introduced in Chapter 4. Third, the authors wanted to develop mass balance data sets that could be used to test the validity of the LLPM.

The laboratory experiments consisted of four individual sand tank experiments in which a known mass of LNAPL was added to the system and the depletion of which was monitored over time. The different experiments were characterized by the application of the two treatment remedies (LNAPL recovery and water table fluctuations), or a combination thereof. A brief description of

each of the experiments is given below and is represented visually in Figure 3. Further details on the experimental design are given in Section 3.2.

- The Base Case experiment was conducted without the application of either LNAPL recovery or water table fluctuations. The purpose of the Base Case experiment was to establish a benchmark scenario by which to compare all subsequent experiments.

- The Recovery experiment was conducted with the application of LNAPL recovery only. The purpose of the Recovery experiment was to examine the effects that LNAPL recovery had on LNAPL longevity when compared to the Base Case experiment.

- The Water Table [WT] Fluctuations experiment was conducted with the application of water table fluctuations only. The purpose of the WT Fluctuations experiment was to examine the effects that water table fluctuations had on LNAPL longevity when compared to the Base Case experiment.

- The Combined experiment was conducted with the application of both LNAPL recovery and water table fluctuations. The purpose of the Combined experiment was to examine the effects that both LNAPL recovery and water table fluctuations had on LNAPL longevity when compared to the Base Case experiment and the sole application of each remedy.

3.2 Methods

The purpose of this section is to describe the methods used to conduct the series of laboratory sand tank experiments to study LNAPL longevity as a function of remedial measures. First, the physical setup of the sand tank is described. Next, a description of the fluids preparation, flow

setup, treatment remedies application, photographic techniques, and sampling procedures is given. Finally, analytical techniques are described.

	No Recovery	Recovery
Constant Water Table	Experiment 1 (Base Case)	Experiment 2 (Recovery)
Water Table Fluctuations	Experiment 3 (WT Fluctuations)	Experiment 4 (Combined)

Figure 3 – Experiment design matrix diagram, treatment conditions are in shaded regions, experiment nomenclature is given in corresponding regions

3.2.1 Sand Tank Setup

The experiments were completed in a closed sand tank system comprised of a two-dimensional glass tank with an aluminum top. The front and back panels of the tank were glass, and the sides and bottom were aluminum. A schematic drawing of the tank setup is shown in Figure 4. The internal tank dimensions were 181.3 cm length, 38.8 cm height, and 5.0 cm depth. Openings in the lid were placed relative to the left (influent) end as follows: water inlet at 4 cm, air inlet at 9 cm, LNAPL inlet at 14 cm, first well at 40.8 cm, second well at 75.8 cm, third well at 110.8 cm, fourth well at 145.8 cm, air outlet at 178.8 cm, and water outlet at 182.5 cm. The aluminum top was sealed to the tank with silicone.

Inlet and outlet screens were placed at either end of the tank to allow flow of water while restricting movement of porous media into inlet and outlet reservoirs. The screens consisted of a stainless steel frame (Round Hole Perforated sheets, McMaster-Carr, Atlanta, GA) covered with stainless steel mesh (type 304 50x50 wire mesh, McMaster-Carr, Atlanta, GA). The frame was bent and cut to measure 38.5 cm high by 2.5 cm wide by 5.0 cm deep.

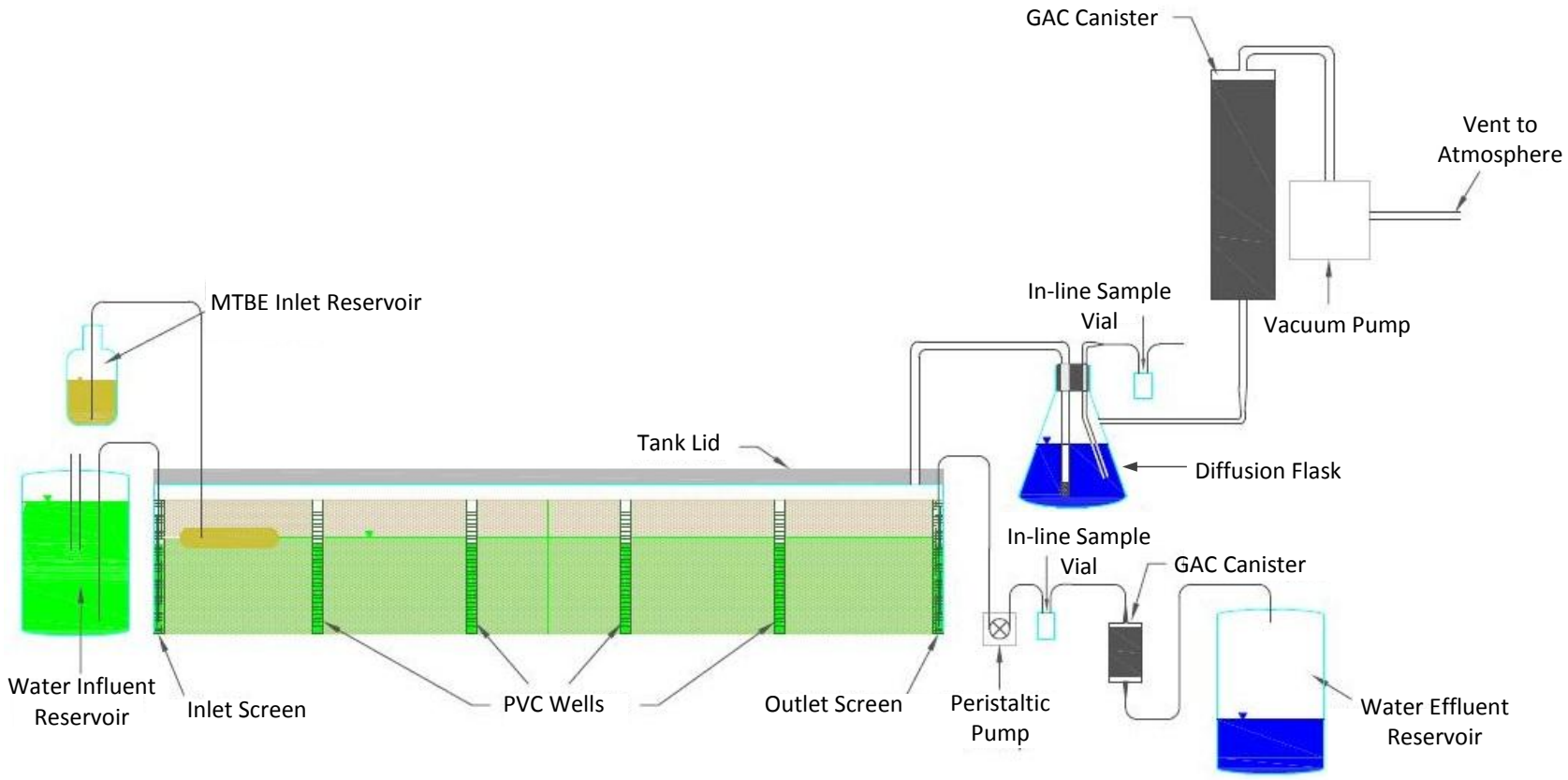

Figure 4 – Schematic drawing of tank setup showing inlet and outlet systems, sampling systems, and well placing, water and vapor flow was from left to right

Four wells were placed at equal intervals throughout the tank. Wells consisted of half sections of 2.54 cm diameter PVC well screen with two sections of 0.5 mm slots (Johnson Screens, Houston, TX). Tygon vinyl tubing (McMaster-Carr, Atlanta, GA) was split length wise and placed on the edges to create a seal between the well and the front glass panel of the tank. Wells were held in place by smaller PVC pipe sections, 0.5 in diameter, wedged between the back glass panel of the tank and the back of each well.

A medium grained, 10-20, uniform sand, (Colorado Silica Sand, Colorado Springs, CO), was used as the porous media. The sand was rained into the tank to achieve a uniform packing. Sand was rained into the tank to a height of approximately 33 cm, leaving a headspace of approximately 5.8 cm. Sand was washed prior to being loaded into the tank. Rinses with tap water were repeated until decanted water appeared considerably clearer than that from the initial wash. Sand was washed to improve photographic quality of the water by removing fines. Once filled with porous media, the tank was flooded with prepared Fluorescein water and allowed to sit overnight. Water from the tank was then pumped out until the desired initial water level was achieved. The initial water level for each of the experiments was approximately 22 cm from the tank bottom.

3.2.2 Fluids Preparation

Fort Collins, Colorado de-aired tap water held at -24 mm Hg for thirty minutes was used to simulate groundwater in the system. The water was dyed with Fluorescein (Sciencelab.com Incorporated, Houston, TX), a UV fluorescent dye, to enhance the photographic quality of the experiments. A “stock solution” was prepared by dissolving 0.5 g of Fluorescein in 50 mL of

deionized [DI] water. The "stock solution" was added in increments of 2.5 mL per liter of de-aired tap water to achieve the desired volume of water for each experiment.

Analytical grade MTBE (OmniSolve, EMD Chemicals, Incorporated, Gibbstown, NJ) was used as the LNAPL. MTBE was chosen because of its high vapor pressure, 3.33 kPa (245 mm Hg) at 25°C (Budavari et al. 1989), and high solubility, 51.26 kg/m^3 at 25°C (U.S. EPA 1993). The high solubility and volatility enabled the experiments to be completed within 14 days of LNAPL addition. The MTBE was dyed with Staybright (BSL 715, Bright Solutions International LLC, Troy, MI) a NAPL soluble fluorescent dye. One percent by volume, 10 mL, of Staybright was added to one liter of MTBE for each experiment.

3.2.3 Flow Setup

Water flow through the system was accomplished in two ways. The inlet reservoir for both setups had a capacity of 20 L. For the Base Case and Recovery experiments, a Marriot syphon was used at the influent end to maintain a constant head. Flow was then induced by a compact multichannel peristaltic pump (REGLO model, ISMATEC, Glattbrugg, Switzerland) at the effluent end per Mahler et al. 2012. For the WT Fluctuations and Combined experiments, flow through the system was maintained by pumping into the influent end of the tank for 12 hours and out of the effluent end for 12 hours each day. For the Base Case and Recovery experiments, an average Darcy groundwater velocity of 1.86×10^{-6} m/s (0.528 ft/day) (assuming a porosity of 0.4, Hawkins 2013) was achieved by pumping water at an average rate of 1.23×10^{-8} m^3/s (0.737 mL/min). For the WT Fluctuations and Combined experiments, a Darcy groundwater velocity of 8.08×10^{-6} m/s (2.29 ft/day) was achieved by pumping water at an average rate of 5.32×10^{-8} m^3/s (3.19 mL/min). This higher flow rate was used for the latter two experiments to achieve the

desired magnitude of water table fluctuations within a 24 hour period. Peristaltic pump tubing of 2.54 mm (0.1 in) inner diameter (Cole-Parmer, Vernon Hills, IL) was used for pumping both water and LNAPL into the system.

Tubing from the water inlet reservoir to a valve was 6.35 mm (0.25 in) FEP tubing (Nalge Nunc International Corporation, Rochester, NY). This tubing was also used in the vapor outlet system along with 12.7 mm (0.5 in) FEP tubing (Nalge Nunc International Corporation, Rochester, NY). From the valve to the water inlet reservoir within the tank 3.175 mm (0.125 in) fluorinated ethylene propylene [FEP] tubing (Cole-Parmer, Vernon Hills, IL) was used. This tubing was also used to skim LNAPL from the wells and in the liquid outlet system.

Air flow was induced by a vacuum pump (115 amp non-lubricated, GAST Manufacturing, Benton Harbor, MI), maximum pressure of 4.14×10^{2} kPa (60psi), connected to the headspace at the effluent end of the tank. The average air flow rate for the four experiments was 3.15×10^{-4} m^3/s (18.9 L/min).

A known mass, between 676 and 750 g, of LNAPL was introduced into the system with a compact multichannel peristaltic pump (REGLO model, ISMATEC, Glattbrugg, Switzerland). FEP tubing (Cole-Parmer, Vernon Hills, IL) of 3.175 mm (0.125 in) diameter was used for LNAPL addition. The end of the tubing was placed approximately ten centimeters above the water table within the porous media. LNAPL was pumped into the sand tank system at an approximate rate of 1.30×10^{-7} m^3/s (7.79 mL/min). This relatively high flow rate and ventilation of the LNAPL inlet reservoir was required to overcome pumping problems associated with the high vapor pressure of MTBE. These LNAPL pumping problems were observed in preliminary experiments but appropriately avoided in the four quantified experiments of the study.

3.2.4 Treatment Remedies Application

LNAPL recovery was initiated 24 hours after LNAPL addition. This provided an equal stabilization period for both the Recovery and Combined experiments. LNAPL recovery was performed via well skimming by 3.175 mm (0.125 in) FEP tubing (Cole-Parmer, Vernon Hills, IL) and a 60 mL luer lock tip plastic syringe (BD, Franklin Lakes, NJ). LNAPL was recovered every hour between 9 am and 5 pm on the first day of LNAPL recovery and every four hours, corresponding to aqueous and vapor phase sample collection, after that until no recoverable LNAPL remained in the wells. Every well did not exhibit recoverable LNAPL at every recovery event. For both the Recovery and Combined experiments, no more recoverable LNAPL entered the wells after 1.5 days of recovery.

Water table fluctuations were initiated 24 hours after LNAPL addition. This provided an equal stabilization period for both the WT Fluctuations and Combined experiments. Water table fluctuations were induced by pumping into the influent end of the tank for 12 hours and then moving the same pump to the effluent end of the tank to pump out for the remaining 12 hours of the day. The flow rate of 5.32×10^{-8} m^3/s (3.19 mL/min) produced a water table fluctuation magnitude of 7.5 cm (2.95 in). Water table fluctuations were continued for the remainder of the WT Fluctuations and Combined experiments.

3.2.5 Photographic Techniques

Lighting and photographic techniques were based on the work of Hawkins 2013. A combination of UV – 40W, T12 black lights (Ace Hardware, Fort Collins, CO) – and white lighting – 10W compact fluorescent single-bulb – was used to enhance the photographic quality of the experiments. Black lights were placed in a horizontal orientation in front of the tank both above

and below the tank. Placement was adjusted to maximize fluorescence and minimize shadow. White lights were placed in the corners of the room facing away from the tank in order to provide enough white light that the UV florescence of the dyed fluids was not overwhelming in the acquired photographic images. Non-reflective black sheeting was used to eliminate the appearance of glare on the glass surface of the tank.

Photographs were taken at regular intervals throughout the experiments using two EOS Rebel T3i cameras (Canon, Melville, NY). One camera was set up to take a photo of the entire tank every 15 minutes. Another camera was set up to take a close up photo of the leading edge of the LNAPL at 7.5 minute intervals; this camera was moved throughout the experiment to follow the leading edge. Remote shooting at the described intervals was accomplished using EOS Utility software (Canon, Melville, NY). Photos were cropped using the batch editing process of Adobe® Photoshop® 7.0 (Adobe, San Jose, CA). Photos of individual experiments were combined to make videos using Windows Live Movie Maker (Microsoft Corporation, Redmond, WA). Videos of individual experiments created with Windows Live Movie Maker were combined using Adobe® Premier® Elements 9 (Adobe, San Jose, CA) to make side by side comparison videos of two experiments. Three videos comparing each of the Recovery, WT Fluctuations, and Combined experiments to the Base Case experiment were created.

3.2.6 Sampling Procedures

Aqueous phase samples were taken using a closed flow through system with a 20 mL vial sample vial. Vapor phase samples, also 20 mL, were taken via a flow through setup similar to the system used to collect aqueous phase samples with one variation as outlined in the following

paragraph. The sample collection systems for both aqueous and vapor phase samples can be seen at the effluent end of the tank setup schematic drawing in Figure 4.

Vapor phase samples were acquired by partitioning the vapor phase MTBE in the vapor effluent flow stream into the aqueous phase. Effluent vapor was diffused via a 70-100 μ POR B diffuser (ACE Glass Incorporated, Vineland, NJ) into water contained in a 4,000 mL sidearm flask. A line placed in the water in the sidearm flask was connected to the 20 mL vapor phase flow through sample vial. A 60 mL luer lock tip plastic syringe (BD, Franklin Lakes, NJ) was used to induce the pressure gradient needed to fill the sample vial at each sampling event.

For the Base Case experiment four aqueous and vapor phase samples were taken at three hour intervals between 8 am and 8 pm each day. The sampling schedule was adjusted for the subsequent experiments such that samples were taken at approximate four hour intervals throughout the day and night. However, for the first four hours after LNAPL addition, hourly samples were taken for these experiments. For the WT Fluctuations and Combined experiments, aqueous phase samples were only taken during the 12 hour periods when effluent was being pumped from the tank.

Sample concentrations, both aqueous and vapor phase, represented average MTBE concentrations leaving the sand tank during the sampling interval. Sample vials were filled and promptly capped with septa crimp caps such that no head space was present in the vials. Samples were stored inverted at 5°C until analyzed. One triplicate sample was taken for every ten samples as a quality control measure. Statistics for triplicates from each experiment are given in Appendix A.

Each effluent flow path was intercepted by 8-20 mesh granular activated carbon (untreated, Sigma-Aldrich, St. Louis, MO) downstream of the sampling systems. This was done to scrub remaining MTBE from each effluent before it entered the storage container for the aqueous phase or came into contact with the vacuum pump for the vapor phase.

3.2.7 Analytical Techniques

Samples were analyzed by gas chromatogram equipped with a flame ionization detector [GC-FID] (Agilent Technologies 6890N Network GC System, Agilent Technologies, Incorporated, Santa Clara, CA) operated in splitless mode equipped with an Agilent restek rtxi-624 MS column (250 μm by 30 m, Agilent Technologies, Incorporated, Santa Clara, CA). The oven program was from 60°C held for two minutes, ramped at 15°C per minute to 250°C for a total runtime of 14.67 minutes. Manual injections of 1 μL headspace sub-samples were performed using a Tekmar™ 7000 HEADSPACE Autosampler (Teledyne Tekmar, Mason, OH).

Samples from the Base Case experiment were initially analyzed without dilution. Results from this preliminary analysis provided a basis for the dilution of samples for the subsequent experiments. Sample dilution was required to produce GC-FID samples with concentrations in the range of analysis established by calibration standards.

Samples were prepared for analysis by subsampling 1 mL from the original 20 mL sample vials via the septa in the vial crimp cap and transferring that volume to a separate 20 mL headspace analysis vial. Each 20 mL headspace analysis vial was filled with the 9 mL of DI water prior to addition of subsample. The total liquid volume in each headspace analysis vial was 10 mL, and the corresponding dilution factor for this preparation method was ten. Subsamples were extracted with a 5 mL gas tight fixed luer lock syringe with a PTFE tipped plunger (SGE

Incorporated, Austin, TX) fitted with a 21 gauge by 2 inch Precision Glide® needle (BD, Becton Dickinson and Company, Franklin Lakes, NJ). Headspace analysis samples were promptly sealed with a septa crimp cap after subsample transfer and original sample vials were resealed.

Sample concentrations were determined by comparing sample analysis results with those of calibration standards. A new set of calibration standards and corresponding calibration curve were created for the analysis of the samples from each experiment. Calibration standards were prepared with analytical grade MTBE (OmniSolve, EMD Chemicals, Incorporated, Gibbstown, NJ) having a density of 740.4 kg/m^3. An example of how the calibration standards were prepared can be seen in Table 2. Figure 5 shows an example of a calibration curve and corresponding equation used to determine experiment sample concentrations. Similar tables and figures for all experiments can be found in Appendix B.

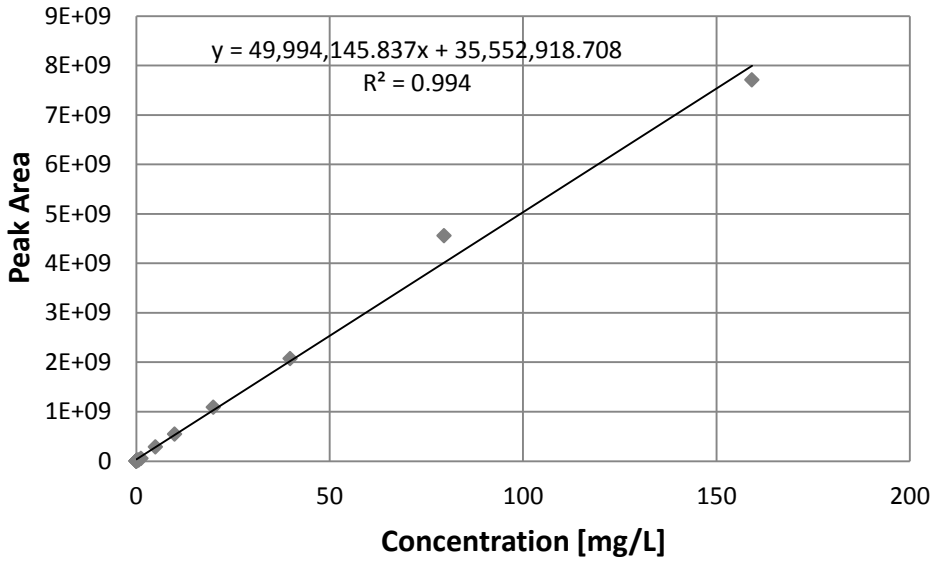

Figure 5 – Calibration curve with equation used to determine sample concentrations of the Base Case experiment samples

Table 2 – Calibration standards for the Base Case experiment

Sample Name	mL/mg MTBE[1]	mL previous	mL DI water	Dilution Factor[2]	Concentration [mg/L]
DIL1	0.1/79.6	-	9.9	100	7,960
DIL2	-	2	8	5	1,592
STD1	-	2	18	10	159.2
STD2	-	10	10	2	79.60
STD3	-	10	10	2	39.80
STD4	-	10	10	2	19.90
STD5	-	10	10	2	9.950
STD6	-	10	10	2	4.975
STD7	-	10	10	2	2.488
STD8	-	10	10	2	1.244
STD9	-	10	10	2	0.6219
STD10	-	10	10	2	0.3109
STD11	-	10	10	2	0.1555
STD12	-	10	10	2	0.07773
STD13	-	10	10	2	0.03887
STD14	-	10	10	2	0.01943
STD15	-	10	10	2	0.009717

[1]0.1 mL of MTBE was pipetted into 9.9 mL of DI water; 79.6 mg was actual scale measured value of added MTBE
[2]Dilution factors refer to dilution power between one sample and the subsequent sample

Flow rates, sampling interval lengths, and sample concentrations were used to calculate mass loss from the system during each sampling interval according to Equation 1

$$\Delta M = C * Q * \Delta t_{SI} \quad \text{[Eq. 1]}$$

where ΔM [M] is the mass loss from the system between sampling events. C [M/L^3] is the sample concentration. The sample concentrations obtained represent the average concentration of the effluent over the sampling interval. The time between sampling events is Δt_{SI} [T] (sampling interval). Finally, Q [L^3/T] is the volumetric flow rate of the effluent. The results of these mass balances were used to parameterize the LLPM.

3.2.7.1 Vapor Phase Fitting Parameter

For the vapor phase effluent samples, a fitting parameter was developed to convert the aqueous concentrations analyzed via GC-FID back into vapor phase concentrations. This fitting parameter was modeled after the dimensionless Henry's coefficient. Using a dimensionless Henry's coefficient aqueous phase concentrations can be converted to vapor phase concentrations according to Equation 2

$$\rho_v = K_{HD} * \rho_{aq} \qquad \text{[Eq. 2]}$$

where ρ_v [M/L^3] is the vapor phase concentration, K_{HD} is the dimensionless Henry's coefficient, and ρ_{aq} [M/L^3] is the aqueous phase concentration. The derivation of Equation 2 and the dimensionless Henry's coefficient is shown in Appendix C.

The fitting parameter was used to complete the mass balance because literature values of the Henry's coefficient for MTBE resulted in vapor phase sample concentrations much too large based on the total initial amount of MTBE introduced to the system. Iterations of the fitting parameter were conducted using GoalSeek in Excel (Microsoft Corporation, Redmond, WA) until Equation 3 reached equality.

$$M_0 = \sum_{i=1}^{n} \rho_{aq_{GC-FID_i}} * Q_{avg_{aq}} * \Delta t_i + \sum_{j=1}^{m} FP * \rho_{v_{GC-FID_j}} * Q_{v_{aq}} * \Delta t_j \qquad \text{[Eq. 3]}$$

In Equation 3, M_0 [M] is the total initial mass added to the system, n is the number of aqueous phase experiment samples taken, m is the number of vapor phase experiment samples taken, $\rho_{aq_{GC-FID_i}}$[M/L^3] is the GC-FID resultant value for aqueous phase sample concentration, $\rho_{v_{GC-FID_j}}$ [M/L^3] is the GC-FID resultant value for vapor phase sample concentration, $Q_{avg_{aq}}$

[L^3/T] is the average aqueous effluent flow rate, Q_{avg_v} [L^3/T] is the average vapor effluent flow rate, Δt_i [T] is the aqueous phase sample interval, Δt_j [T] is the vapor phase sample interval, and FP is the fitting parameter. In Equation 3, $\rho_{v_{GC-FID_j}}$ represents the vapor phase MTBE that was partitioned into the aqueous phase for sampling according to the procedures outlined in Section 3.2.6.

Ideally system conditions would have remained the same between experiments such that a constant value of FP could be used for all the experiments; however, this was not the case. The value of FP required to close the mass balance varied for each experiment. This suggests that equilibrium conditions controlling the partitioning of vapor phase MTBE in the vapor effluent into the aqueous phase in order to be sampled were different for each experiment. See Appendix C for a table of the FP values for each experiment.

3.3 Results

This section presents the results of the laboratory LNAPL longevity study. First, panels of photographs showing the daily time lapse of each experiment are presented and discussed. The longevity of each experiment is presented and compared. The mass balance for all the experiments has been represented as a plot of mass remaining versus time. These mass balances are presented and implications regarding the model are discussed. Finally, the relative amounts of LNAPL lost by the various loss mechanisms, volatilization, dissolution, and LNAPL recovery, for each experiment are presented and discussed as these values relate to the longevity and mass balance results.

3.3.1 Photographic Time Lapse

Figure 6 through Figure 9 in this section are made up of the photographs taken during the series of laboratory sand tank experiments. One photograph from each day was chosen to make the panels of daily time lapses. The photographic time lapse panels begin with day one as the top photograph and proceed downward one day at a time. The chosen photographs were all taken at approximately the same time each day. The photographic time lapse ends for each experiment once the LNAPL was visually depleted from the system. This also marked the LNAPL longevity for each experiment as will be discussed further in Section 3.3.2. It is interesting to note that even though the LNAPL was introduced to the system in the same manner for each experiment the LNAPL distribution isn't identical between any of the experiments.

The photographic time lapse for the Base Case experiment is shown in Figure 6. It can be observed that the LNAPL was visually depleted by day seven. Figure 6 also shows that most of the LNAPL mass depletion for the Base Case experiment occurred above the water table as the mass that was partitioned below the water table represent the majority of mass that persisted past day four. Mass seemed to persist near the wells in the Base Case experiment more so than in all other experiments.

The photographic time lapse for the Recovery experiment is shown in Figure 7. It can be observed that the LNAPL was visually depleted by day five. Due to LNAPL recovery, the thickness of the MTBE pool on day two of the Base Case and Recovery experiments is notably different. By comparing Figure 6 and Figure 7 it is obvious that LNAPL recovery had a relatively large impact on LNAPL longevity for the sand tank system. One reason this impact was thought to be so large is because the LNAPL recovery was applied to the system when the

LNAPL release would have been considered early stage. If LNAPL recovery had been applied at different life cycle stages of the release, different levels of effectiveness might have been observed.

The photographic time lapse for the WT Fluctuations experiment is shown in Figure 8. It can be observed that the LNAPL was visually depleted by day seven. By comparing Figure 6 and Figure 8 the effects of water table fluctuations on the distribution of mass between the continuous and discontinuous fraction can be seen. As soon as day two, the mass has been spread vertically between the maximum and minimum water table levels. The mass distribution was most effected by water table fluctuations; however, water table fluctuations did appear to have an effect on longevity also. When compared to the time lapse of the Base Case experiment, it can be seen that water table fluctuations did not decrease LNAPL longevity. Water table fluctuations arguably increased the LNAPL longevity. By comparing the day six photographs from Figure 6 and Figure 8 it can be seen that much more LNAPL visibly remains in the WT Fluctuations experiment than in the Base Case experiment (more LNAPL is even present in day six of the WT Fluctuations experiment than in day five of the Base Case experiment). From this observation, it can be concluded that water table fluctuations acted to somewhat increase LNAPL longevity within the sand tank system. Possible explanations for this result are given in Section 3.3.4.

The photographic time lapse for the Combined experiment is shown in Figure 9. As was expected after evaluating the previous experiments, the visual LNAPL longevity for the Combined experiment fell between that of the Recovery and WT Fluctuations experiments. The LNAPL appeared to be visually depleted by day six (and close to depleted by day five). This supports the result obtained from the WT Fluctuations experiment that water table fluctuations

acted to increase LNAPL longevity. After LNAPL recovery was completed, by the middle of day three, a substantially smaller amount of mass was left to be depleted by volatilization and dissolution according to the mass distribution imposed by water table fluctuations in the Combined experiment than in the WT Fluctuations experiment.

3.3.2 LNAPL Longevity

The LNAPL longevity of each experiment was determined visually by examining the photographs taken at 15 minute intervals throughout each experiment. Longevity was not quantified based solely on the photographs chosen to represent each day in the photographic time lapses of Section 3.3.1. For this work, LNAPL longevity was defined as the time between the beginning of LNAPL addition and the point when LNAPL was no longer visibly present in the tank. The longevities of the LNAPL from each of the experiments are represented graphically in Figure 10.

It is interesting to note that the longevities for the Base Case, WT Fluctuations, and Combined experiments are all similar even though the evolution of LNAPL distribution, as seen in the photographic time lapse figures of Section 3.3.1, is different for these experiments. When compared to the Base Case, LNAPL recovery resulted in a 31.4% decrease in longevity, water table fluctuations resulted in a 7.44% increase in longevity, and the combination of LNAPL recovery and water table fluctuations resulted in decrease in longevity of 8.34%. Possible explanations relating the percentages of the different types of losses that occurred in the system to the longevity of each experiment are presented in Section 3.3.4.

Base Case Experiment

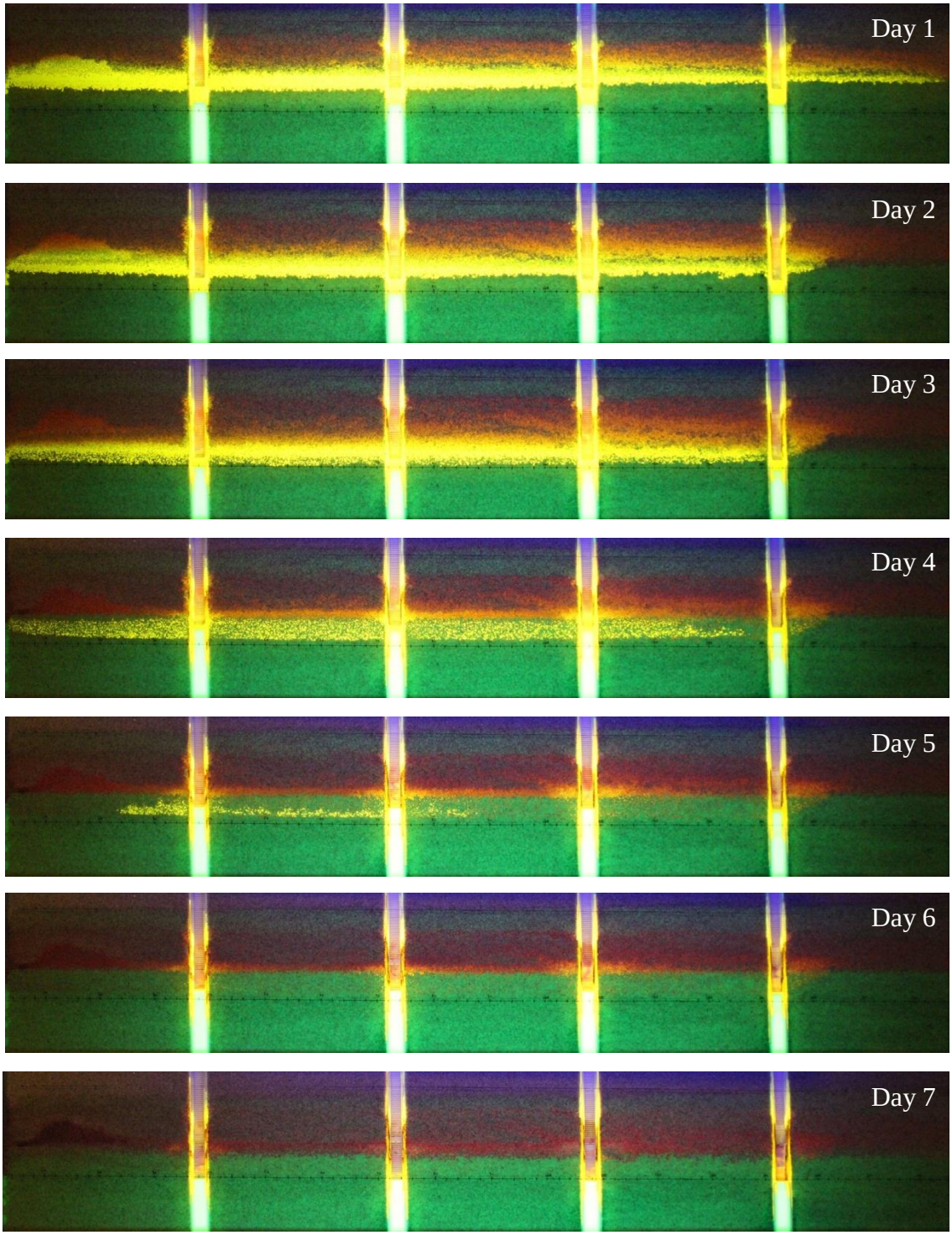

Figure 6 – Evolution of LNAPL (yellow colored) for the Base Case experiment in daily increments starting at the top with day one and continuing downward to day seven with water shown as green colored

Recovery Experiment

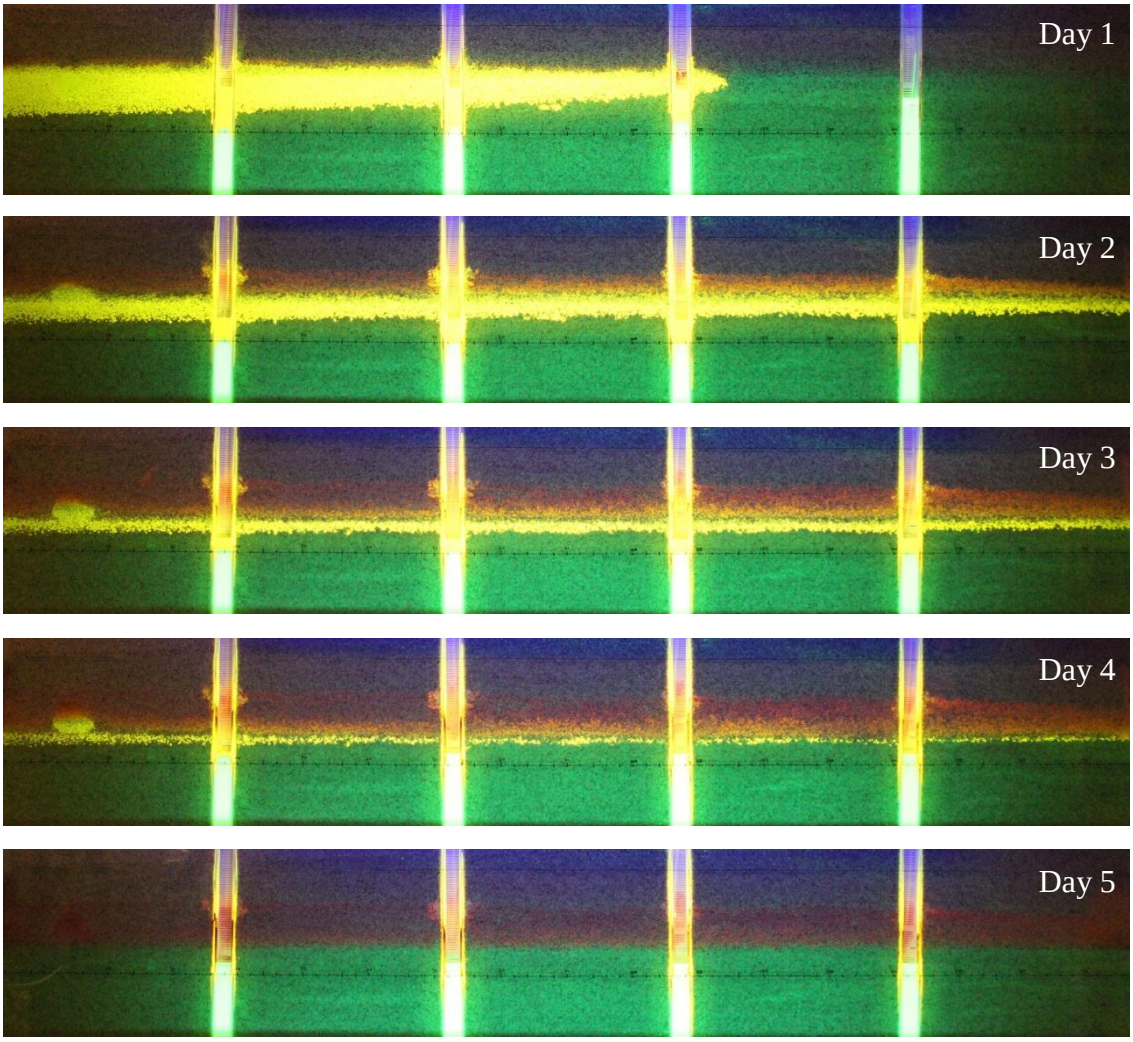

Figure 7 – Evolution of LNAPL (yellow colored) for the Recovery experiment in daily increments starting at the top with day one and continuing downward to day five with water shown as green colored

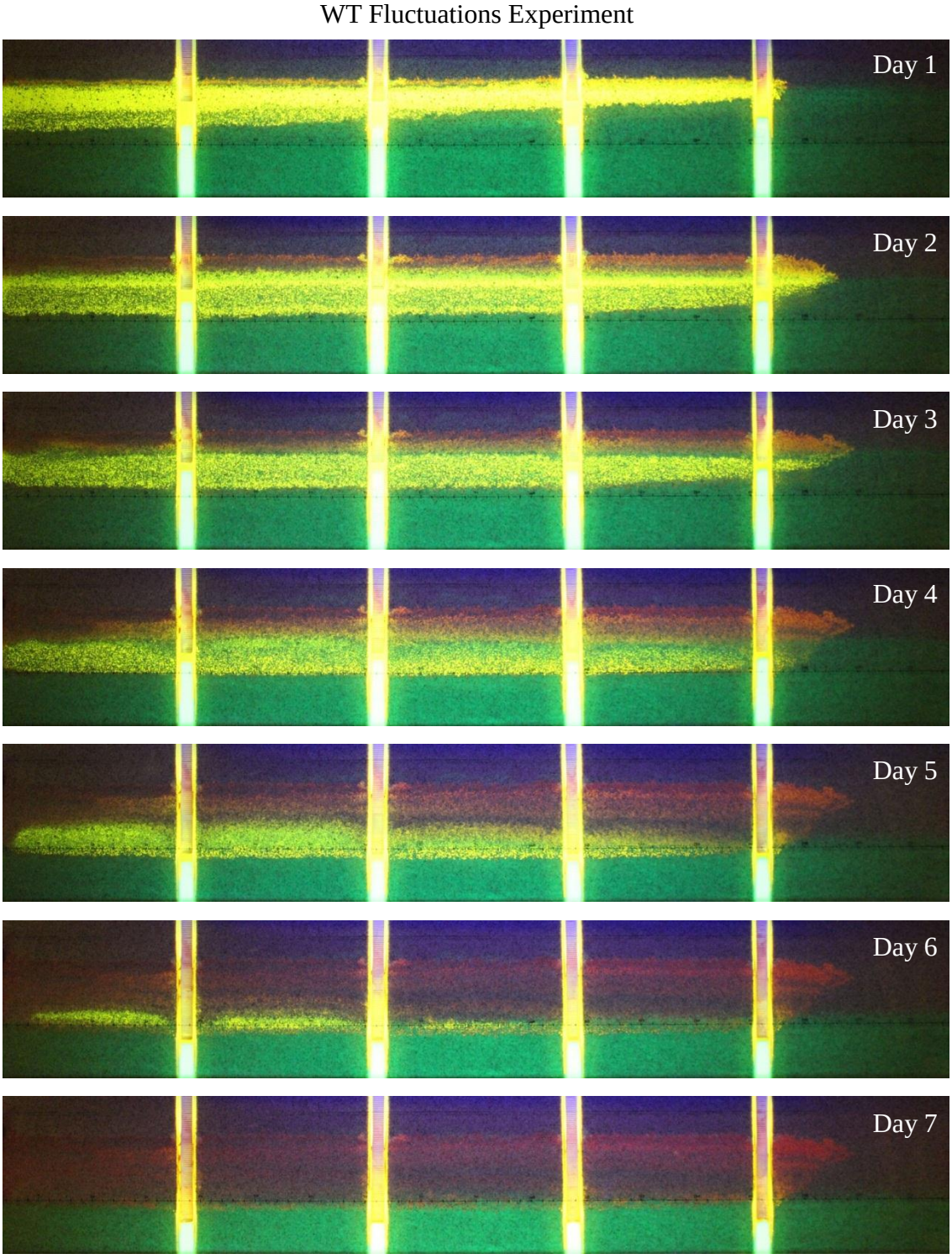

Figure 8 – Evolution of LNAPL (yellow colored) for the WT Fluctuations experiment in daily increments starting at the top with day one and continuing downward to day seven with water shown as green colored

Combined Experiment

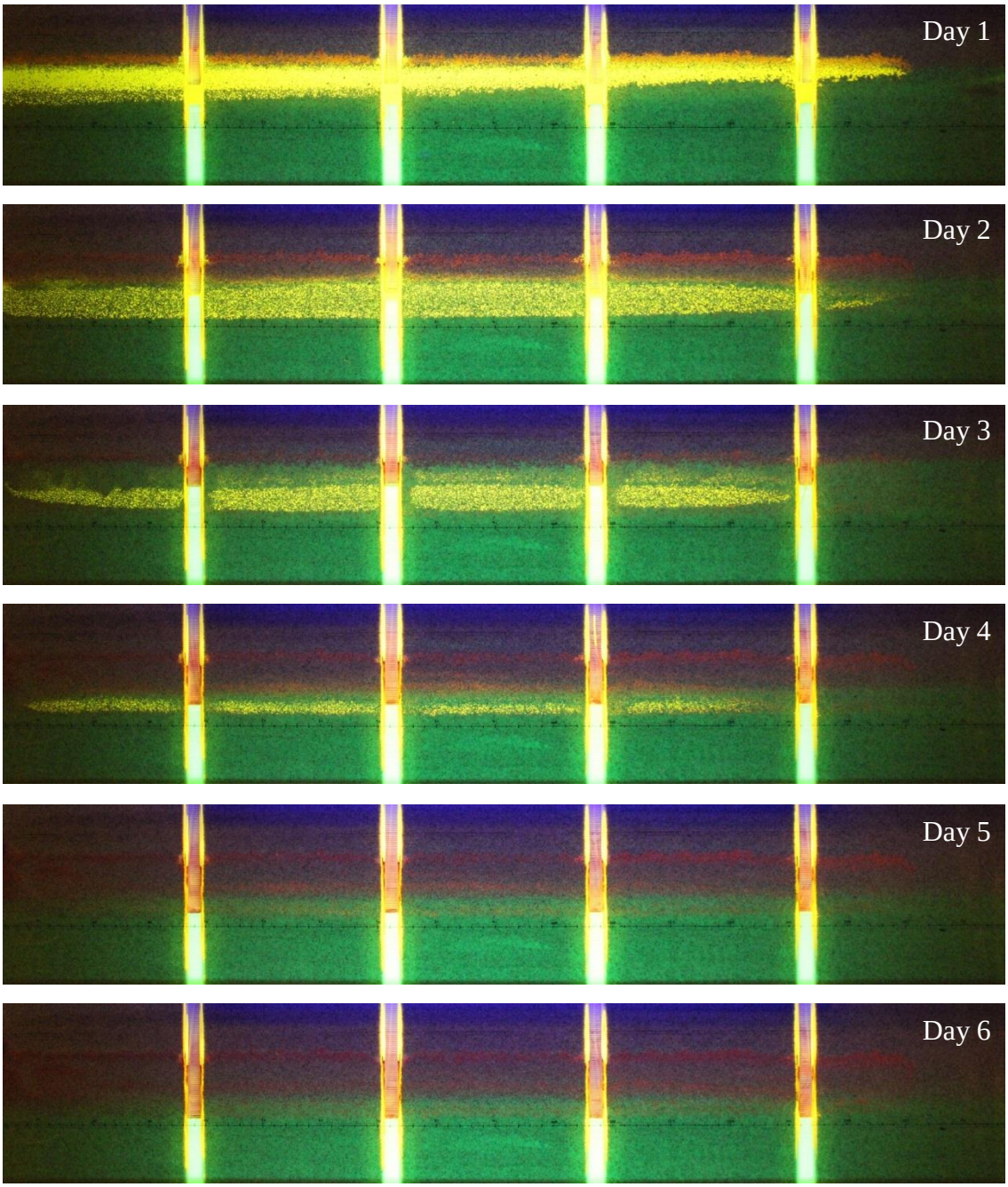

Figure 9 – Evolution of LNAPL (yellow colored) for the Combined experiment in daily increments starting at the top with day one and continuing downward to day six with water shown as green colored

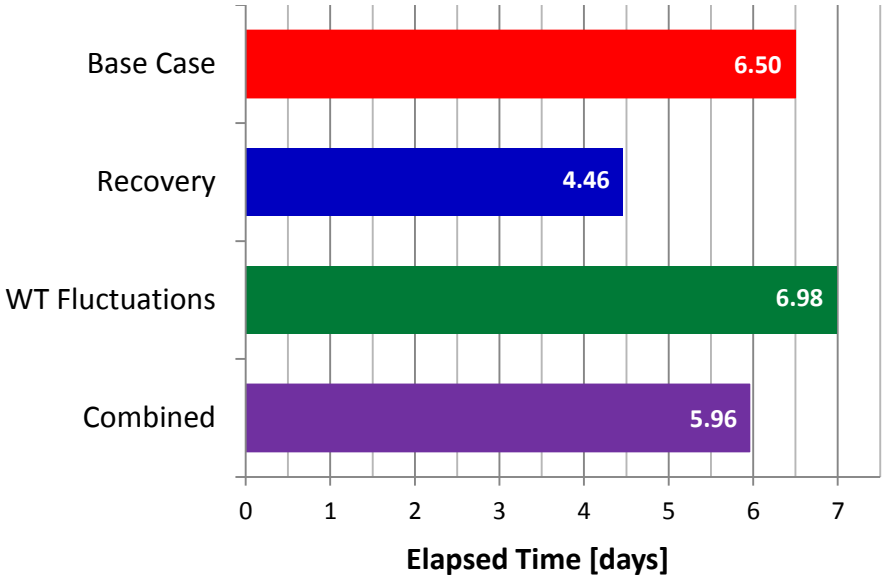

Figure 10 – Bar graph of LNAPL longevity for sand tank experiments

3.3.3 Mass Balance

Figure 11 shows the results of the mass balance for each experiment as normalized mass [%] remaining versus time [days]. Values for normalized remaining mass are relative to total initial mass in the system and calculated using Equation 4

$$\mathrm{M(t)}_{norm} = \frac{M(t)}{M_0} \qquad \text{[Eq. 4]}$$

where $\mathrm{M(t)}_{norm}$ [%] is the normalized mass remaining at any given time, $M(t)$ [M] is the mass remaining at any given time, and M_0 [M] is the initial mass introduced to the system.

The relatively constant slope (straight line shape) of the curves supports the assumption that natural losses, particularly losses due to volatilization and dissolution, can be modeled using zero order reaction rate equations. Straight line segments for the experiments involving LNAPL recovery begin after approximately 2.5 days (after recovery was complete). Small oscillations are seen in the slopes of the experiments involving water table fluctuations due to the change in

mass available for either volatilization or dissolution throughout the experiment; however the overall shape still suggests a zero order process (or a combination of two zero order processes).

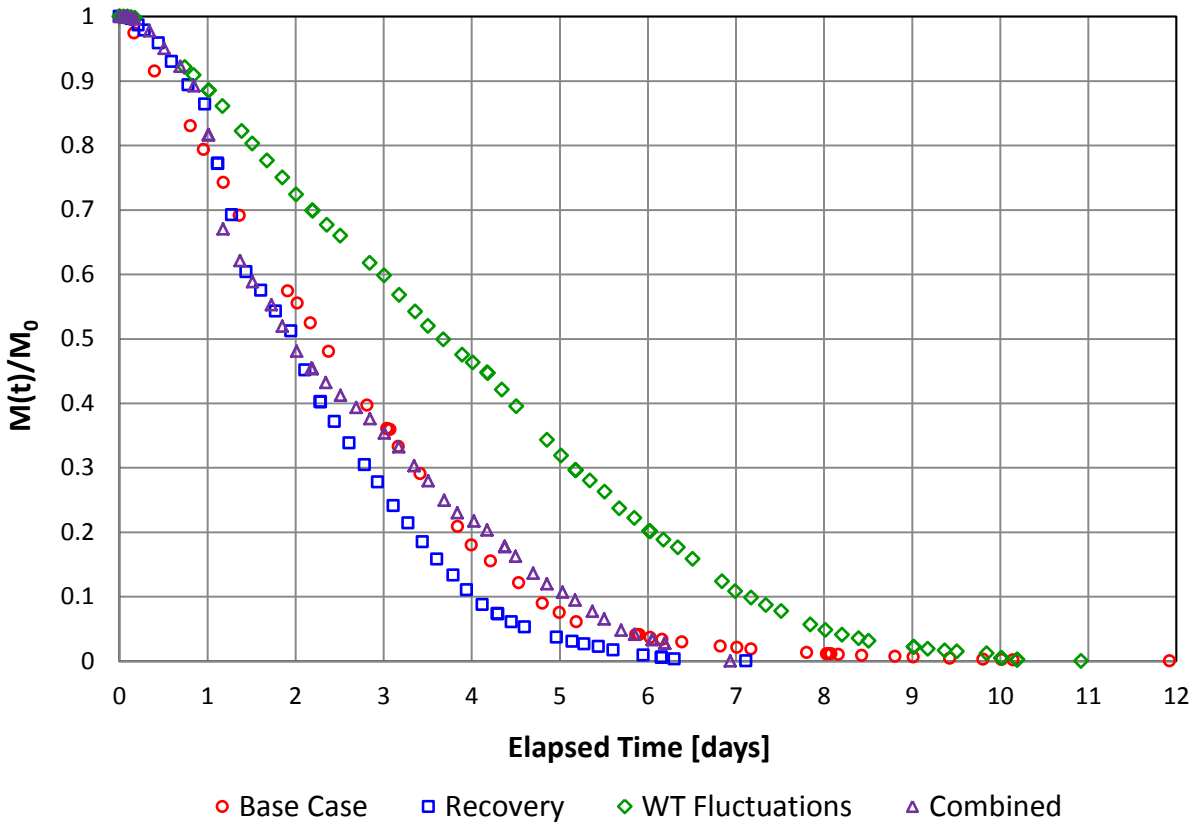

Figure 11 – Plot of normalized mass remaining versus time for the four laboratory LNAPL longevity experiments

Interestingly the curve for each experiment appears to consist of two straight line segments connected by a curvilinear section. One possible explanation is that these curvilinear sections represent a transition period from one zero order reaction rate to another. A possible explanation of this transition period is that for a certain period of time the mass distribution is such that the LNAPL area exposed to volatilization and dissolution is constant. Then at some point, enough LNAPL has been depleted that this exposed area is changed enough that the reaction rate of LNAPL loss begins to decrease until it reaches another nearly constant zero order rate. For this experiment, a possible scenario is that initially the LNAPL pool is shrinking along its top and

bottom edges only, and at some point begins to shrink from the up gradient, down gradient, front, and back edges as well, causing a change in geometry. The loss measurements acquired from these experiments are technically averages over the plan view surface area of the porous media. Therefore, as less LNAPL occupies the tank a smaller portion of the total porous media plan view surface area will be experiencing losses. In other words, the total LNAPL loss rate in the system is constant per unit surface area of LNAPL but not for the total porous media plan view surface area of the tank.

It is important to note that the mass balance curves shown in Figure 11 may indicate greater LNAPL longevities than the visual LNAPL longevities discussed in Section 3.3.2. This is because even when LNAPL was visually gone from the sand tank system, non-zero aqueous and vapor phase sample concentrations were still observed for multiple days. The longevities that could be extrapolated from Figure 11 would represent the total longevity of all MTBE phases not the longevity of the MTBE LNAPL alone.

One other important observation that can be made in Figure 11 is the effect that water table fluctuations appeared to have on the overall LNAPL loss rate (or slope of the mass balance curve). When comparing the magnitudes of the slopes of the mass balance curves of the WT Fluctuations experiment to the Base Case experiment and the Combined experiment to the Recovery experiment, the magnitudes of the slopes of the WT Fluctuations experiment and Combined experiment appear to be smaller. This suggests that water table fluctuations somehow act to decrease the overall LNAPL loss rate of the system. Possible reasons for this are discussed in Section 3.3.4.

3.3.4 Types of Losses

In general, volatilization of the LNAPL release was responsible for approximately 52%-98% more mass loss than LNAPL recovery or dissolution. The amount of mass loss due to dissolution increased when water table fluctuations were included in the experiment design. Approximately the same fraction of mass was recovered via well skimming in both the Recovery and Combined experiments. Similar fractions of mass were lost through dissolution in both the WT Fluctuations and Combined experiments. These observations can be seen in Figure 12 and are expanded upon in the subsequent paragraphs.

For the Base Case experiment volatilization accounted for 99.4% of losses, while dissolution accounted for the remaining 0.6% of mass loss. Loss percentages through volatilization and dissolution were 75.5% and 1.1%, respectively for the Recovery experiment. LNAPL recovery was responsible for 23.4% of mass losses in this experiment. For the WT Fluctuations experiment volatilization accounted for 91.1% and dissolution accounted for 8.9% of mass loss. Volatile losses made up 69.8% of mass loss for the Combined experiment, dissolution accounted for 8.6%, and approximately 21.6% of LNAPL mass was recovered via well skimming for this experiment.

In both experiments involving LNAPL recovery, approximately the same portion of LNAPL mass was recovered. This supports the assumption that LNAPL recovery can be modeled as a first order loss rate equation. The differences in longevity reduction of the Recovery and Combined experiments when compared to the Base Case experiment supports the statement made in Huntley and Beckett 2002 that hydraulic recovery will not be equally effective for various site conditions. Even though approximately the same portion of mass was recovered via

well skimming in both experiments, different percentages of longevity reduction compared to the Base Case experiment were observed because of other site conditions (i.e. water table fluctuations).

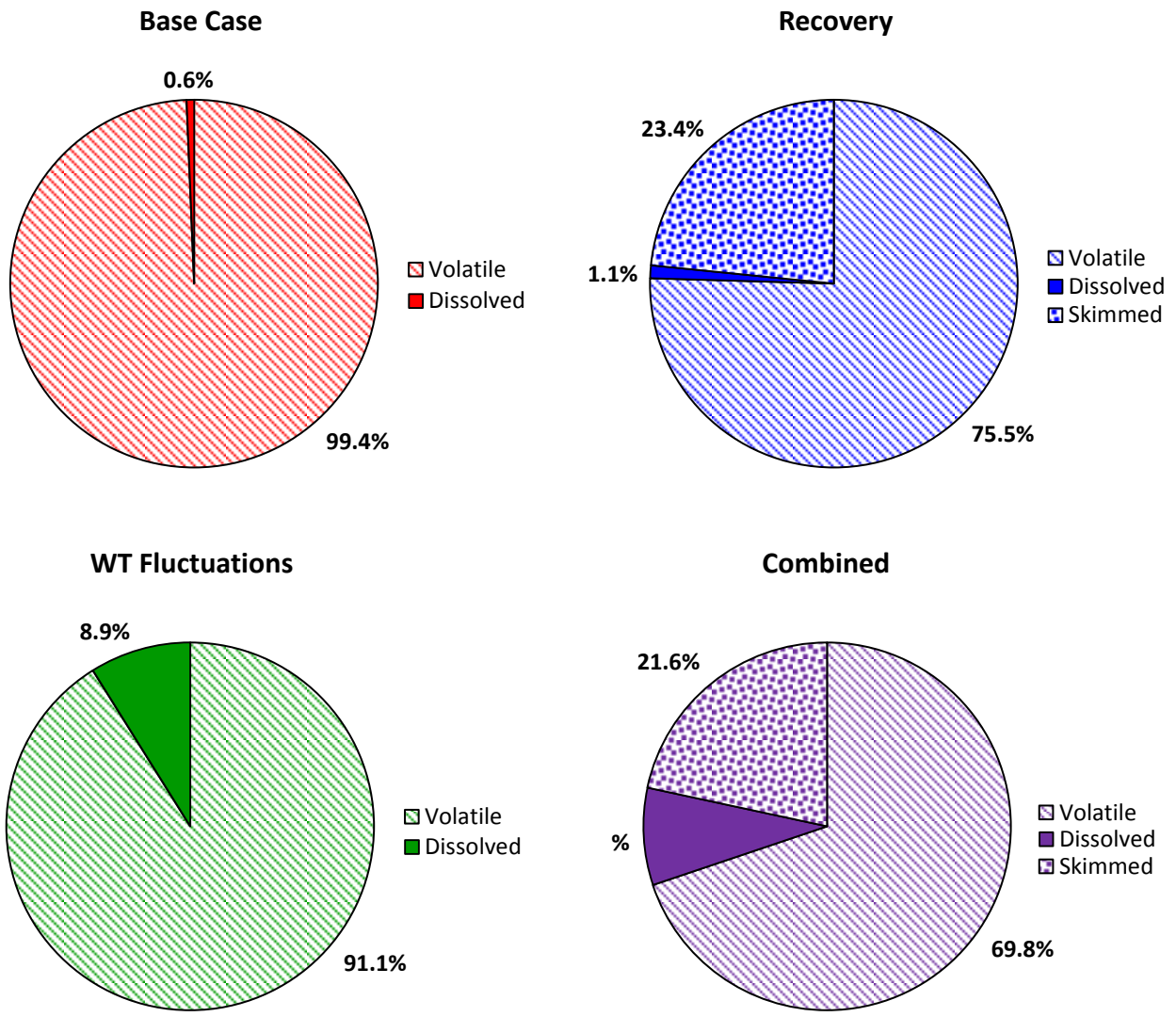

Figure 12 – Type of loss pie charts for each laboratory experiment showing percentages of mass lost through each of the loss mechanisms

The fact that recovery of 23.4% of the total LNAPL mass in the Recovery experiment resulted in a corresponding reduction in longevity of 31.4% when compared to the Base Case experiment

suggest that LNAPL recovery can be an appropriate remediation approach for early stage releases. However no recoverable LNAPL was present in the wells after two days of LNAPL recovery. This suggests that as LNAPL releases evolve, LNAPL recovery may become a less beneficial and less appropriate remediation approach.

When comparing the WT Fluctuations experiment to the Base Case experiment and the Combined experiment to the Recovery experiment, it can be seen that both LNAPL longevity and the portion of mass lost through dissolution relatively increased for the WT Fluctuations and Combined experiments. It is hypothesized that the rate of dissolution occurring in the system was much slower than the rate at which volatilization was occurring based on vapor and water flow rates, the chemical properties of the LNAPL, and the experimental results. Therefore, one possibility why relative longevity increases were observed in these experiments is that more LNAPL was prone to dissolution because more LNAPL was present below the water table at various times throughout these experiments. It follows that since dissolution was assumed to occur at a slower rate than volatilization, more mass loss through dissolution would result in increased longevity. Another possible explanation is that the water table fluctuations limited the amount of LNAPL subject to volatilization at various times throughout these experiments. Because volatilization was possibly the dominant process in the system, limiting of the effectiveness of volatilization would increase LNAPL longevity.

The relative effects of combinations of treatment remedies can be explored by comparing the results of the Combined experiment to those of the Recovery and WT Fluctuations experiments. When compared to the Recovery experiment, the longevity of the Combined experiment represented a 33.6% increase. When compared to the WT Fluctuations experiment, the longevity of the Combined experiment represented a 14.7% decrease. The percent changes from the Base

Case longevity observed in the Recovery and WT Fluctuations experiments were a 31.4% decrease and a 7.44% increase, respectively. By comparing these two sets of results, it can be concluded that the two treatment remedies employed did not affect the LNAPL independently of one another. This suggests it will be important to incorporate the interactions of multiple remedies in order to develop an accurate analysis of LNAPL losses as a function of time and the overall longevity of LNAPL.

4. LNAPL LONGEVITY PREDICTIVE MODEL

This chapter describes a novel LNAPL longevity predictive model [LLPM]. First, an introduction to this novel effort is given. Second, assumptions made and methods used in the development of the LLPM are discussed. Next, required model inputs and resulting outputs are described. Finally, a demonstration of the model applied to the laboratory data gathered from the laboratory sand tank experiments described in Chapter 3 is presented.

The primary objective of the model is to provide a predictive tool that can be used by practitioners to support sustainable remediation planning decisions by improving the understanding of the relationships between different loss mechanisms. A secondary objective of the modeling was to gain an improved conceptual understanding of how different loss mechanisms affect LNAPL longevity.

Critically the LLPM is different than LNAST, Huntley and Beckett 2002. LNAST focuses on mass transport processes and their effect on aqueous and vapor phase concentrations. This is based on the premise that aqueous and vapor phase concentrations are the primary metrics of concern. Within the LLPM, the primary concern is the long--term persistence of LNAPL. Longevity is predicted by modeling the interactions of governing processes to complete a mass balance for the lifetime of the LNAPL release.

A limitation of this model is that it is largely untested with respect to field data. This is because field data describing LNAPL longevity is apparently unavailable. Continued efforts to find field data by which to compare the LLPM are necessary. Future work will also be necessary to verify the developed equations and further develop input parameters.

4.1 Model Assumptions

This section provides a summary list of critical assumptions made in the development of the LLPM. The assumptions previously stated in Section 1.1 also apply to the development of the LLPM. The authors realize that the following are highly simplifying assumptions; however, it is hypothesized that the LLPM will provide an adequate estimate of LNAPL longevity nonetheless.

Key assumptions for the model include:

- The mass balance volume consists of the entire LNAPL pool.
- The mass input rate term in the mass balance equation is equal to zero.
- The LNAPL distribution is laterally uniform across the mass balance volume.
- Losses occur uniformly across the mass balance volume and throughout the lifetime of the LNAPL.
- Loss terms for all LNAPL components can be integrated into an average value for each loss mechanism.
- A mass balance can be constructed for each mass fraction separately. These mass balances can then be linked by an equation relating water table fluctuations to the mass distribution between continuous and discontinuous fractions.
- Water table fluctuations affect the distribution of LNAPL between continuous and discontinuous fractions. A sinusoidal equation can be used to model fluctuations in this distribution.

- Temperature fluctuations affect the magnitude of biological degradation of LNAPL. A sinusoidal equation can be used to model annual fluctuations in temperature.

- The biological degradation rate will be determined by a step function. When the temperature in the subsurface is above a specified value, an optimal biological degradation rate will apply. When the temperature in the subsurface is below a specified value, a non-optimal biological degradation rate will apply.

4.2 Methods

This section describes the mathematical techniques used to quantitatively address the governing processes that were assumed to be important in the prediction of LNAPL evolution. First a general mass balance for an LNAPL release is developed. Next, the application of the various loss mechanisms are discussed. The computational methods employed are introduced and the derivation of the final mass balance equations are presented. The equations used to distribute mass between the continuous and discontinuous fractions by water table fluctuations are given. Finally, the equations used to vary the rate of biological degradation according to annual temperature fluctuations are given.

4.2.1 Mass Balance

The mass balance volume shown in Figure 13 represents the LNAPL pool for which the mass balance to produce the LLPM was employed. The mass balance volume consists of the entire area affected by LNAPL and the entire LNAPL mass. LNAPL mass can be present in one of two compartments as either continuous fraction above the water table or discontinuous fraction

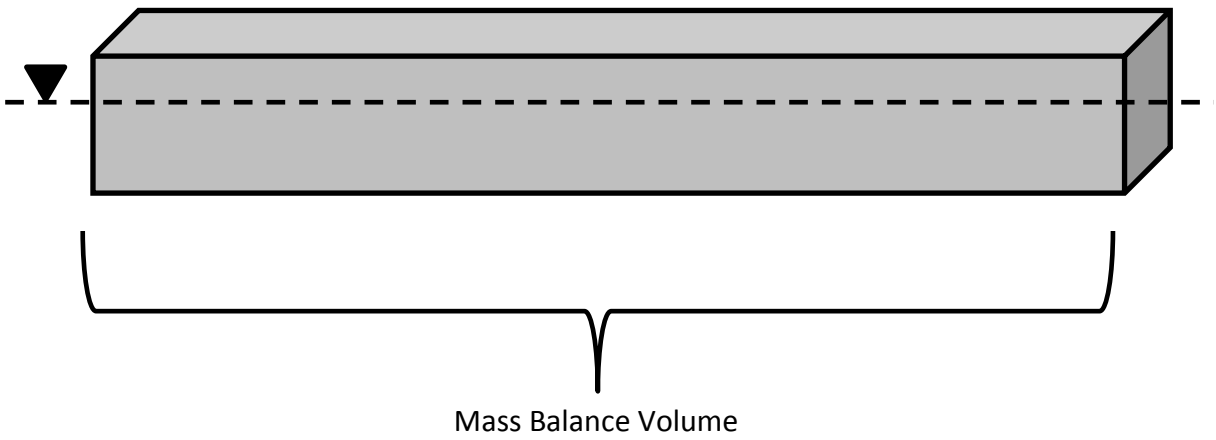

Figure 13 – Mass balance volume consisting of the entire effected area and containing all LNAPL mass as either continuous or discontinuous fraction; where continuous LNAPL can be located above and below the water table, and discontinuous LNAPL is only located below the water table

below the water table. Equation 5 is the expression written to represent the mass balance applied to the mass balance volume.

$$\dot{M}_{in} + \dot{M}_{out} = \frac{dM}{dt} \qquad \text{[Eq. 5]}$$

In Equation 5, $\dot{M}_{in}$ [M/T] is the rate of mass input, $\dot{M}_{out}$ [M/T] is the rate of mass output (i.e. losses), and $\frac{dM}{dt}$ [M/T] is the rate of change of mass within the mass balance volume. Based on the assumptions that there is no mass input and a mass balance can be constructed for each mass fraction separately, Equation 6 and Equation 7 can be written for the discontinuous and continuous fractions, respectively. In Equation 6 and Equation 7, components are the same as for Equation 5 except they each relate to a specific portion of the LNAPL mass.

$$\dot{M}_{out_{disc}} = \frac{dM_{disc}}{dt} \qquad \text{[Eq. 6]}$$

$$\dot{M}_{out_{cont}} = \frac{dM_{cont}}{dt} \qquad \text{[Eq. 7]}$$

Equation 8 can be used to represent the mass balance for the total mass of the mass balance volume.

$$\frac{dM_T}{dt} = \frac{dM_{disc}}{dt} + \frac{dM_{cont}}{dt} \qquad \text{[Eq. 8]}$$

4.2.2 Loss Mechanisms

Loss mechanisms of volatilization, dissolution, biological degradation, and hydraulic recovery and/or SVE (including the LNAPL recovery employed in the laboratory sand tank experiments) are included in the LLPM. Reaction rates were assigned different reaction orders and designated to act on the different fraction compartments of LNAPL mass based on the foundation established in Chapter 2.

Ordinary differential equations [ODEs] for zero and first order reaction rates are shown in Equation 9 and Equation 10, respectively

$$\lambda_{0th} = -\frac{dM}{dt} \quad \text{[Eq. 9]}$$

$$\lambda_{1st} * M(t) = -\frac{dM}{dt} \quad \text{[Eq. 10]}$$

where λ_{0th} [M/T] is the zero order reaction rate, λ_{1st} [T^{-1}] is the first order reaction rate, $\frac{dM}{dt}$ [M/T] is the rate of change in mass relative to time represented in derivative form, and $M(t)$ [M] is the mass remaining in the system at any given time.

Hydraulic recovery and/or SVE were modeled as a first order reaction rate based on the findings of Sale 2001. Volatilization and dissolution were designated as zero order reaction rates based

on the experimental results presented in Section 3.3.3. Biological degradation was designated as a zero order reaction rate based on the findings of McCoy 2012.

Hydraulic recovery and/or SVE acts on the continuous fraction mass compartment in the LLPM. This designation was made based on the discussion of the importance of LNAPL fractions in Chapter 2. Volatilization was assigned to act on the continuous fraction LNAPL because this fraction is in contact with soil vapor. Dissolution was assigned to act on the discontinuous fraction LNAPL because this fraction is in contact with groundwater. Biological degradation was assigned to act on both fractions of LNAPL represented in the LLPM because evidence of biological degradation has been found throughout LNAPL bodies where both continuous and discontinuous LNAPL fractions are present.

The assumption that volatilization and dissolution affect different portions of the mass can be supported by the results of the laboratory sand tank experiments. The losses due to volatilization changed by 23.9%, of total losses, between the Base Case and Recovery scenarios; while the percentage of losses due to dissolution between those two experiments was approximately the same. The application of LNAPL recovery appeared to decrease the amount of mass available for volatilization. This suggests that LNAPL recovery was removing mass from the same compartment that volatilization was acting on. Because it is generally accepted that LNAPL recovery acts on continuous fraction LNAPL (Huntley and Beckett 2002), it was assumed that volatilization was acting on the continuous fraction mass separately of dissolution acting on the discontinuous fraction mass.

4.2.3 Computational Methods

The LLPM uses numerical methods to solve Equation 8. The derivation of the LLPM utilized finite difference methods to estimate the mass remaining at each time step throughout the model time frame. For the complete derivation of the final expressions for mass in the discontinuous and continuous compartments presented in this section see Appendix D. The model was built in Excel (Microsoft Corporation, Redmond, WA). Excel is a common computational platform that enables the design of a graphical user interface [GUI] to simplify the utilization of the model.

The final expression for estimating discontinuous mass at the future time step is given by Equation 11

$$M_{disc}^{i+1} = M_{disc}^{i} - \Delta t * (\lambda_{dis} + f_{disc} * \lambda_{bio}) \quad \text{[Eq. 11]}$$

where M_{disc}^{i+1} [M] is the discontinuous mass remaining in the system at the future time step, M_{disc}^{i} [M] is the discontinuous mass remaining in the system at the current time step, Δt [T]is the time step interval, λ_{dis} [M/T] is the zero order reaction rate due to dissolution, f_{disc} [%] is the fraction of LNAPL mass in the discontinuous fraction, and λ_{bio} [M/T] is the zero order reaction rate due to biological degradation.

The final expression for estimating continuous mass at the future time step is given by Equation 12

$$M_{cont}^{i+1} = \frac{M_{cont}^{i} * \left(1 - \frac{\Delta t * \lambda_{rec}}{2}\right) - \Delta t * (\lambda_{vol} + f_{cont} * \lambda_{bio})}{\left(1 + \frac{\Delta t * \lambda_{rec}}{2}\right)} \quad \text{[Eq. 12]}$$

where M_{cont}^{i+1} [M] is the continuous mass remaining in the system at the future time step, M_{cont}^{i} [M] is the continuous mass remaining in the system at the current time step, λ_{rec} [T^{-1}] is the first order reaction rate due to LNAPL recovery, λ_{vol} [M/T] is the zero order reaction rate due to volatilization, and f_{cont} [%] is the fraction of LNAPL mass in the continuous fraction. The total mass present in the system at any given time is the sum of the mass in each of the compartments.

Finally, the total modeled mass at the future time step can be found by combining Equation 11 and Equation 12. Equation 13 is the final expression used within the LLPM. Appendix D contains the full derivation of the governing equations of the LLPM.

$$M_T^{i+1} = M_{disc}^{i} - \Delta t * (\lambda_{dis} + f_{disc} * \lambda_{bio}) + \frac{M_{cont}^{i} * \left(1 - \frac{\Delta t * \lambda_{rec}}{2}\right) - \Delta t * (\lambda_{vol} + f_{cont} * \lambda_{bio})}{\left(1 + \frac{\Delta t * \lambda_{rec}}{2}\right)} \quad \text{[Eq. 13]}$$

4.2.4 Water Table Fluctuations

Water table fluctuations are used in the model to partition mass between the two compartments. As previously discussed, these compartments are delineated by whether they consist of the continuous or discontinuous fraction of mass. This would make the LLPM comparable to the WT Fluctuations and Combined experiments and field conditions. A cyclic function was developed based on the general equation for a cosine wave function, Equation 14

$$y = A * \cos\left(\frac{2*\pi}{\lambda} * x\right) + D \quad \text{[Eq. 14]}$$

where A is the amplitude in units of y, λ is the period in units of x, D is a non-zero center of amplitude in units of y, and x and y are position coordinates. The date – or time and date depending on period length – of the low water level, period of the water level cycle, and the

range of the portion of mass in the continuous fraction (high and low value) within the water level cycle period were used to establish a cosine function of fraction of continuous fraction mass at any given time. Equation 15 calculates the fraction of mass in the continuous fraction at any given time, $f(t_{WL})_{cont}$ [%]

$$f(t_{WL})_{cont} = \frac{f_{cont}^{max} - f_{cont}^{min}}{2} * \cos\left(\frac{2*\pi}{\lambda_{WL}} * t_{WL}\right) + \frac{f_{cont}^{max} + f_{cont}^{min}}{2} \quad \text{[Eq. 15]}$$

where f_{cont}^{max} [%] and f_{cont}^{min} [%] are the period maximum and minimum fraction of mass in the continuous fraction, respectively, λ_{WL} [T] is the period of the water level cycle, and t_{WL} [T] is the number of days since the low water level. The period low water level will correspond to the same day f_{cont}^{max} is achieved for that period.

4.2.5 Temperature Fluctuations

The capability to include seasonal subsurface temperature fluctuations is part of the LLPM to address the effect temperature has on the biological degradation reaction rate. This was accomplished by establishing a date the annual high subsurface temperature is observed, the annual subsurface temperature range (high and low values), and assuming the period of subsurface temperature fluctuation, λ_{temp}, is 365 days. These inputs were used to establish a cosine function of seasonal temperature variation that produces the subsurface temperature at any given time, $T(t_{temp})$ [°C]. Equation 16 is based on time, t_{temp} [T] in days, since the annual high temperature was observed

$$T(t_{temp}) = \frac{T_{max} - T_{min}}{2} * \cos\left(\frac{2*\pi}{\lambda_{temp}} * t_{temp}\right) + \frac{T_{max} + T_{min}}{2} \quad \text{[Eq. 16]}$$

where T_{max} [°C] and T_{min} [°C] are the maximum and minimum annual subsurface temperatures, respectively. Equation 14 also served as a basis for Equation 16.

The biological degradation reaction rate is a function of this temperature. The biological degradation reaction rate for a given time step is assigned the value of either 4.68 m^3/hectare/yr (500 gal/acre/yr) if the temperature for that time step is less than 18°C, or 46.8 m^3/hectare/yr (5,000 gal/acre/yr) if the temperature for that time step is greater than or equal to 18°C. This is represented in equation form by a step equation, Equation 17.

$$\lambda_{bio} = \begin{matrix} C * 500 \frac{gal}{acre*yr}, when\ T(t_{temp}) < 18°C \\ C * 5000 \frac{gal}{acre*yr}, when\ T(t_{temp}) > 18°C \end{matrix} \quad \text{[Eq. 17]}$$

In Equation 17, C [M*L^2/L^3] is a conversion factor used to change λ_{bio} into units of [M/T] that are utilized by the LLPM in Equation 13. The critical temperature for this step function is based on values determined by Zeman 2012. The values for the two possible biological degradation reaction rates are based on McCoy 2012. Because biological degradation was not a loss mechanism in the laboratory study of LNAPL longevity, the inclusion of temperature fluctuations was not necessary for application of this model to the sand tank experiment results.

The LLPM also has the capability to include the effects of thermally enhanced LNAPL attenuation. Application of this passive treatment alternative has been explored by the work of Zeman 2012, Irianni Renno 2013, and Akhbari 2013. Inclusion of thermally enhanced LNAPL attenuation functions to maintain the critical temperature of 18°C within the system for a specified annual time frame. This in turn dictates that the higher value of the biological degradation reaction rate is active during that annual time frame as long as the treatment remedy

is active on site. For dates outside the annual time frame of thermal enhancement and when the treatment remedy is not active, Equation 16 controls temperature.

4.3 Model Inputs

This section introduces and describes each of the parameters needed to run the LLPM. The input worksheet of the model requires user specified parameters in three different categories: site characteristics, contamination characteristics, and loss and remedy characteristics. The GUI created in Excel (Microsoft Corporation, Redmond, WA) used to facilitate the input of the user specified parameters is shown in Figure 14. In Figure 14, drop down arrows open lists containing options related to the parameter they are adjacent to. Cells with "units?" drop downs provide a list of possible units the adjacent parameter can be defined in terms of. Cells with "yes/no?" drop downs allow the user to choose whether or not to include the adjacent site characteristic or treatment method. Further instructions appear in the darker shaded cells adjacent to these drop downs to instruct the user on how to proceed with parameter entry once a site characteristic or treatment method has been included or excluded.

As general information, the start date the user would like to define as the initial time reference point of the model is required. The final field-scale LLPM performs 150 years of calculations with a time step of 30 days.

The length of the model time step and the period of water table fluctuations must be compatible. For example, a period of water table fluctuations of 30 days is not compatible with a model time step of 30 days because the same water table level would be observed at each time step. This means the model time step would need to be adjusted to accommodate tidal water table

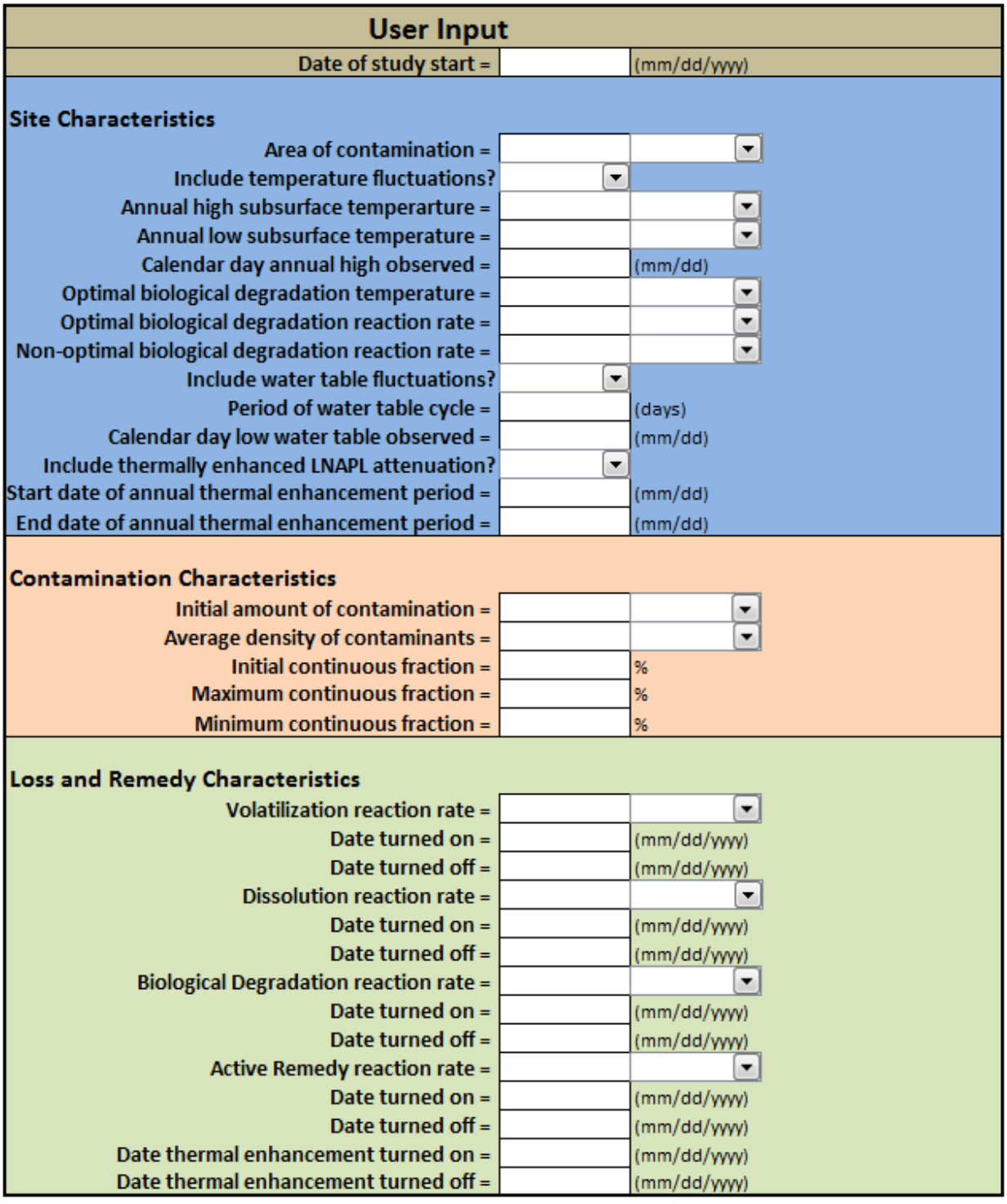

Figure 14 – Graphical user interface to facilitate user specified parameter entry

fluctuations. This could be accomplished with any time step that is out of sync with tides. For example, a time step of 0.25 days would a high and low value of water table for each 0.5 day period.

4.3.1 Site Characteristics

Inputs for the site characteristics category include:

- Area of contamination
- Choice of whether to include temperature fluctuations
- Annual high subsurface temperature
- Annual low subsurface temperature
- Calendar day annual high temperature observed
- Temperature for optimal biological degradation
- Optimal biological degradation reaction rate
- Non-optimal biological degradation reaction rate
- Choice of whether to include water table fluctuations
- Period of water table cycle
- Calendar day low water table observed for period
- Choice of whether to include thermally enhanced LNAPL attenuation
- Start date of annual thermal enhancement period
- End date of annual thermal enhancement period

The area of contamination is used, along with the average density of contaminants from the contamination characteristics category, to convert the loss mechanism reaction rates entered in the loss and remedy characteristics category into units of [M/T].

When temperature fluctuations are included, temperature varies based on the next three inputs from the above list and Equation 16. When temperature fluctuations are not included, the next three inputs from the above list are not required, and the reaction rate for biological degradation is held constant at the rate indicated by the user in the loss and remedy characteristics category.

When water table fluctuations are included, the fraction of mass in the continuous fraction varies at each time step according to Equation 15. Equation 15 requires the next two inputs from the above list, and the maximum and minimum fraction in the continuous fraction inputs from the contamination characteristics category. The maximum fraction in the continuous fraction corresponds to the calendar day the annual low water level is observed. When water table fluctuations are not included, the initial continuous fraction input from the contamination characteristic category is used as a starting point for the distribution of mass between the two compartments. In either case, Equation A11-3 is used to calculate the corresponding fraction of discontinuous fraction mass either at each time step for the first scenario or initially for the second scenario.

When thermally enhanced LNAPL attenuation is included, the next two inputs from the above list are used to bracket a range of annual dates when the temperature is maintained at 18°C. This in turn dictates the biological degradation reaction rate as long as the thermal enhancement treatment is active, as specified by the dates input in the loss and remedy characteristics category. When thermal enhancement is not active, the biological degradation reaction rate is

controlled by whether or not temperature fluctuations have been chosen to be included in the model.

Figure 15 shows three plots that will populate as decisions regarding the inclusion of temperature fluctuations, water table fluctuations, and thermally enhanced LNAPL attenuation are made. These plots can be used to guide the input of the parameters associated with inclusion of the above phenomena. To simplify the interpretation of the top panel of Figure 15, the units of λ_{bio} are shown in [M/T] matching the operating units of the LLPM rather than the unit system chosen by the user from the appropriate drop down list within the GUI.

4.3.2 Contamination Characteristics

Inputs for the contamination characteristics category include:

- Initial amount of contamination
- Average density of contaminants
- Initial continuous fraction
- Maximum continuous fraction
- Minimum continuous fraction

The initial amount of contamination is used along with the average density of contaminants to give a starting point of total mass for the finite difference mass balance. The average density of contaminants is used, along with the area of contamination from the site characteristics category, to convert the loss mechanism reaction rates entered in the loss and remedy characteristics category into units of [M/T].

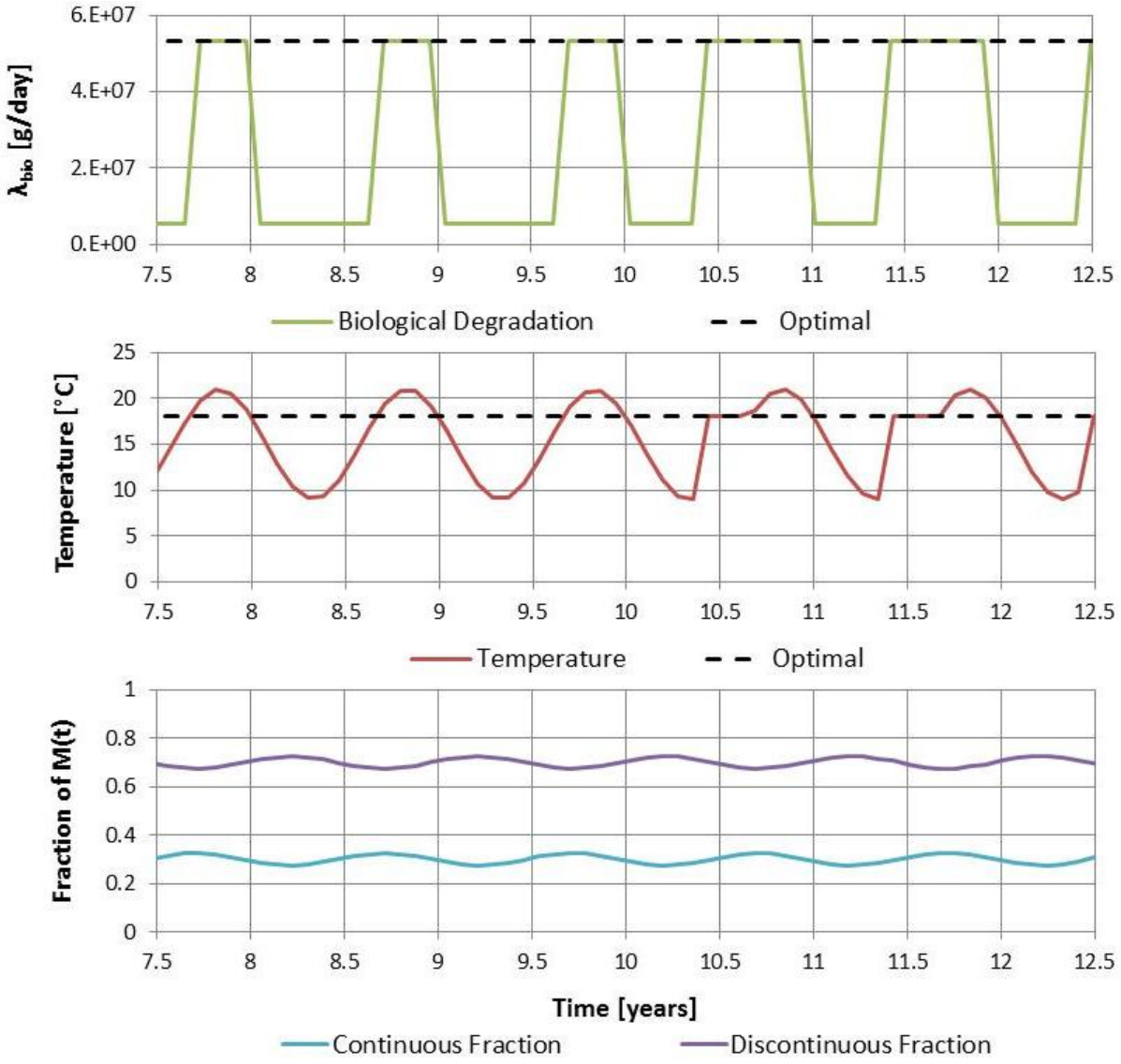

Figure 15 – Plots of biological degradation reaction rate, temperature, and continuous and discontinuous fractions versus time for a period 2.5 years prior to and 2.5 years after the beginning of application of both hydraulic recovery and thermally enhanced LNAPL attenuation

The maximum and minimum continuous fractions [f_{cont}] are used, along with inputs from the site characteristics category, to control the mass distribution between the continuous and discontinuous fraction compartments throughout the model time frame. The maximum continuous fraction will correspond to the low water table for that period and the minimum continuous fraction to the high water table.

4.3.3 Loss and Remedy Characteristics

Inputs for the loss and remedy characteristics category include:

- Volatilization reaction rate
- Date volatilization is turned on
- Date volatilization is turned off
- Dissolution reaction rate
- Date dissolution is turned on
- Date dissolution is turned off
- Biological degradation reaction rate
- Date biological degradation is turned on
- Date biological degradation is turned off
- LNAPL recovery reaction rate
- Date LNAPL recovery is turned on
- Date LNAPL recovery is turned off
- Date thermal enhancement is turned on
- Date thermal enhancement is turned off

The loss mechanism reaction rates are converted into units of [M/T] with the average density of contaminants from the contamination characteristics category and the area of contamination from the site characteristics category. If one of these rates is left blank, it assumed to be equal to a value of zero for calculation purposes.

The on and off dates for each of the loss mechanisms or treatments is used to establish the period of time within the model domain for which the corresponding loss mechanism is active. If one

of the on dates is left blank, the corresponding loss mechanism is assumed to be not active within the system. If one of the off dates is left blank, its value is assumed to be the maximum time value in the simulation (i.e. the loss mechanism is assumed to be active for the remainder of the model time frame if an on date is included).

For thermal enhancement these dates are different than the dates specified in the site characteristics category. The dates in the site characteristics category refer to the annual period of time within a year when the temperature will be maintained above 18°C to stimulate biological degradation. The on and off dates in the loss and remedy characteristics category refer to the period of time that thermally enhanced LNAPL attenuation as a treatment remedy is applied. For example, in Chapter 5, field-scale simulations are carried out where a treatment remedy application of thermally enhanced LNAPL attenuation with an annual period of maintained temperature of six months is turned on ten years after the beginning of the model time frame and left on for the remainder of the model time frame.

4.4 Model Outputs

This section introduces and describes the metrics used to quantify the performance of remedies employing multiple LNAPL loss mechanisms. The LLPM tracks total mass and mass in each of the compartments separately at each time step. From this data set, a mass balance plot over time, similar to the ones shown for the experiments in Section 3.3.3, can be produced. This plot will show the model estimate for the LNAPL longevity based on the user specified parameters. The mass loss rate at each time step is calculated in terms of the total mass, each mass compartment, and loss mechanism type. This data set can be used to produce plots of mass loss rate versus time. Mass balance plots were produced for each of the laboratory sand tank experiment model

scenarios. Mass loss rate plots were only produced for the field-scale application of the LLPM which will be described in Chapter 5.

4.5 Application to Laboratory Data

This section describes the application of the LLPM to the data from the laboratory sand tank studies presented in Chapter 3. Input parameters for the model were based on the experimental procedures applied, which are discussed in detail in Section 3.2, and linear fitting of the experimental mass balance data to produce values for the loss mechanism reaction rates.

A version of the model with laboratory-scale inputs was used for this portion of the work. Because the experimental time frame was only a matter of days, a smaller time step of 1 hour was used. Comparisons of the model to experimental data for all experiments can be seen in Figure 16. Figure 17shows the relative portions of mass that was lost through each of the simulated loss mechanisms.

In Figure 16, it can be seen that the LLPM obtained a relatively good fit to the experimental data. There appears to be a transition between the early time and late time data from a more rapid to a slower total mass loss rate in the experimental data, as discussed in Section 3.3.3. One weakness of the fit of the model to experimental data is that the model does not capture that curvilinear transition period between the early and late time data. In spite of this weakness, the application of the LLPM to the laboratory data can be considered a success, especially when looking at the fit of the model to the Recovery and Combined experiments. The curved sections of data due to LNAPL recovery and water table fluctuations are depicted by the model of these scenarios. Also the predicted longevities are similar to those presented in Section 3.3.2.

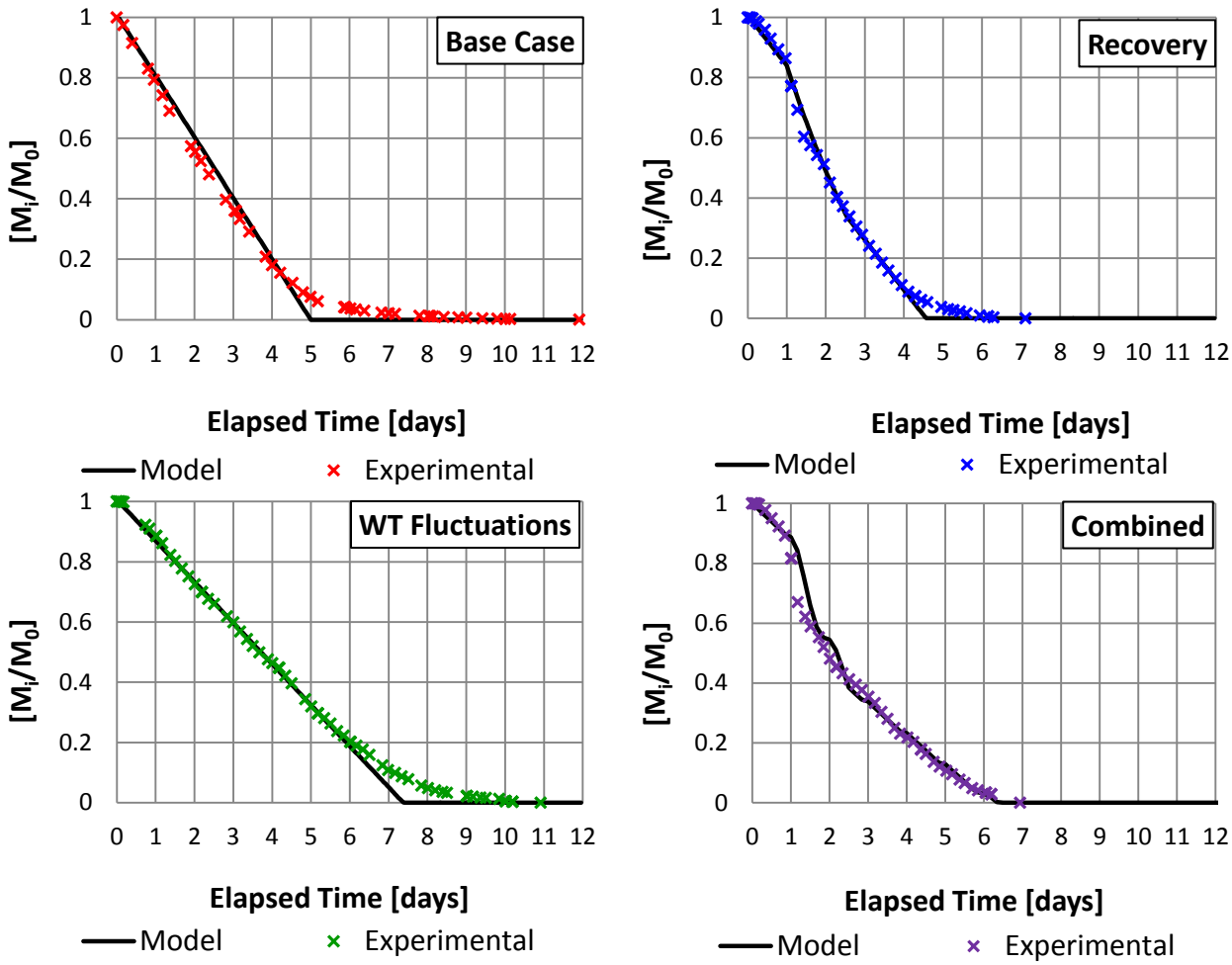

Figure 16 – Mass balance plots of laboratory data and model solutions for each experiment

In Figure 17, it can be seen that the LLPM produces similar results to those observed in the laboratory experiments. This can be seen by comparing Figure 12 and Figure 17. Once again, the portion of losses due to dissolution is higher for the simulations that included water table fluctuations. Also, LNAPL recovery again appears to affect only the continuous phase. The portions of volatile losses for the simulations with LNAPL recovery are less than those of the simulations without recovery, and the portions of dissolved losses stay relatively unchanged. This is seen by comparing the results of the Recovery simulation to those of the Base Case simulation and the Combined simulation to the WT Fluctuations simulation in Figure 17.

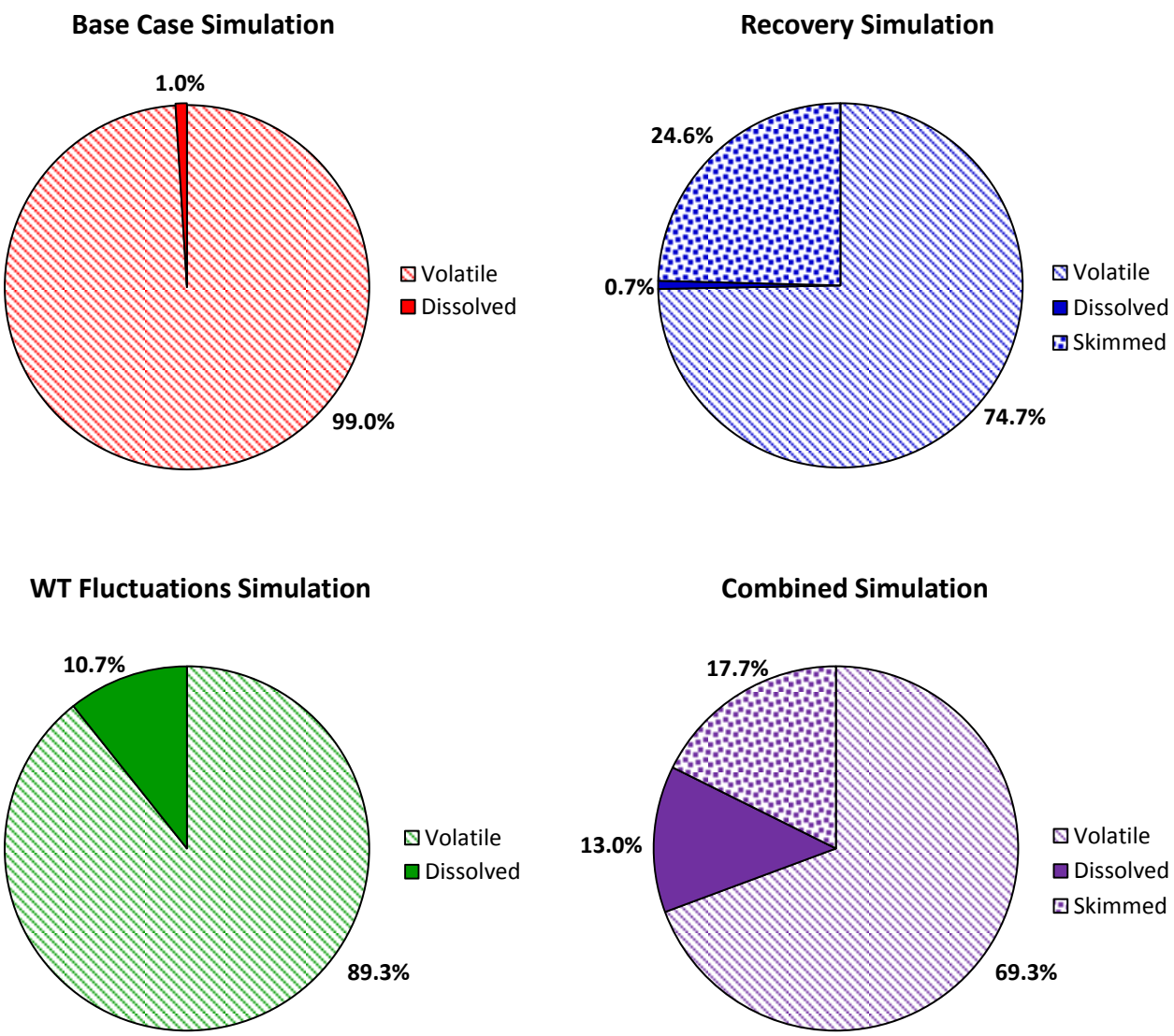

Figure 17 – Type of loss pie charts for the laboratory simulations with the LLPM showing percentages of mass lost through each of the loss mechanisms

Model parameters that were used to simulate the experimental data from the laboratory sand tank experiments are shown in Table 3. The loss mechanism reaction rates of volatilization and dissolution were estimated by linear best fit analysis of the mass balance data corresponding to each rate. An example of this fitting process applied to the Base Case mass balance data can be seen in Appendix E.

Table 3 – Model parameter values used so simulate laboratory study of LNAPL longevity experiments

	Base Case	Recovery	WT Fluctuations	Combined
Parameter	**Value**	**Value**	**Value**	**Value**
initial contamination [g]	749.45	676.05	745.24	747.29
initial f_{cont}	0.99	0.99	-	-
Volatilization Reaction Rate [m^3/hectare/yr]	7,592	5,817	4,471	4,259
Dissolution Reaction Rate [m^3/hectare/yr]	28.44	94.65	522.6	739.5
LNAPL Recovery Reaction Rate half-life [days]	-	2.46	-	2.32
inclusion of water table fluctuations?	no	no	yes	yes
water table cycle period [days]	-	-	1	1
f_{cont} range	-	-	0.90-0.10	0.99-0.01

5. FIELD-SCALE APPLICATION OF THE LLPM

The purpose of this chapter is to demonstrate a field-scale application and capabilities of the LLPM. This involved a sensitivity analysis for primary model input parameters. First, the objectives of applying the model to field-scale scenarios are introduced. Second, an important difference between the laboratory-scale and field-scale versions of the model is discussed. Third, the methods used to construct the field-scale models and sensitivity analysis are given. Fourth, the results of this section of work are described. Finally, limitations of the current model are discussed.

There were three main objectives for the field-scale application and sensitivity analysis of the LLPM. The first was to examine the applicability of the model to field-scale data. Part of this objective includes an evaluation of whether or not the LLPM gave reasonable outputs given input parameters that are consistent with field-scale LNAPL releases. The second main objective was to resolve the relative importance of the governing processes included in the model. The third, and final, main objective was to identify areas where additional work may be required and improvements can be made.

5.1 Laboratory versus Field-Scale Loss Mechanisms

An important difference between the laboratory-scale and field-scale application of the model is that volatilization was the primary natural loss mechanism during the laboratory study of LNAPL longevity described in Chapter 3, but biological degradation is the expected primary natural loss mechanism at field sites.

In Huntley and Beckett 2002, it is proposed that a large amount of volatilization of LNAPL from the water table zone to the surface doesn't likely occur due to counter acting conditions such as groundwater recharge and geologic heterogeneity that act to impede vapor flow to the surface. However, substantial volatilization may occur before the LNAPL comes to rest at the water table as it trickles down through the vadose zone; this is particularly true for more volatile components. This is part of the reasoning for not including a volatilization reaction rate in the field-scale model simulations.

Additional factors that would differ between the theoretical field-scale system and the laboratory-scale system comprising Chapter 3 are the vapor pressure of the LNAPL(s) and the size of the vadose zone. The vapor pressure of MTBE is higher than the vapor pressure of many components of typical petroleum hydrocarbons. Thus, less volatilization would be expected at the theoretical field site because it is a former petroleum refinery and multiple component LNAPLs are going to be present. There will also be a large difference in the thickness of the vadose zones between the two systems. A thicker vadose zone for the theoretical field site would result in less volatilized LNAPL mass reaching the ground surface due to a smaller vapor concentration gradient.

Another reason volatilization would account for less LNAPL mass depletion in the theoretical field-scale system is because volatilized mass would potentially be intercepted and depleted by the site microbial community. A large portion of the mass that leaves the LNAPL pool by both volatilization and dissolution will be biologically degraded at a later point in time. This is one of the ideas introduced in McCoy 2012 according to work done at the former Casper refinery. Estimates for the field-scale biological degradation reaction rate parameters were based off of this work; therefore, the field-scale applications contained in this chapter do not include

volatilization and dissolution reaction rates separate from biological degradation reaction rates. It is recognized that significant volatilization and dissolution can occur independent of biological degradation; this is apparent by the existence of extensive vapor and aqueous phase plumes. However those types of cases were not simulated here.

5.2 Methods

Within this section the theoretical field site will be introduced, the modeled treatment scenarios and methods for conducting the sensitivity analysis will be described, and the basis for comparing the different modeled treatment scenarios and the parameter variations within the sensitivity analysis will be given.

A theoretical field site was defined based on a former petroleum refinery located near Casper, Wyoming. This site was used because other researchers at the Center for Contaminant Hydrology at Colorado State University (see Irianni Renno 2013 and Akhbari 2013) have done work to characterize the site; therefore, some of the necessary inputs were known or could be derived from available data sets. Estimates of the initial amount of contamination, annual temperature fluctuation, and the effects of a hydraulic recovery treatment period were available. Geologic data indicate that the site consists of an alluvial aquifer.

5.2.1 Modeled Treatment Scenarios

The application, or lack thereof, of two different treatment remedies to the theoretical field site was the basis for the design of the field-scale modeled treatment scenarios. The two treatment remedies for this study were hydraulic recovery and thermally enhanced LNAPL attenuation.

Recently a thermally enhanced LNAPL attenuation pilot study has been conducted at the site which provided information to estimate some of the necessary inputs (Irianni Renno 2013 and Akhbari 2013). Building on the work of Zeman 2012, these studies operate under the hypothesis that biological communities can be stimulated by relatively low levels of heat addition to the subsurface such that the annual period of optimal biological degradation can be extended. Thus, the annual biological degradation of an LNAPL release could be notably increased by a passive remedy. The application periods of hydraulic recovery and thermal enhancement overlap for the modeled scenarios in order to evaluate the effects of simultaneous treatment remedies. This is not necessarily reflective of reality as the thermal enhancement pilot began recently in site history, whereas hydraulic recovery was completed decades ago. However, this variation was necessary to make the desired comparisons.

Four field-scale scenarios were considered. A No Action scenario was modeled where no treatment remedy was applied. An All Treatments scenario was modeled where both the hydraulic recovery and thermal enhancement treatment remedies were applied. One scenario was modeled for each of the treatment remedies applied singly: Hydraulic Recovery Only and Thermal Enhancement Only scenarios. The model parameters used to establish the modeled treatment scenarios are listed in Table 4. It can be seen that the input is the same for each of the scenarios except for the input parameters that control the treatment remedies. Hydraulic recovery and thermal enhancement were employed in the same manner for each of the modeled treatment scenarios for which they are applied. Thus comparison of the modeled treatment scenarios will be a comparison of the effects of treatment remedies –and combinations thereof – and nothing else.

Table 4 – Input parameters for the four modeled treatment scenarios of the field-scale model application order by longest longevity to shorter

Parameter [units]	No Action	All Treatments	Hydraulic Recovery Only	Thermal Enhancement Only
	Value			
model time frame start	1/1/1950	1/1/1950	1/1/1950	1/1/1950
area of contamination [km^2]	5.18	5.18	5.18	5.18
include temperature fluctuations	yes	yes[1]	yes	yes
annual temperature range [°C]	9-21	9-21	9-21	9-21
calendar day annual high observed [mm/dd]	10/15	10/15	10/15	10/15
include water table fluctuations	yes	yes	yes	yes
calendar day cycle low observed [mm/dd]	09/01	09/01	09/01	09/01
period of water table cycle [days]	365	365	365	365
include thermally enhanced biological	no	yes	no	yes
optimal temperature for biological degradation [°C]	-	18°C	-	18°C
optimal biological degradation reaction rate [m^3/hectare/yr]	-	46.8	-	46.8
non-optimal biological degradation reaction rate [m^3/hectare/yr]	-	4.68	-	4.68
initial amount of contamination [m^3/hectare]	2,806	2,806	2,806	2,806
average density of contaminants [kg/m^3]	800	800	800	800
range of f_{cont}	0.275-0.325	0.275-0.325	0.275-0.325	0.275-0.325
initial f_{cont}	-	-	-	-
biological degradation time frame	01/01/1950-end	01/01/1950-end	01/01/1950-end	01/01/1950-end
half-life of LNAPL recovery [years]	-	1	1	-
schedule of hydraulic recovery	-	01/01/1960-01/01/1965	01/01/1960-01/01/1965	-
annual period of thermal enhancement [mm/dd]	06/01-09/01	06/01-09/01	06/01-09/01	06/01-09/01
schedule of thermally enhanced biological	-	01/01/1960-end	-	01/01/1960-end

[1]Biological degradation reaction rate will be dependent of temperature

5.2.2 Parameter Sensitivity Analysis

Ten primary model input parameters, thought to have important impacts on site LNAPL evolution within the model, were designated. They were chosen from the list given in Section 4.3. Three levels of each parameter were defined: low, medium/base, and high values. For most of the parameters, the low level was equal to half of the base level, and the high level was equal to twice the base level. This was not the case for the magnitude of the f_{cont} range or the average of the f_{cont} range. The halving and doubling pattern was not followed for these parameters because it was thought that the levels chosen would produce a larger range of results which would make comparison easier. These parameters were then varied within each scenario for which they were applicable. These parameters, along with the values for each level, are shown in Table 5.

The ten primary model input parameters are defined below:

- Initial amount of contamination – model start value for contamination in terms of [M], [L^3], or [L^3/L^2]
- Magnitude of f_{cont} range – difference between the maximum and minimum continuous fraction in terms of [%]
- Average of f_{cont} range – average of the maximum and minimum continuous fraction in terms of [%]
- Initial f_{cont} – initial continuous fraction in terms of [%], required when water table fluctuations aren't included

- Biological degradation reaction rate – rate at which biological degradation occurs in terms of [$M/L^2/T$] or [$L^3/L^2/T$], required when water table fluctuations or thermally enhanced biological treatment remedy are not included
- Half-life of hydraulic recovery – estimated time required for half of LNAPL to be depleted by hydraulic recovery in terms of [T]
- Length of hydraulic recovery application – length of time that the hydraulic recovery treatment remedy is applied in terms of [T]
- Scheduling of hydraulic recovery – period of time when the hydraulic recovery treatment remedy is applied relative to the start of the model time frame in terms of [T]
- Length of annual period of maintained temperature – length of time that the subsurface temperature is annually maintained at the optimal temperature for biological degradation in terms of [T]
- Scheduling of thermal enhancement – period of time when the thermally enhanced biological degradation treatment remedy is applied relative to the start of the model time frame in terms of [T]

Each of the four modeled treatment scenarios described in Section 5.1.1 was modeled with base level parameters to provide a base case for the variation of the above mentioned parameters within each scenario. The sensitivity analysis was conducted by producing a modeled parameter scenario for all levels of each of the primary input parameters. One parameter was varied per modeled parameter scenario while all others were held at base levels. This was done for each of the treatment scenarios. This resulted in output that would provide insight into what parameters had the greatest effect on LNAPL longevity and how their effects varied between the treatment scenarios.

To apply the initial f_{cont} parameter, water table fluctuations were excluded to produce the modeled parameter scenarios where low, medium, and high values of initial f_{cont} were used. Similarly, to apply the biological degradation reaction rate parameter, temperature fluctuations were excluded to produce the modeled parameter scenarios where low, medium, and high values of biological degradation reaction rate were used.

Table 5 – Parameter level values used in the sensitivity analysis

Parameter [units]	Level Value		
	Low	Medium/Base	High
initial amount of contamination [gal/acre]	1,403	2,806	5,612
magnitude of f_{cont} range [%]	5[1]	10	20
average of f_{cont} range [%]	10	50[2]	90
initial f_{cont} [%]	25	50[3]	75
biological degradation reaction rate [m^3/hectare/yr]	16.4	32.8	65.6
half-life of hydraulic recovery reaction rate [years]	0.5	1	2
length of hydraulic recovery application [years]	2.5	5	10
scheduling of hydraulic recovery [years since t_0]	5	10	20
length of annual period of maintained temperature	3	6	12[4]
scheduling of thermal enhancement [years since t_0]	5	10	20

[1]This is the base level for this parameter
[2]This is the medium value used in the parameter level variation portion of the sensitivity analysis, the base level value for the modeled treatment scenario comparisons was 30%
[3]This is the medium value used in the parameter level variation portion of the sensitivity analysis, the base level value the modeled treatment scenario comparisons was 30%
[4]Parameter level variation scenarios with a high value of nine months were also evaluated

5.2.3 Basis for Comparison

Outputs that were used to compare the modeled treatment scenarios and modeled parameter scenarios include LNAPL longevity, mass balance plots, cumulative type losses plots, and loss mechanism loss rates plots. Relative LNAPL longevities from one scenario to another gave a

metric for the effectiveness of the scenarios relative to one another. Mass balance plots depict the evolution of the total mass and the distribution of mass between the continuous and discontinuous compartments. Cumulative type losses plots show the evolution of LNAPL losses due to hydraulic recovery and biological degradation and provide insight into the periods of treatment remedy effectiveness. Loss mechanism loss rates plots also provide insight into the periods of treatment remedy effectiveness. These plots show the evolution of the loss rates of hydraulic recovery and biological degradation.

5.3 Results

This section contains the results of the field-scale application and sensitivity analysis of the LLPM. First, results of the four modeled treatment scenarios are presented and discussed. Result topics include LNAPL longevity, mass balance, cumulative type losses, and loss mechanism loss rates outputs. Finally, the most significant results of the parameter level variation of the sensitivity analysis are presented and discussed.

5.3.1 LNAPL Longevity

The resulting LNAPL longevity outputs of the field-scale modeled treatment scenarios were in agreement with what was expected. The scenarios with progressively more aggressive treatment remedies resulted in shorter LNAPL longevities. The modeled treatment scenarios arranged in order of decreasing longevity are No Action, Thermal Enhancement Only, Hydraulic Recovery Only, and All Treatments. Figure 18 shows the values of longevity for each of the modeled treatment scenarios. Relative to the No Action modeled treatment scenario the longevities given in Figure 18 associated with the All Treatments, Hydraulic Recovery Only, and Thermal

Enhancement Only scenarios represent a 70.5%, 59.2%, and 30.4%decrease in LNAPL longevity, respectively.

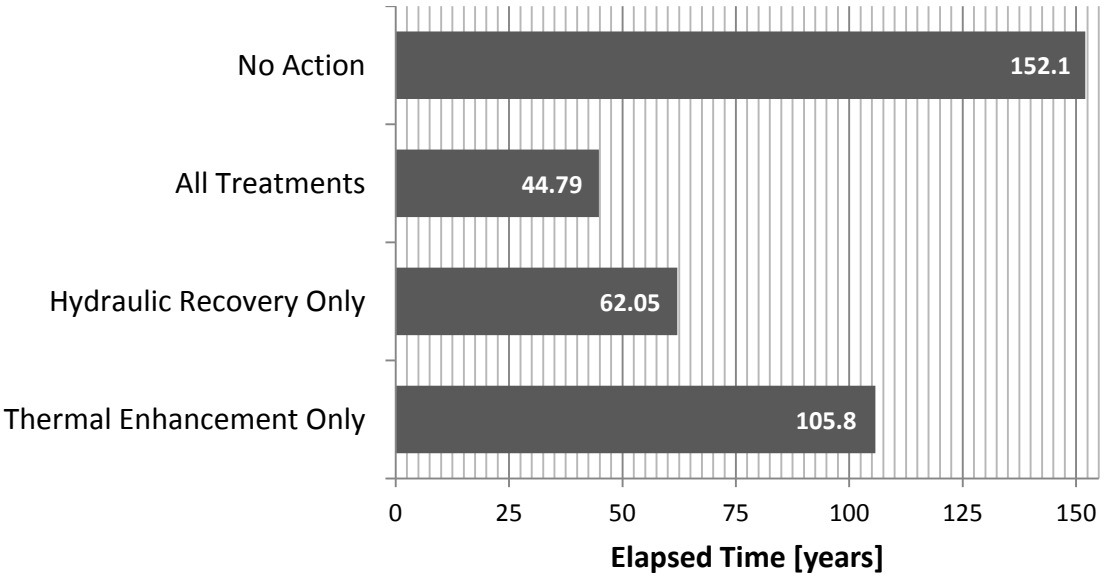

Figure 18 – LNAPL longevities for the four modeled treatment scenarios

5.3.2 Mass Balance

The output plots of relative mass remaining versus elapsed time for each of the modeled treatment scenarios are shown in Figure 19. Relative masses are the mass remaining in the system at any time divided by the total initial mass at t_0, as previously described in Section 3.3.3. The oscillations in the relative mass curves for the continuous and discontinuous fractions are due to the cyclic pattern of mass partitioning imposed on the scenarios because of the inclusion of annual water level fluctuations. The oscillations in the relative total mass curves are due to the fluctuation of the biological degradation reaction rate because of the inclusion of temperature fluctuations. From Figure 19 one can see the benefit of the output from the LLPM for comparing possible treatment scenarios for LNAPL releases in terms of mass evolution and distribution.

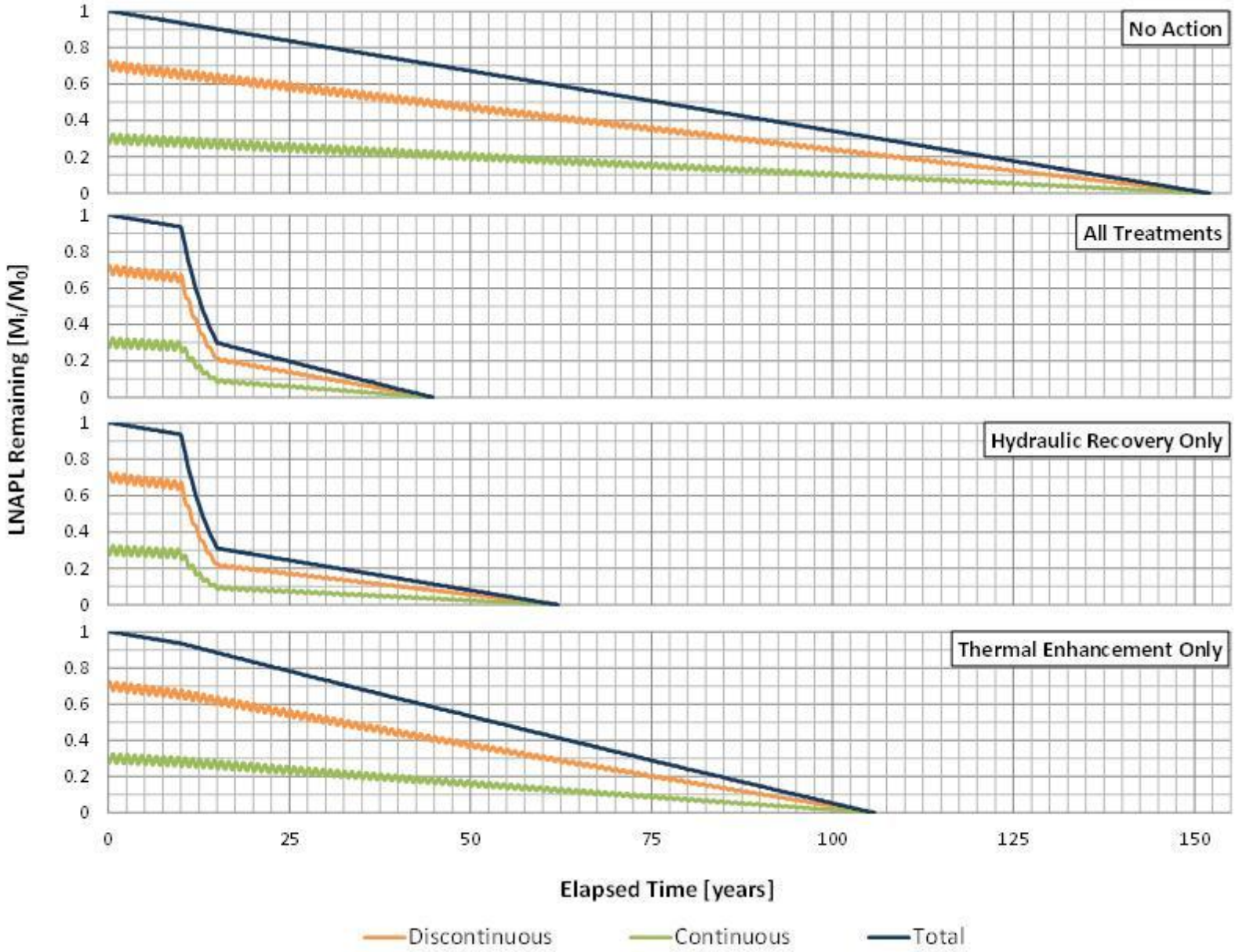

Figure 19 – Mass balance over time for all modeled treatments scenarios showing total mass and discontinuous and continuous fraction mass

Once again the LNAPL longevity for each of the modeled treatment scenarios relative to one another can be observed in Figure 19. In Figure 19, the specific LNAPL evolution and mass distribution can also be observed. The impact of the specific application of hydraulic recovery used for the All Treatments and Hydraulic Recovery Only scenarios is shown in Figure 19. This could be due to the fact that hydraulic recovery was applied early in the model time frame. If hydraulic recovery was applied later in the model time frame (or any number of conditions were different that limited the effectiveness of hydraulic recovery), different results would be observed. This idea is discussed further in Section 5.2.5.

5.3.3 Cumulative Type Losses

The individual contributions of hydraulic recovery and biological degradation to total mass loss for each of the modeled treatment scenarios are shown in Figure 20. Figure 20 shows that for the All Treatments and Hydraulic Recovery Only scenarios the cumulative losses due to hydraulic recovery made up a larger portion of the total losses. Once again, if hydraulic recovery was applied later in the model time frame, different results would be observed. Additionally if the effectiveness of hydraulic recovery was decreased, by conditions such as a longer LNAPL half-life under hydraulic recovery or less mass was contained in the continuous fraction, one would expect the cumulative losses due to biological degradation to overtop those due to hydraulic recovery. The idea is discussed further in Section 5.2.5. From Figure 20 one can see the benefit of the output from the LLPM for comparing possible treatment scenarios for LNAPL releases in terms of mass loss evolution and distribution.

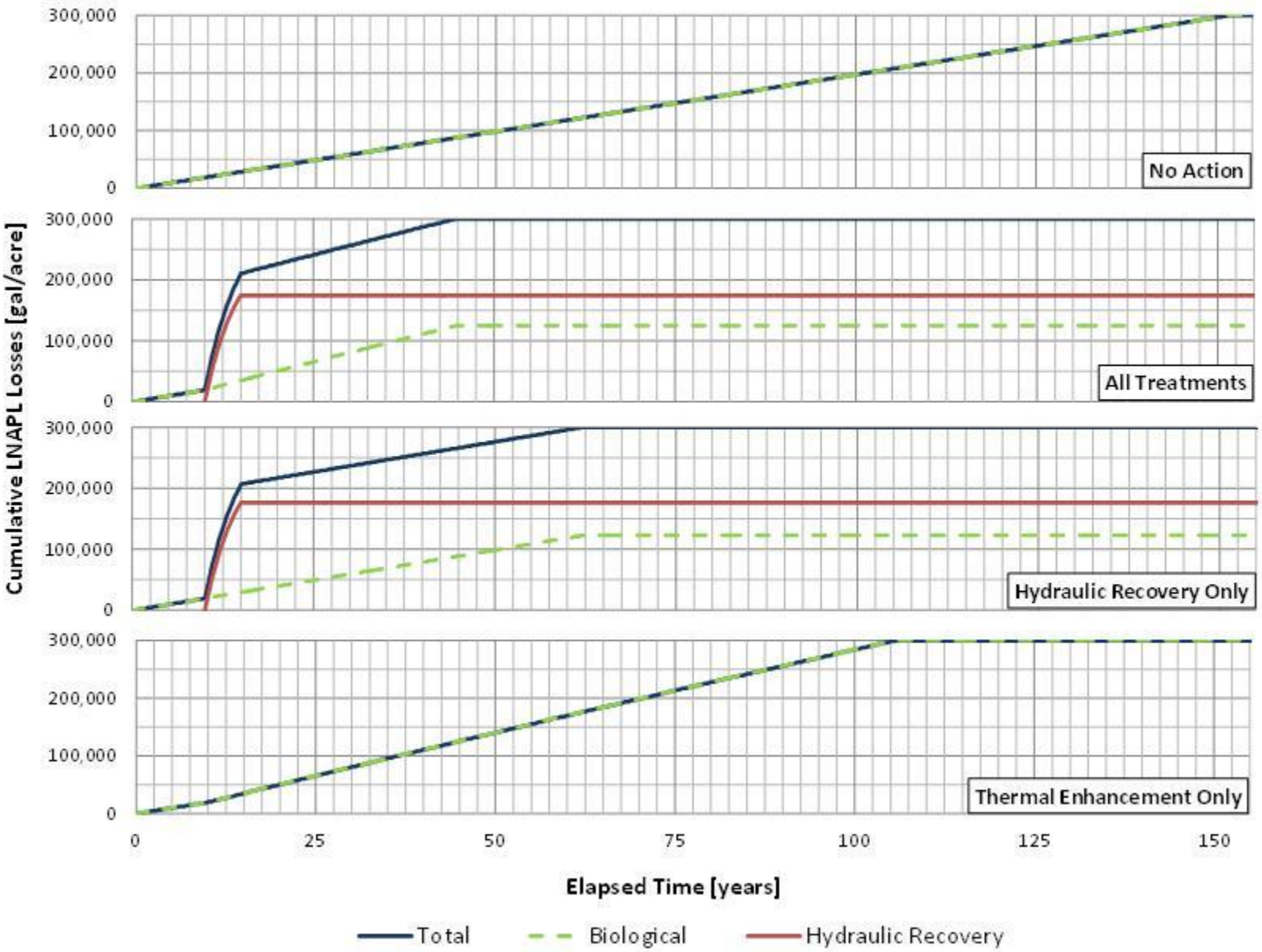

Figure 20 – Cumulative losses versus time for all modeled treatment scenarios showing total, biological, and hydraulic recovery losses

5.3.4 Loss Mechanism Loss Rates

The total mass loss rate and the mass loss rates dues to hydraulic recovery and biological degradation are shown for each of the modeled treatment scenarios in Figure 21. Figure 21 shows that for the periods when hydraulic recovery is active, the loss rate associated with hydraulic recovery is always higher than that of biological degradation. This can be seen in the panels for the All Treatments and Hydraulic Recovery Only modeled treatment scenarios. However, the loss rate associated with hydraulic recovery decays throughout the hydraulic recovery application period. It can be assumed that at some point the biological degradation loss rate would be greater than that of hydraulic recovery.

According to Figure 21, it can also be assumed that the hydraulic recovery loss rate would decay to a value less than the biological degradation loss rate more quickly if LNAPL mass wasn't continually cycled into the continuous fraction by water table fluctuations (or other conditions that would limit the effectiveness of hydraulic recovery. This idea is discussed further in Section 5.2.5. From Figure 21 one can see the benefit of the output from the LLPM for comparing possible treatment scenarios for LNAPL releases in terms of the loss rates associated with various loss mechanisms.

5.3.5 Parameter Sensitivity Analysis

This section presents the results of the parameter sensitivity analysis. These results give insight into the important factors that affect the governing processes of LNAPL depletion within the model. The relative effects of each parameter at each level – low, medium/base, and high – are compared in terms of the model outputs previously described as part of the results of modeled

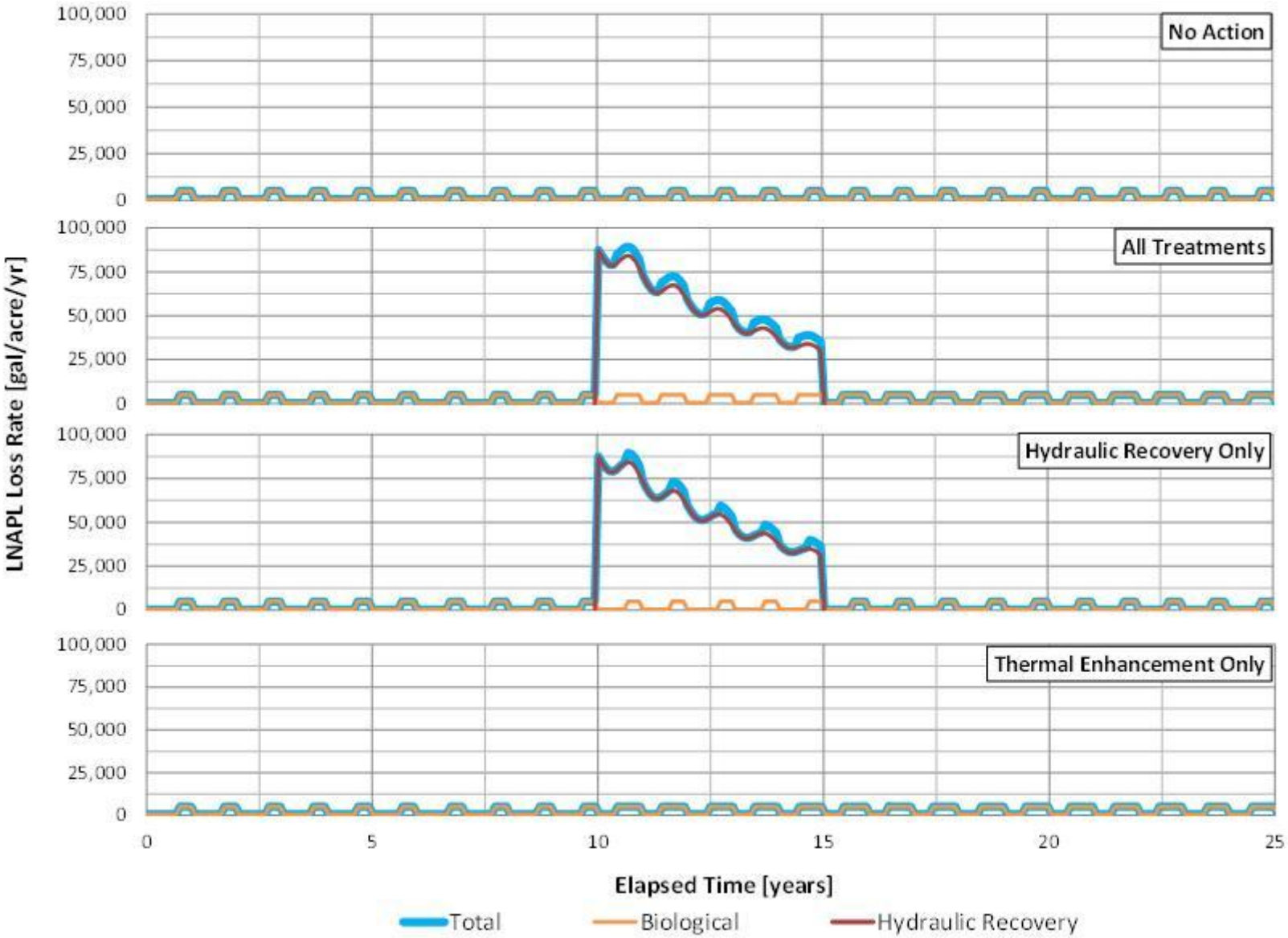

Figure 21 – LNAPL loss rates versus time for all modeled treatment scenarios in terms of total, biological degradation, and hydraulic recovery

treatment scenarios in Sections 5.2.1-5.2.4. Each parameter is discussed according to the modeled treatment scenarios for which it is relevant.

The longevity related outputs of the parameter level variation of the sensitivity analysis are shown in Figure 22, Figure 23, and Figure 24. The single best way to display the results of the sensitivity analysis did not present itself outright. The dotted lines in each of this figures was used to separate the parameters that applied to certain treatment scenarios. The first five parameters from the left applied to all of the treatment scenarios. The next three were only applicable to the treatment scenarios that included hydraulic recovery. The final two were only applicable to the treatment scenarios that included thermal enhancement.

Figure 22 displays the results directly in terms of longevity for every parameter level scenario that was designated. This is the rawest representation of the sensitivity analysis output. Figure 23 shows the output in terms of the standard deviation of the longevities resulting from the three levels tested for each parameter and treatment scenario. Figure 24 shows the outputs in terms of the coefficient of variation of the longevities resulting from the three levels tested for each parameter and treatment scenario. The results show differences between each of the representation methods; however, similar conclusions can be drawn from each of the representations.

The percent changes in longevity for each parameter level scenario of the four modeled treatment scenarios are shown in Table 6. Parameters that are irrelevant to a certain modeled treatment scenario are excluded from that section. For example, the length of the half- life for hydraulic recovery was not evaluated in the No Action or Thermal Enhancement Only scenarios because hydraulic recovery was not included.

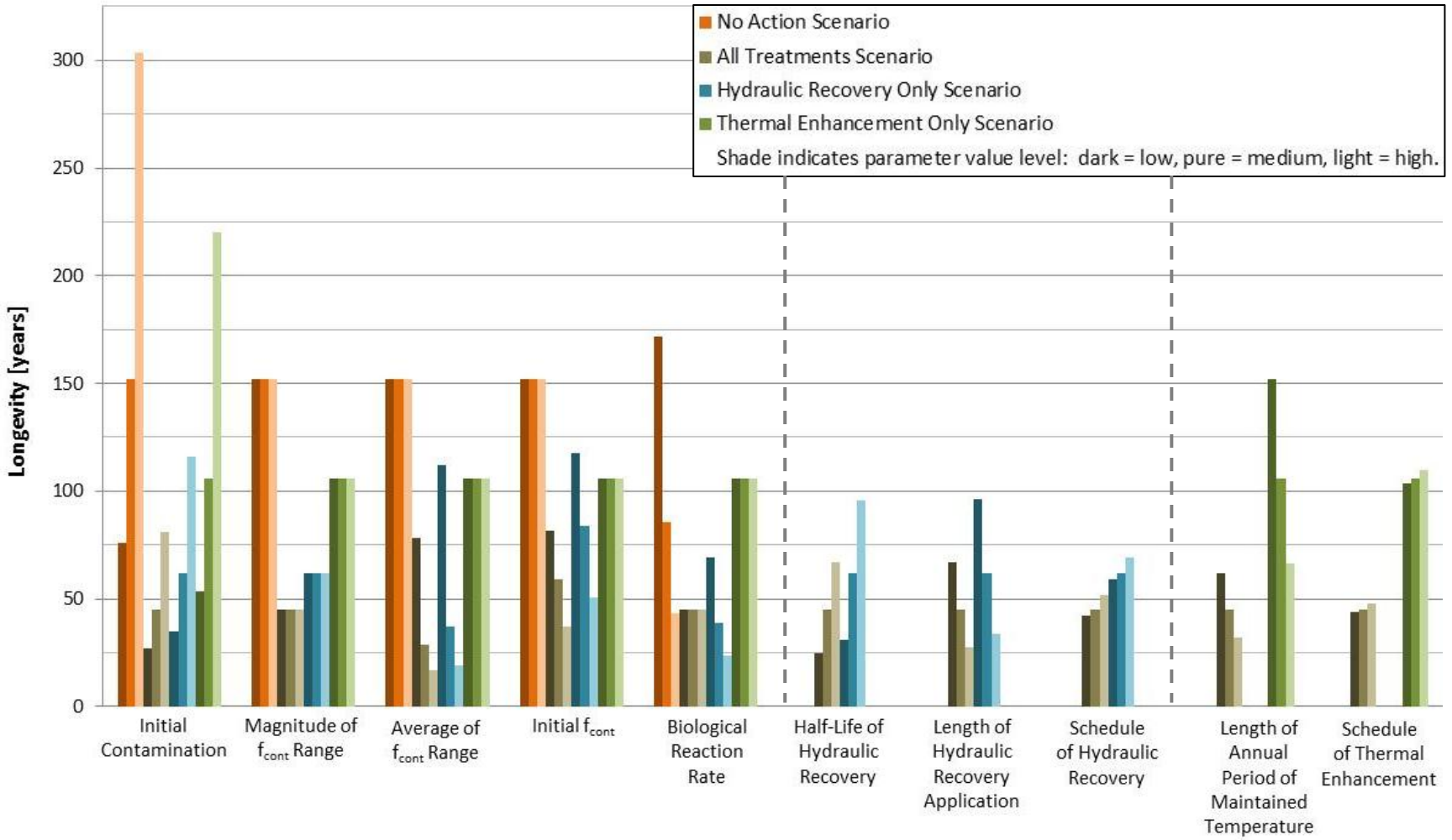

Figure 22 – Longevities of various parameter level variation model runs; parameter groups are designated along the x axis, each color represents a different treatment scenario, the three shades of each color represent the three levels of each parameter

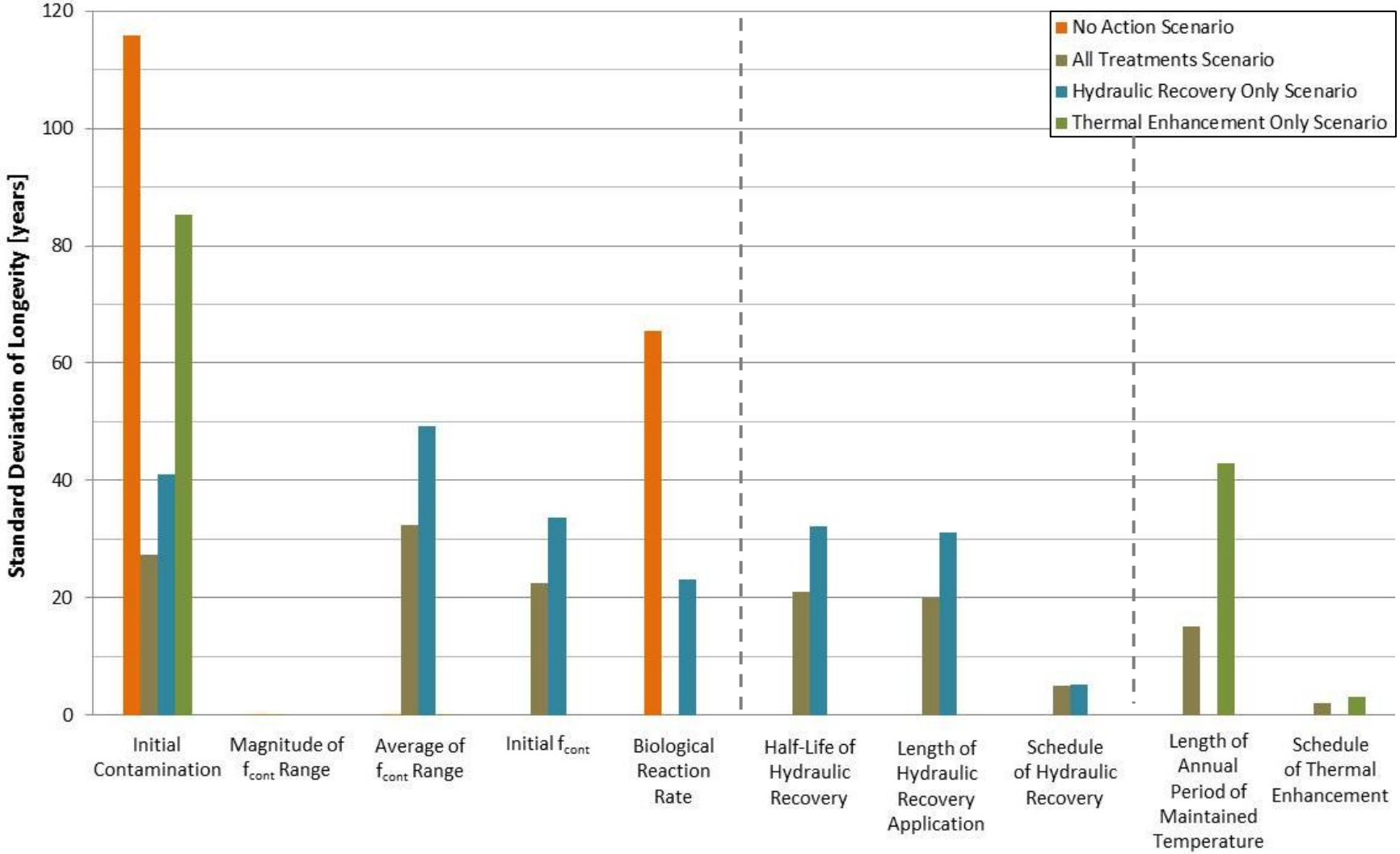

Figure 23 – Standard deviations of longevity according to parameter level; parameter groups are designated along the x axis, each color represents a different treatment scenario

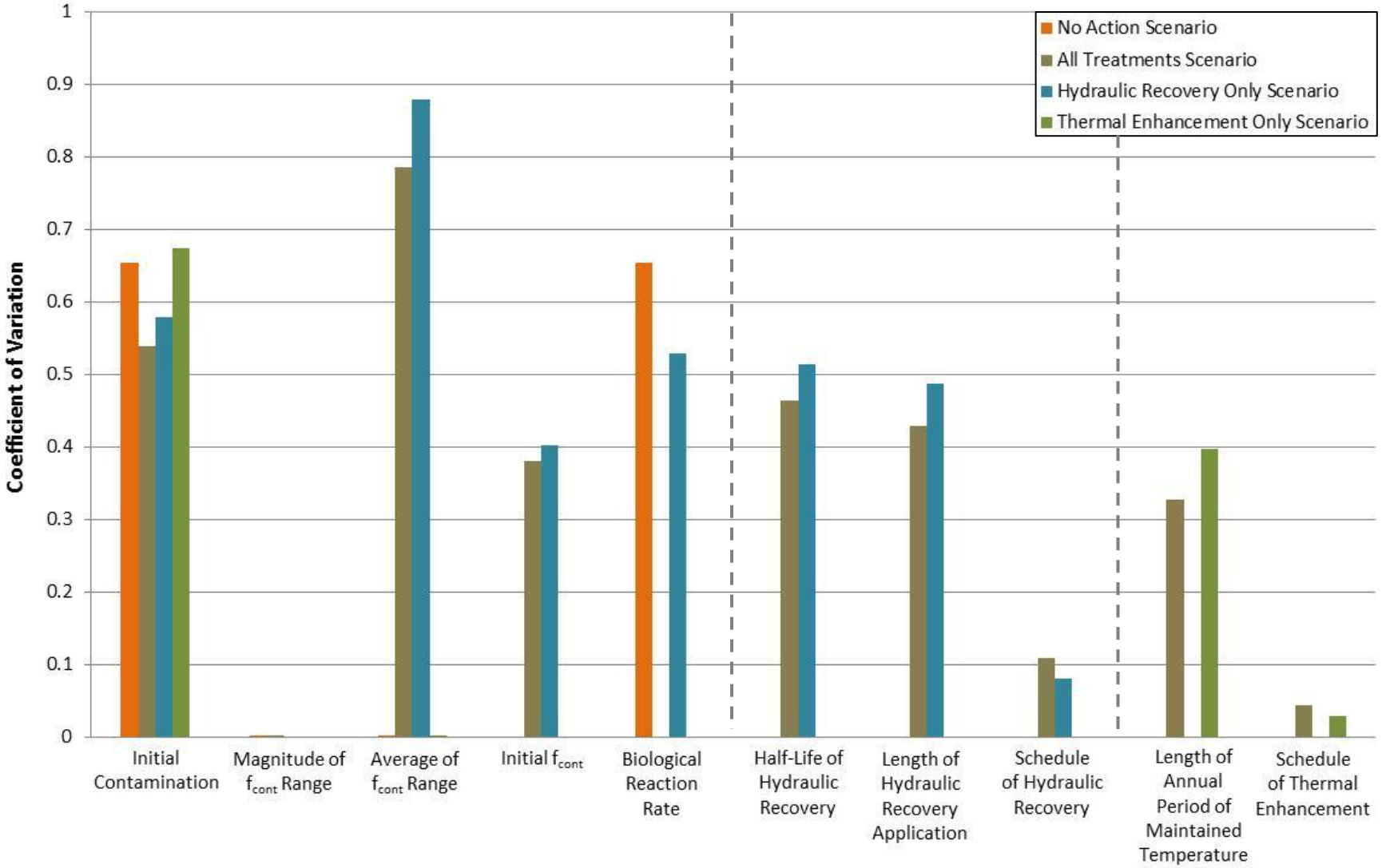

Figure 24 – Coefficients of variation of longevity according to parameter level; parameter groups are designated along the x axis, each different color represents a different treatment scenario

5.3.5.1 Initial Amount of Contamination

The variation of the initial amount of LNAPL mass had a predictively substantial effect on LNAPL longevity for each of the treatment scenarios. Applying multiples of 0.5 and 2.0 of the initial LNAPL mass to each treatment scenario approximately reduced or increased the LNAPL longevity by the same respective factor relative to the base parameter level scenario. LNAPL mass balance and distribution was similarly affected as the LNAPL evolution was stretched over a longer time frame for the high parameter level scenarios. Similar results were seen for the cumulative losses due to the different loss mechanisms in that the initial amount of contamination appeared to act as a time frame scaling factor. The loss rate of hydraulic recovery was distinctly different between the high and low level parameter scenarios for the All Treatments and Hydraulic Recovery Only scenarios. This was to be expected because the loss rate of hydraulic recovery is dependent of the amount of mass present. It was also interesting to note that the hydraulic recovery loss rate decayed at the same rate for both the high and low parameter levels for both the All Treatments and Hydraulic Recovery Only scenarios.

5.3.5.2 Magnitude of f_{cont} Range

Variation of the magnitude of the annual fluctuations of mass in the continuous fraction did not have a major effect on LNAPL longevity. This is most likely because the average f_{cont} was the same for each of the range levels, see definitions in Section 5.1.2. Similarly variation of this parameter had no effect on the total LNAPL evolution, relative proportions of hydraulic recovery and biological degradation losses, or the loss rates associate with each loss mechanism. This was true for each of the treatment scenarios.

Table 6 – Percent changes in longevity for parameter level variation analysis relative to base parameter levels for relevant modeled treatment scenario

Treatment Scenario	Parameter	Parameter Level		
		Low	Medium/Base	High
		Percent Change in Longevity from Base[1]		
No Action	initial amount of contamination	-49.9	-[2]	99.7
	magnitude of f_{cont} range	-	-0.0541	-0.0541
	average of f_{cont} range	-0.0541	-0.0541	0
	initial f_{cont}	-0.108	-0.108	-0.108
	biological reaction rate	12.9	-43.6	-71.7
All Treatments	initial amount of contamination	-39.4	-	80.7
	magnitude of f_{cont} range	-	0.183	0
	average of f_{cont} range	74.1	-36.1	-62.0
	initial f_{cont}	82.8	31.4	-17.8
	half-life of hydraulic recovery reaction rate	-44.8	-	49.4
	length of hydraulic recovery application	49.9	-	-38.9
	scheduling of hydraulic recovery	-6.42	-	15.2
	length of annual period of maintained temperature	38.5	-	-28.8/-20.2[3]
	scheduling of thermal enhancement	-1.65	-	6.79
Hydraulic Recovery Only	initial amount of contamination	-43.4	-	86.8
	magnitude of f_{cont} range	-	0	0
	average of f_{cont} range	80.4	-40.1	-69.3
	initial f_{cont}	89.9	35.2	-18.8
	biological reaction rate	11.4	-37.5	-62.0
	half-life of hydraulic recovery reaction rate	-50.1	-	53.9
	length of hydraulic recovery application	55.0	-	-45.4
	scheduling of hydraulic recovery	-5.03	-	11.1
Thermal Enhancement Only	initial amount of contamination	-49.3	-	108
	magnitude of f_{cont} range	-	0	0
	average of f_{cont} range	0.0777	0	0.155
	initial f_{cont}	-0.0777	-0.0777	-0.0777
	length of annual period of maintained temperature	43.7	-	-37.2/-25.6
	scheduling of thermal enhancement	-1.94	-	3.73

[1]Negative values indicate a decrease in longevity, positive values indicate an increase in longevity
[2]Dash indicates this parameter level results in the base parameter values for the modeled treatment scenario
[3]Second value is for an annual heating period of nine months

5.3.5.3 Average of f_{cont} Range

The variation of the average of the f_{cont} range resulted in relatively large differences in LNAPL longevity for the scenarios that included hydraulic recovery. This effect was slightly more pronounced for the Hydraulic Recovery Only treatment scenario. This result supports the idea that the distribution of LNAPL between the continuous and discontinuous fractions is one of the most important factors in the effectiveness of hydraulic recovery. The overall shapes of the total LNAPL evolution curves were also affected by the variation of the average of the f_{cont} range. As the value of this parameter increased, the curvilinear portion of the LNAPL evolution curves became more pronounced. At the medium and high level values for this parameter the total cumulative losses due to hydraulic recovery were greater than those due to biological degradation. At the low level values to opposite was true. This shows that hydraulic recovery has a greater losses potential when more of the LNAPL mass is located in the continuous fraction. Variation of this parameter also caused changes in the LNAPL loss rate due to hydraulic recovery. Once again, this was because this rate is dependent on the amount of mas present, or more particularly for this case, the amount of mass present in the continuous fraction.

5.3.5.4 Initial f_{cont} Value

To vary the initial f_{cont} value water table fluctuations had to be turned off for each of the treatment scenarios. Variation of this parameter only affected the LNAPL longevity for the scenarios including hydraulic recovery. Once again the affect was more pronounced for the Hydraulic Recovery Only treatment scenario than the All Treatments scenario. Another distinct difference that was seen with the variation of this parameter was that the continuous fraction LNAPL is depleted sooner than the discontinuous fraction of LNAPL. This can be seen in

Figure 25. This is different than what was observed for the scenarios when water table fluctuations were included. For those scenarios the continuous and discontinuous fractions were depleted at different rates but appear to be fully depleted at approximately the same time. This pattern can be seen in Figure 19. For both treatment scenarios that involved hydraulic recovery, the total cumulative losses due to biological degradation were greater than those due to hydraulic recovery for the low and medium levels of this parameter. The opposite was true for the high level of this parameter. Once again this shows that hydraulic recovery has a greater loss potential when more mass is located in the continuous fraction. Variation of this parameter also caused relatively large changes in the LNAPL loss rate due to hydraulic recovery. Once again, this was because this rate is dependent on the amount of mas present, or more particularly for this case, the amount of mass present in the continuous fraction.

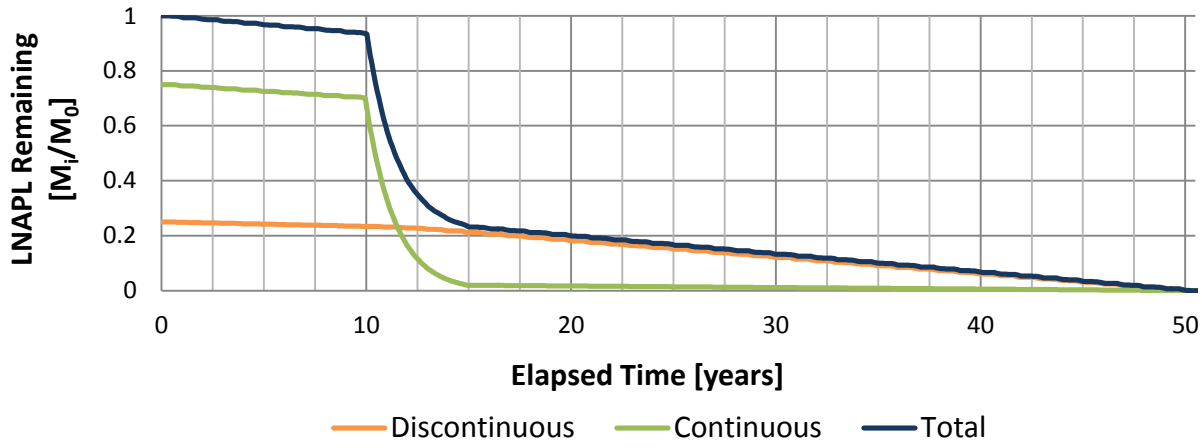

Figure 25 – Mass balance over time for the Hydraulic Recovery Only, high value of initial f_{cont} parameter level scenario

In general, when water table fluctuations were not included, the effects of the variation of all parameters related to hydraulic recovery were less pronounced than for the parameter level scenarios when water table fluctuations were included. For example, the relative LNAPL longevity reduction due to hydraulic recovery is smaller when water table fluctuations are not

included. This is because water table fluctuations are not present to continually redistribute mass into the continuous fraction where it is available for hydraulic recovery. Therefore, the rate of hydraulic recovery continues to decline from the beginning of the hydraulic recovery application. While in the parameter level scenarios when water table fluctuations are included, this rate has an annual peak at the point in each year when the water table is lowest – and therefore the value of f_{cont} is at its yearly maximum.

5.3.5.5 Biological Degradation Reaction Rate

To vary the biological degradation reaction rate temperature fluctuations had to be turned off. This was only applicable to the treatment scenarios that did not include thermal enhancement as a treatment remedy because when thermal enhancement was included the equations associated with temperature fluctuations were automatically included as well. Variation of the biological degradation reaction rate had a relatively large effect on LNAPL longevity. Applying multiples of 0.5 and 2.0 of the medium level biological degradation reaction rate to the No Action treatment scenario resulted in a proportional increase and decrease, respectively in LNAPL longevity. This was not true for the same variations of the Hydraulic Recovery Only treatment scenario most likely because biological degradation had to compete with hydraulic recovery in this treatment scenario. The effect of increasing this parameter on the LNAPL evolution was to produce generally steeper curves (as well as shorter LNAPL longevities as previously discussed). For the Hydraulic Recovery Only treatment scenario total cumulative losses due to biological degradation were greater than those due to hydraulic recovery for the high level parameter scenario. The mass loss rate due to hydraulic recovery decreased as the biological degradation reaction rate was increased in these parameter level scenarios for the Hydraulic Recovery Only treatment scenario. This is thought to be because as the biological degradation reaction rate was

increased the amount of mass present in the continuous fraction at the beginning of the application of hydraulic recovery decreased because biological losses affect both mass compartments.

5.3.5.6 Half-Life of Hydraulic Recovery

The variation of the half-life of LNAPL due to hydraulic recovery could only be done for the treatment scenarios that included hydraulic recovery as a treatment remedy. Applying multiples of 0.5 and 2.0 of the base level value of this parameter did not produce linear results. Decreasing this base level parameter by a factor of 0.5 resulted in approximately a factor of 0.5 decrease in LNAPL longevity; however, increasing this base level parameter by a factor of 2 resulted in approximately a factor of 1.5 increase in LNAPL longevity. The LNAPL evolution was affected by the variation of this parameter in that as it was increased hydraulic recovery had less of effect. The total cumulative losses due to hydraulic recovery decreased as this parameter was increased, and for the high parameter value scenario for both the All Treatments and Hydraulic Recovery Only treatment scenarios the total cumulative losses due to hydraulic recovery were surpassed by the total cumulative losses due to biological degradation. As this parameter was increased the mass loss rate due to hydraulic recovery decreased.

5.3.5.7 Length of Hydraulic Recovery Application

The variation of the length of hydraulic recovery application could only be done for the treatment scenarios that included hydraulic recovery as a treatment remedy. The variation of this parameter had a greater effect on LNAPL longevity for the Hydraulic Recovery Only treatment scenario. Similar to the variation of the half-life of LNAPL due to hydraulic recovery variation of the length of hydraulic recovery application did not result in linear variations in LNAPL

longevity. As this parameter was increased hydraulic recovery was able to have more of an impact on LNAPL evolution. Even with an application length of ten years the effectiveness of hydraulic recovery did not appear to greatly decrease. The total cumulative mass loss due to hydraulic recovery was more than that due to biological degradation for both the base and high parameter level scenarios for both treatment scenarios which included hydraulic recovery. The mass loss rate due to hydraulic recovery followed the same evolution for each of the parameter level scenarios. For the application length of ten years was close to becoming less than the rate due to biological degradation.

5.3.5.8. Scheduling of Hydraulic Recovery

The variation of the scheduling of hydraulic recovery could only be done for the treatment scenarios that included hydraulic recovery as a treatment remedy. As hydraulic recovery began at later points in the LNAPL life cycle the reduction in LNAPL longevity due to hydraulic recovery was smaller. This speaks to the importance of beginning hydraulic recovery soon after a release is detected. Also, this reiterates the idea that hydraulic recovery will not have equal results at all LNAPL sites. The LNAPL evolution was only affected by this parameter in that the effects of hydraulic recovery were shifted to later times. The total cumulative losses due to hydraulic recovery were greater at each level of this parameter; however the total cumulative losses due to biological degradation were almost equal to those due to hydraulic recovery for the All Treatment, high parameter level scenario. The evolution of the loss rates for both the hydraulic recovery and biological degradation loss mechanisms were the same for each level of this parameter.

5.3.5.9 Annual Period of Maintained Temperature

The variation of the annual period of maintained temperature could only be done for the treatment scenarios that included thermal enhancement as a treatment remedy. Increasing this parameter had a relatively greater effect on LNAPL longevity than decreasing this parameter. Increasing this parameter resulted in a general increase in the slope of the LNAPL evolution curves. Slightly more cumulative losses due to biological degradation were achieved as this parameter was increased for the All Treatments treatment scenario. The shapes of the loss mechanisms loss rates curves were similar for each parameter level scenario; the maximum total loss rate was greatest for the high parameter level scenario.

5.3.5.10 Scheduling of Thermal Enhancement

The variation of the scheduling of thermal enhancement could only be done for the treatment scenarios that included thermal enhancement as a treatment remedy. Variation of the scheduling of thermal enhancement did not have as substantial of an effect on LNAPL longevity as did the same parameter for hydraulic recovery. This supports the idea that the application of passive remedies can be appropriate for LNAPL releases in various points in the evolution of LNAPL life cycle. The only a slight difference in the overall slope of the LNAPL mass evolutions for each of the parameter level scenarios was observed. Slightly less cumulative losses due to biological degradation were achieved as this parameter was increased for the All Treatments treatment scenario. The shapes of the loss mechanisms loss rates curves were similar for each parameter level scenario; the maximum total loss rate was greatest for the high parameter level scenario. This may seem counter intuitive. This occurs because the more mass is lost due to biological degradation when the scheduling of thermal enhancement is earlier such that less

LNAPL mass is present at the beginning of the hydraulic recovery application; therefore, a lower maximum loss rate due to hydraulic recovery (and relatedly a lower maximum total loss rate) occurs.

5.4 Limitations

One of the major limitations of the LLPM is that it is a first order approximation for LNAPL longevity and evolution. This is due to the assumptions that were made for the model and the way input parameters were correspondingly designated. All of the reaction rates acting within the model are averages over time, space, and for all LNAPL components. The LNAPL distribution generated by the relevant input parameters is averaged across the entire LNAPL extent. These are two limitations associated with not including heterogeneity in the LLPM. Long-term trends in temperature variations over periods of year are also not included. In addition to the above factors that lead to the first order approximation nature of the LLPM there are several other factors that limit the accuracy or utility of the model.

The current method may not be the most appropriate for dealing with fluctuations in the LNAPL distribution between the continuous and discontinuous fractions. The results of the sensitivity analysis showed that the scheduling of hydraulic recovery did affect the model output; however, the effect was not as pronounced as one would expect based on real world experiences at field sites. Also, because an asymptote for hydraulic recovery was not directly included in the development of the programmed equations of the model the accuracy of predictions related to hydraulic recovery may be limited. Both of these issues may relate to how the distribution of LNAPL is currently achieved within the model.

Another parameter that fluctuated within the model was the rate of biological degradation. Fluctuations of this parameter were dependent on the modeled subsurface temperate. Although data by which the theoretical field site was developed suggest that a sinusoidal wave function is appropriate for this site, this may not be true for different field-scale applications. The equation that controls temperature fluctuation may need to be changed on a site to site basis.

The assumption that biological degradation occurs as a zero order reaction rate process may be contentious. This assumption was made based on site specific data for the theoretical field site; however, numerous sources exist in the relevant literature that concluded biological degradation occurs as a first order reaction rate process. One could therefore assume that the field-scale application of this model would accurately match LNAPL evolution data for the Casper, Wyoming site if it was available. If the same data was available for a site that was thought to exhibit first order biological degradation, the current version of the LLPM may not achieve the same level of accuracy.

How thermal enhancement is applied within the model does not precisely agree with how the pilot study in Casper, Wyoming was conducted. Once again the current version of the model approaches this parameter as an average. The model assumes that temperature can be uniformly maintained across the entire LNAPL extent and does not include the compounding and self-heating effects of exothermic reactions that are part of the biological degradation of LNAPL.

The generation of figures to display output is largely manual for this version of the LLPM. Variations of scenarios would have to be calculated and the results assembled separately. Also multiple runs are needed if the lifetime of LNAPL exceeds 150 years because the number of calculations the model performs and the model time step must be manually adjusted. This was

necessary for the high level initial contamination parameter scenarios as part of the parameter sensitivity analysis.

6. CONCLUSION

This chapter provides a summary of the preceding chapters. First, the main ideas and themes of this thesis are reiterated. Next, the main results of the work are highlighted. Finally, suggestions for future work to advance the ideas of the current study are made.

6.1 Main Ideas and Themes

LNAPL longevity and evolution over time are important parameters to consider in remediation planning and design. Decision makers would benefit from a tool that was able to predict LNAPL longevity as part of mass balance calculations over the lifetime of an LNAPL release. This work was completed to develop a beta version of a novel modeling tool (the LLPM) and provide a basis for continued improvement of this tool.

A conceptual model for LNAPL depletion over time was developed by reviewing the available relevant literature. From this it was concluded that a model could be developed to predict LNAPL longevity as a function of natural losses and remedial measures. Five important attributes of the LLPM were recognized by the literature review. First, the LLPM must demonstrate the significant effects natural loss mechanisms can have on the longevity of LNAPL bodies. Second, the effects that temperature can have on the rate of biological degradation, and thus LNAPL longevity, must be included. Third, the important role of the distribution of mass between the continuous and discontinuous fractions must be represented. Fourth, the effects of water table fluctuations on the distribution of LNAPL mass must be included. Fifth, output of the LLPM must provide a basis for the comparison of treatment remedies. The LLPM was developed using Excel (Microsoft Corporation, Redmond, WA) by applying numerical methods to combinations of differential equations for zero and first order reaction rates. Equations to

support functionality to include of the five important attributes determined from the literature review were also developed in Excel.

Laboratory experimentation was necessary to develop a better understanding of the processes governing LNAPL longevity, test the assumptions listed in Section 1.1, and provide estimates of input parameters for the LLPM. The results of the laboratory sand tank experiments were used to develop and examine the accuracy of the LLPM to laboratory-scale data. A lack of longevity and evolution data for existing LNAPL field sites presented a problem for the verification of the model to field-scale data. A theoretical field-scale site was developed to examine the field-scale applicability and demonstrate field-scale results of the LLPM.

6.2 Main Results

Laboratory experiments were successfully conducted that resulted in mass balance data for the evolution of a LNAPL release. This mass balance data was successfully used to develop a beta version model that predicts LNAPL evolution and longevity. In this section, the results of both of these efforts are summarized.

6.2.1 Laboratory Study of LNAPL Longevity

The results of the laboratory experimentation validated the assumption that LNAPL releases can be fully depleted over time. The LNAPL longevities of the releases simulated in the laboratory sand tank experiments ranged from approximately four to seven days as concluded by the time when LNAPL was visually depleted. LNAPL recovery had an important influence on the longevity of the LNAPL releases in the laboratory experiments and resulted in decreased LNAPL longevity. Water table fluctuations acted to increase LNAPL longevity in the

experiments because more mass was lost through dissolution in the experiments that included water table fluctuations. This occurred in part because more mass was distributed into the discontinuous fraction in these experiments. The mass balance curves for the laboratory sand tank experiments supported the assumption that natural losses, particularly volatilization and dissolution, could be modeled as zero order processes, while LNAPL recovery could be modeled as a first order process.

Both laboratory experimentation and the field-scale application of the LLPM showed that natural losses can have an important impact on LNAPL longevity. Furthermore, the ability to enhance natural type losses at LNAPL sites can have relatively large implications as far as LNAPL longevity is concerned because these natural losses have the potential to act upon the entire LNAPL mass and not one fraction.

6.2.2 LNAPL Longevity Predictive Model

The LLPM described in Chapter 4 was able to successfully predict the experimental data – excluding the late time curvilinear section – from the laboratory study described in Chapter 3. This indicated that the LLPM had the potential to predict the longevity and evolution of field-scale LNAPL releases. This was accommodated by making appropriate changes to the model to allow for field-scale inputs and the calculation of field-scale outputs.

The LLPM produced field-scale results that showed its potential utility as a method of comparing treatment remedy scenarios. The application of the model to four different treatment scenarios showed that a combined remedy was the most effective remediation approach. This conclusion was based on outputs of LNAPL longevity, the evolution of LNAPL mass, cumulative losses due

to the two included loss mechanisms, and loss rates associated with the two included loss mechanisms over the LNAPL life time.

The sensitivity analysis of the LLPM produced field-scale results that showed the parameters that affected the distribution of mass between the continuous and discontinuous fractions had the most substantial impact on the evolution of LNAPL releases for the treatment scenarios that included hydraulic recovery. These results also showed that the mass distribution at LNAPL sites could largely affect which and when certain loss mechanisms are most important. These two observations highlight how important it is to have accurate predictions of the mass distribution at LNAPL sites in order to make appropriate remediation decisions that will best impact LNAPL longevity and evolution. The input parameter that most affected the model output when hydraulic recovery was not included in the treatment scenario was the initial amount of contamination.

Variation of the LNAPL half-life due to hydraulic recovery, length of hydraulic recovery application, and the length of the annual period of maintained temperature also resulted in relatively large changes of the model output. The scheduling of hydraulic recovery was found to have a more notable impact on LNAPL longevity than did the scheduling of thermal enhancement of biological degradation. This highlights the importance of conducting hydraulic recovery early in release history. More importantly perhaps, it demonstrates the idea that not all sites can be effectively remediated by hydraulic recovery alone. Many sites will required multiple types of remedial approaches as they evolve over time with respect to transport and mobility. An accurate prediction of LNAPL evolution over the lifetime of releases is needed to make informed and sustainable decisions regarding remediation planning.

6.3 Future Work

The author realizes that the current LLPM is a simplified approximation of LNAPL evolution. The continuation of this novel effort could result in an improved understanding of the governing processes that affect LNAPL evolution. Suggestions for future work have been made herein. These suggestions include studies of multi-component LNAPL releases, studies to further examine the effects that scheduling of treatments and the distribution of mass have on LNAPL longevity and evolution, continued work to improve the utility of the LLPM.

6.3.1 Multi-Component LNAPL Laboratory Sand Tank Studies

In the field, LNAPL sites usually contain a suite of contaminants or contaminant components. In the laboratory study of LNAPL longevity for this work, a single component LNAPL was used. This provided a simplified case for which to build a preliminary understanding of LNAPL evolution and longevity and the relevant parameters affecting these metrics. A laboratory study of LNAPL longevity which utilizes a multi-component LNAPL might be able to provide a more thorough understanding of these principles by building on the conceptual model arrived at via the single component studies conducted herein. The LLPM is considered to be a beta version model for LNAPL longevity and evolution. Improvements to this model could be made through the application of the findings of multi-component LNAPL laboratory sand tank studies.

Improved photographic quality may be achieved in these experiments by using a lower concentration of NAPL soluble dye (i.e. a lower percent by volume). The intensity of the LNAPL fluorescence in the laboratory study for this work was so intense as to cause washout of adjacent colors. The resulting images may not have described the LNAPL content of the system as accurately as may be achieved with a lower dye concentration.

6.3.2 Scheduling of LNAPL/Hydraulic Recovery

LNAPL recovery resulted in an apparently large reduction of LNAPL longevity in the laboratory sand tank experiments. It is hypothesized that this was because the releases simulated in the study had LNAPL recovery applied during the early stage time frame. Different effects on longevity may have been observed if LNAPL recovery was employed during the middle or late stage time frame in these studies. A series of laboratory sand tank studies that employed LNAPL recovery on early, middle, and late stage LNAPL releases may provide further insight as to when LNAPL recovery is no longer an efficient treatment remedy relative to LNAPL mass remaining at a site. This type of laboratory sand tank experiments could also aid in the evaluation of the ability of the LLPM to predict the relative effects of the scheduling of hydraulic recovery at the field-scale. The evaluation of additional real world field-scale data would also be beneficial to this effort.

6.3.3 Distribution of LNAPL Mass

Changes to how the distribution of mass between the continuous and discontinuous fraction compartments is performed may improve the accuracy of the LLPM. The simplified methods used to distribute LNAPL mass between the continuous fraction and discontinuous fraction in this beta version of the LLPM are not theoretically rigorous. Factors other than water table fluctuations affect this distribution. A further review of relevant literature would be beneficial in the development of more rigorous methods. Literature that discusses the relationship between LNAPL distribution and factors such as vapor pressure, capillary pressure, heterogeneity, and degradation rates (among numerous others) would give beneficial insight into this problem.

One idea is that when fluctuations in the mass distribution occur, a one-to-one transfer between the two compartments may not always be the case. For example, perhaps the equation controlling the mass distribution should be skewed to the discontinuous fraction over time. Further review of the processes and factors effecting LNAPL distribution may indicate that 100% of the LNAPL that enters the discontinuous fraction is not transferred back to the continuous fraction. This would result in all continuous fraction mass being depleted before the discontinuous fraction mass.

6.3.4 Model Utility

The inclusion of functionality that further dictates the fluctuation of temperature within the model may be beneficial. As discussed in Section 5.3 temperature fluctuations may not occur as a yearly sinusoidal function at all field sites. A more accurate approximation of site temperature fluctuations may be achieved if the user were able to easily choose or define a function for temperature fluctuations from the model input GUI.

More literature should be reviewed in order to determine the best way to apply biological degradation. Of main importance is whether biological degradation occurs according to a zero or first order reaction rate. The applicability of the model to various field sites might be improved if functionality was included that enabled the user to choose the reaction rate order of biological degradation according to what has been observed on a site specific basis.

The inclusion of supplemental worksheets to facilitate the estimation of user specified input parameters, such as loss mechanism reaction rates, would result in a more user friendly version of the LLPM. Along those same lines, inclusion of more straightforward methods of outputting data to tables and figures would also produce a more user friendly model. The model utility

could be also improved by including functionality that would enable the user to define the model time frame and time step such that the amount of model calculations necessary to achieve their desired results could be minimized and adjusted on a field scenario specific basis.

7. REFERENCES

Akhbari, D. 2013. Transport and Generation of Heat in LNAPL Bodies. MS thesis. Colorado State University, 2012. Fort Collins, CO: Colorado State University, Libraries.

Amos, R. T., K. U. Mayer, B. A. Bekins, G. N. Delin, and R. L. Williams 2005. Use of dissolved and vapor-phase gases to investigate methanogenic degradation of petroleum hydrocarbon contamination in the subsurface, Water Resour. Res.,41, W02001,doi:10.1029/2004WR003433

Brooks, R. H. and A. T. Corey. 1964. Hydraulic Properties of Porous Media. Hydrology Paper Number 3, Civil Engineering Department, Colorado State University, Fort Collins, CO.

Budavari, S., M. J. O'Neil, A. Smith, P. E. Heckelman (Eds.). 1989. The Merck Index, 11th ed. Merck & Co., Inc., Rahway, NJ, p. 951.

Davis, S. N., R. J. M. DeWiest. 1966. Hydrogeology. New York, New York: John Wiley & Sons.

Johnson, P., P. Lundegard, and Z Liu. 2006. Source Zone Natural Attenuation at Petroleum Hydrocarbon Spill Sites – I: Site-Specific Assessment Approach. Groundwater Monitoring & Remediation, Vol 26, No. 4, pp. 82-92.

Mahler, N. 2010. A Mass Balance Approach to Resolving the Stability of LNAPL Bodies. MS thesis. Colorado State University, 2010. Fort Collins, CO: Colorado State University, Libraries.

Mahler, N., T. Sale and M. Lyverse 2012. A Mass Balance Approach to Resolving LNAPL Stability. Journal of Ground Water, Vol 50, No. 6, pp. 861-871.

McCoy, K. M. 2012. Resolving Natural Losses of LNAPL Using CO_2 Traps. MS thesis. Colorado State University, 2012. Fort Collins, CO: Colorado State University, Libraries.

U.S. EPA. 1993. U.S. Environmental Protection Agency. Technical Information Review. Methyl tertiary Butyl Ether (CAS No. 1634-04-4). Office of Pollution Prevention and Toxics, U.S. EPA, Washington, D.C. (from http://www.epa.gov/chemfact/s_mtbe.txt)

Hawkins, A. M. 2013. Processes Controlling the Behavior of LNAPLs at Groundwater Surface Water Interfaces. MS thesis. Colorado State University, 2013. Fort Collins, CO: Colorado State University, Libraries.

Huntley, D., and G. D. Beckett. 2002. Evaluating Hydrocarbon Removal from Source Zones and its Effect on Dissolved Plume Longevity and Magnitude. American Petroleum Institute: Regulatory Analysis and Scientific Affairs Department, Publ. Number 4715.

Irianni Renno, M. I. 2013. Baseline Microbial Ecology of an LNAPL Body. MS thesis. Colorado State University, 2012. Fort Collins, CO: Colorado State University, Libraries.

Sale, T. 2001. Methods for Determining Inputs to Environmental Petroleum Hydrocarbon Mobility and Recovery Models. API Publication Number 4711. American Petroleum Institute.

Zeman, N. R. 2012. Thermally Enhanced Bioremediation of LNAPL. MS thesis. Colorado State University, 2012. Fort Collins, CO: Colorado State University, Libraries.

Zimbron, J. A., T. C. Sale, M. Lyverse. 2013. Gas Flux Measurement Using Traps. US Patent Application Publication. Pub. No.: US 2013/0031955 A1.

8. APPENDIX A

8.1 Triplicate Statistics for the Base Case Experiment

Table 7 – Triplicate Statistics for the Base Case Experiment

Aqueous					Vapor				
Sample #	**Conc. [mg/L]**	**AVG [mg/L]**	**STD [mg/L]**	**Relative STD [%]**	**Sample #**	**Conc. [mg/L]**	**AVG [mg/L]**	**STD [mg/L]**	**Relative STD [%]**
12-1	311.04	278.49	43.78	15.72	12-1	756.35	862.74	110.66	12.83
12-2	295.70				12-2	977.22			
12-3	228.72				12-3	854.65			
22-1	546.17	615.30	63.31	10.29	22-1	122.92	130.85	6.896	5.270
22-2	670.46				22-2	135.45			
22-3	629.26				22-3	134.17			
30-1	548.06	531.86	37.81	7.108	30-1	32.230	33.92	3.310	9.759
30-2	558.87				30-2	31.798			
30-3	488.65				30-3	37.736			

8.2 Triplicate Statistics for the Recovery Experiment

Table 8 – Triplicate Statistics for the Recovery Experiment

Aqueous					Vapor				
Sample #	**Conc. [mg/L]**	**AVG [mg/L]**	**STD [mg/L]**	**Relative STD [%]**	**Sample #**	**Conc. [mg/L]**	**AVG [mg/L]**	**STD [mg/L]**	**Relative STD [%]**
10-1	18.553	20.40	1.759	8.626	10-1	3910.1	4300.4	341.46	7.940
10-2	20.578				10-2	4544.2			
10-3	22.057				10-3	4446.8			
17-1	258.20	328.25	61.57	18.76	17-1	3353.0	3566.8	423.35	11.87
17-2	373.82				17-2	4054.4			
17-3	352.73				17-3	3292.9			
29-1	1077.5	939.09	127.99	13.63	29-1	1714.9	1707.7	80.59	4.719
29-2	825.06				29-2	1623.8			
29-3	914.67				29-3	1784.5			
38-1	1634.3	1584.5	71.73	4.527	38-1	282.38	288.59	13.04	4.518
38-2	1617.0				38-2	303.58			
38-3	1502.3				38-3	279.82			

8.3 Triplicate Statistics for the WT Fluctuations Experiment

Table 9 – Triplicate Statistics for the WT Fluctuations Experiment

Aqueous					Vapor				
Sample #	**Conc. [mg/L]**	**AVG [mg/L]**	**STD [mg/L]**	**Relative STD [%]**	**Sample #**	**Conc. [mg/L]**	**AVG [mg/L]**	**STD [mg/L]**	**Relative STD [%]**
8-1	591.85	607.23	139.29	22.93	10-1	6795.1	6917.0	801.33	11.59
8-2	476.28				10-2	6183.6			
8-3	753.58				10-3	7772.3			
16-1	3720.2	4195.5	411.98	9.820	17-1	6160.5	6064.4	685.91	11.31
16-2	4450.0				17-2	6697.2			
16-3	4416.4				17-3	5335.5			
21-1	4619.7	5021.6	424.78	8.459	29-1	3637.2	4499.4	896.48	19.93
21-2	5466.1				29-2	5426.6			
21-3	4979.0				29-3	4434.3			
26-1	957.75	867.83	117.24	13.51	34-1	6571.9	7050.6	697.99	9.900
26-2	735.24				34-2	6728.6			
26-3	910.51				34-3	7851.5			
					57-1	775.15	835.72	63.17	7.559
					57-2	901.201			
					57-3	830.78			
					62-1	314.55	317.88	9.236	2.906
					62-2	328.32			
					62-3	310.76			

8.4 Triplicate Statistics for the Combined Experiment

Table 10 – Triplicate Statistics for the Combined Experiment

Aqueous					Vapor				
Sample #	**Conc. [mg/L]**	**AVG [mg/L]**	**STD [mg/L]**	**Relative STD [%]**	**Sample #**	**Conc. [mg/L]**	**AVG [mg/L]**	**STD [mg/L]**	**Relative STD [%]**
13-1	5417.1	6263.3	735.88	11.75	10-1	6653.5	7195.0	652.00	9.062
13-2	6753.2				10-2	7012.8			
13-3	6619.7				10-3	7918.7			
19-1	1016.2	644.31	352.31	54.64	17-1	6007.7	6241.6	206.93	3.315
19-2	316.17				17-2	6316.2			
19-3	600.59				17-3	6400.9			
					29-1	4129.1	4324.2	169.58	3.922
					29-2	4435.8			
					29-3	4407.8			
					39-1	1559.8	1524.3	107.06	7.024
					39-2	1609.2			
					39-3	1404.0			

9. APPENDIX B

This appendix contains calibration curve data that was used to determine the sample concentrations for experiments 2-4. Corresponding data for experiment 1 is given in Section 3.2.

9.1 Recovery Experiment Calibration Data

Table 11 – Calibration standards for the Recovery experiment

Sample Name	mL/mg MTBE	mL previous	mL DI water	Dilution Factor	Concentration [mg/L]
DIL1	0.1/71.0	-	9.9	100	7,100
STD1	-	4	16	5	1,420
STD2	-	10	10	2	710.0
STD3	-	10	10	2	355.0
STD4	-	10	10	2	177.5
STD5	-	10	10	2	88.75
STD6	-	10	10	2	44.38
STD7	-	10	10	2	22.19
STD8	-	10	10	2	11.09
STD9	-	10	10	2	5.547
STD10	-	10	10	2	2.773
STD11	-	10	10	2	1.387
STD12	-	10	10	2	0.6934
STD13	-	10	10	2	0.3467
STD14	-	10	10	2	0.1733
STD15	-	10	10	2	0.08667
STD16	-	10	10	2	0.04334

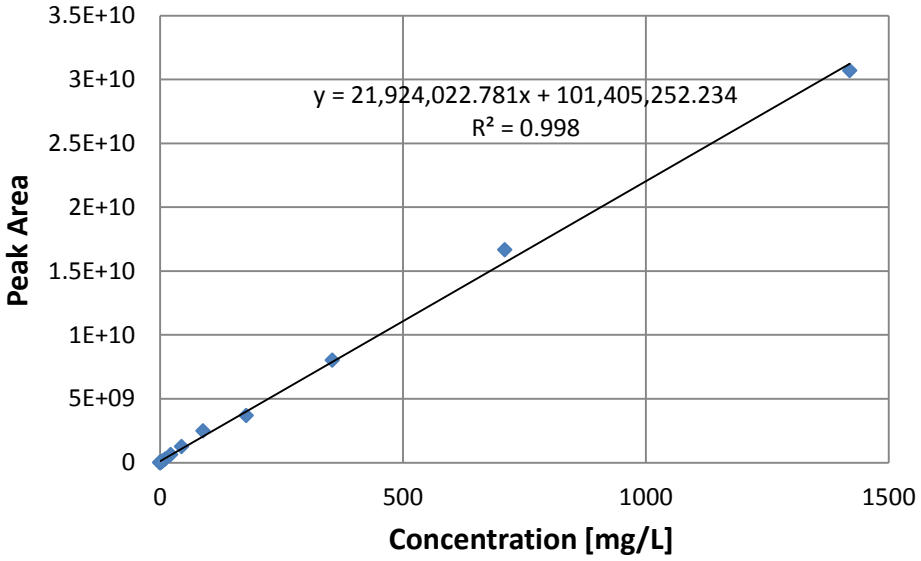

Figure 26 – Calibration curve with equation used to determine sample concentrations of the Recovery experiment samples

9.2 WT Fluctuations Experiment Calibration Data

Table 12 – Calibration standards for the WT Fluctuations experiment

Sample Name	mL/mg MTBE	mL previous	mL DI water	Dilution Factor	Concentration [mg/L]
DIL1	0.1/71.1	-	9.9	100	7,110
STD1	-	4	16	5	1,422
STD2	-	10	10	2	711.0
STD3	-	10	10	2	355.5
STD4	-	10	10	2	177.8
STD5	-	10	10	2	88.88
STD6	-	10	10	2	44.44
STD7	-	10	10	2	22.22
STD8	-	10	10	2	11.11
STD9	-	10	10	2	5.555
STD10	-	10	10	2	2.777
STD11	-	10	10	2	1.389
STD12	-	10	10	2	0.6943
STD13	-	10	10	2	0.3472
STD14	-	10	10	2	0.1736
STD15	-	10	10	2	0.08679
STD16	-	10	10	2	0.04340

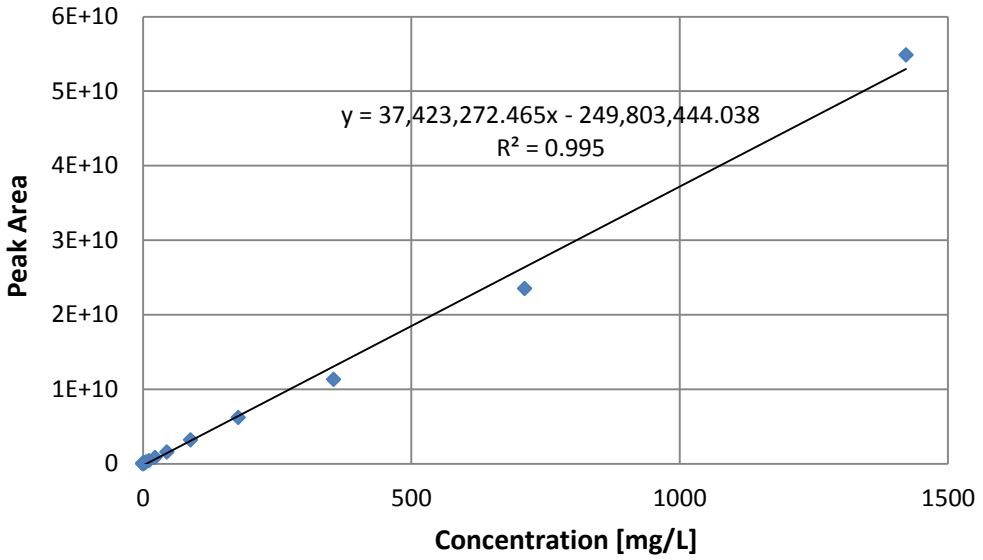

Figure 27 – Calibration curve with equation used to determine sample concentrations of the WT Fluctuations experiment samples

9.3 Combined Experiment Calibration Data

Table 13 – Calibration standards for the Combined experiment

Sample Name	mL/mg MTBE	mL previous	mL DI water	Dilution Factor	Concentration [mg/L]
DIL1	0.1/79.1	-	9.9	100	7,910
STD1	-	4	16	5	1,582
STD2	-	10	10	2	791.0
STD3	-	10	10	2	395.5
STD4	-	10	10	2	197.8
STD5	-	10	10	2	98.88
STD6	-	10	10	2	49.44
STD7	-	10	10	2	24.72
STD8	-	10	10	2	12.36
STD9	-	10	10	2	6.180
STD10	-	10	10	2	3.090
STD11	-	10	10	2	1.545
STD12	-	10	10	2	0.7725
STD13	-	10	10	2	0.3862
STD14	-	10	10	2	0.1931
STD15	-	10	10	2	0.09656
STD16	-	10	10	2	0.04828

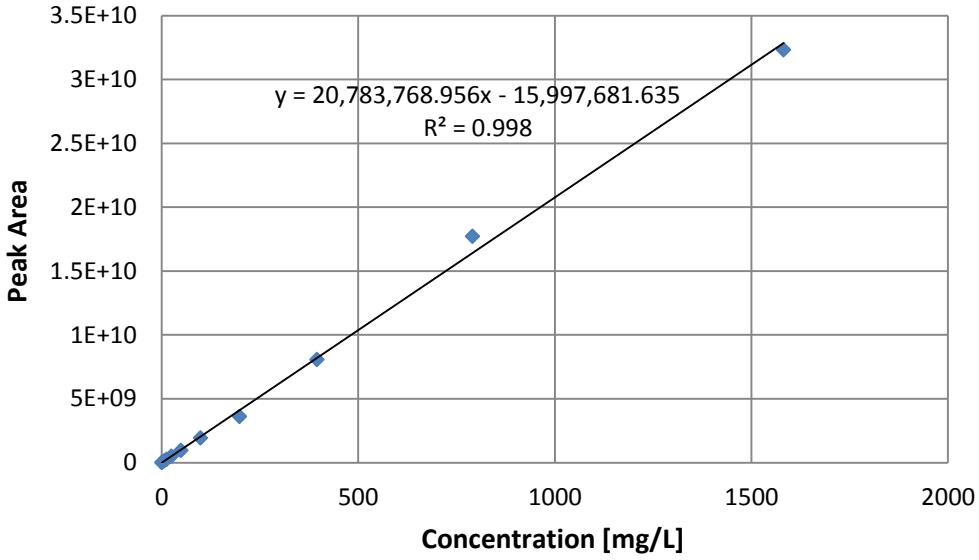

Figure 28 – Calibration curve with equation used to determine sample concentrations of the Combined experiment samples

10. APPENDIX C

10.1 Derivation of Equation 2

Henry's law states:

$$K_H = \frac{P_v}{C_{aq}}$$

Where K_H [L*atm/mol] is the Henry's coefficient for a given gas phase solute relative to water, P_v [atm] is the partial pressure of the gas phase constituent, and C_{aq} [mol/L] is the molar concentration of the solute in water.

Substitution of the following equations can be made:

$$C_{aq} = \frac{\rho_{aq}}{MW}$$

and

$$P_v = \frac{\rho_v * R * T}{MW}$$

where MW is the molecular weight of the solute. R is the ideal gas constant [L*atm/(K*mol)] and T [K] is temperature. Equation 1 is then derived from Henry's law as follows:

$$K_H = \frac{\frac{\rho_v * R * T}{MW}}{\frac{\rho_{aq}}{MW}}$$

$$K_H = \frac{\rho_v * R * T}{\rho_{aq}}$$

$$K_{HD} = \frac{K_H}{R * T}$$

$$K_H = \frac{\rho_v}{\rho_{aq}}$$

$$\rho_v = K_{HD} * \rho_{aq} \qquad \text{[Eq. 1]}$$

10.2 Table of FP Values

Table 14 – FP values used to convert GC-FID measured concentrations into vapor phase concentrations

Experiment	FP Value
Base Case	6.24×10^{-3}
Recovery	1.12×10^{-3}
WT Fluctuations	5.65×10^{-4}
Combined	6.84×10^{-4}

11. APPENDIX D

This appendix contains supplemental equations and explanations pertinent to the final model and the full derivation of the final model as described in Chapter 4.

11.2 Implementation of Mass Estimate for First Order (Mass Dependent) Reaction Rates

Because first order reaction rates are dependent of the mass present at the time the calculation is made (see Equation 10), the average of the mass at the current time step and the next time step was used to estimate the mass at the next time step.

$$\lambda_{1st} * M(t) = -\frac{dM}{dt} \quad \text{[Eq. 10]}$$

Estimating the derivatives as incremental changes (delta values) gives:

$$\lambda_{1st} * M = -\frac{\Delta M}{\Delta t}$$

Estimating the first order mass reaction rate with the average mass between one time step and the next where $M_{i+1/2} = \frac{M_{i+1}+M_i}{2}$ gives:

$$-\lambda_{1st} * M_{i+1/2} = \frac{M_{i+1}-M_i}{\Delta t}$$

The result of the above substitution gives:

$$-\lambda_{1st} * \frac{M_{i+1}+M_i}{2} = \frac{M_{i+1}-M_i}{\Delta t} \quad \text{[Eq. A11-1]}$$

11.1 Definition of Fractional Biological Degradation Reaction Rate

Because the biological degradation loss mechanism was included in both compartments, a fractional factor, based on Equation A11-2 and Equation A11-3, was applied to the biological degradation reaction rate in the equations for both compartments

$$f_{cont} = \frac{M_{cont}}{M_{total}} \qquad \text{[Eq. A11-2]}$$

$$f_{disc} = 1 - f_{cont} \qquad \text{[Eq. A11-3]}$$

where f_{cont} [%] is the fraction of total mass contained in the continuous compartment, M_{cont} [M] is the mass of LNAPL in the continuous compartment, M_{total} [M] is the total amount of mass in the system, and f_{disc} [%] is the fraction of total mass contained in the discontinuous compartment.

11.3 Derivation of Finite Difference Expression for Discontinuous Fraction Mass

This derivation arrives at Equation 11 by combining multiples of Equation 9 with Equation 6.

$$\dot{M}_{out_{disc}} = \frac{dM_{disc}}{dt} \qquad \text{[Eq. 6]}$$

The left hand side of Equation 6 can be populated with multiple zero order reaction rates, according to the loss mechanisms that are assumed to act on the discontinuous compartment, based on the left hand side of Equation 9 resulting in Equation A11-4

$$\lambda_{dis} + f_{disc} * \lambda_{bio} = \frac{dM_{disc}}{dt} \qquad \text{[Eq. A11-4]}$$

where λ_{dis} [M/T] is the zero order reaction rate associated with the dissolution loss mechanism and λ_{bio} [M/T] is the zero order reaction rate associated with the biological degradation loss mechanism.

$\frac{dM_{disc}}{dt}$ can be estimated as $\frac{\Delta M_{disc}}{\Delta t}$ and ΔM_{disc} can be expanded as $M_{disc}^{i+1} - M_{disc}^{i}$ resulting in Equation A11-5.

$$\lambda_{dis} + f_{disc} * \lambda_{bio} = \frac{M_{disc}^{i+1} - M_{disc}^{i}}{-\Delta t} \qquad \text{[Eq. A11-5]}$$

$$-\Delta t * (\lambda_{dis} + f_{disc} * \lambda_{bio}) = M_{disc}^{i+1} - M_{disc}^{i}$$

$$M_{disc}^{i+1} = M_{disc}^{i} - \Delta t * (\lambda_{dis} + f_{disc} * \lambda_{bio}) \quad \text{[Eq. 11]}$$

11.4 Derivation of Finite Difference Expression for Continuous Fraction Mass

This derivation arrives at Equation 12 by combining multiples of Equation 9 and Equation 10 and the estimate of $M_{i+1/2}$ with Equation 7.

$$\dot{M}_{out_{cont}} = \frac{dM_{cont}}{dt}. \quad \text{[Eq. 7]}$$

The left hand side of Equation 7 can be populated with multiple zero and first order reaction rates, according to the loss mechanisms that are assumed to act on the continuous compartment, based on the left hand side expressions of Equation 9 and Equation 10 resulting in Equation A11-6

$$\lambda_{vol} + f_{cont} * \lambda_{bio} + \lambda_{hydr} * M_{cont}^{i+1/2} = \frac{dM_{cont}}{dt} \qquad \text{[Eq. A11-6]}$$

where λ_{vol} [M/T] is the zero order reaction rate associated with the volatilization loss mechanism, λ_{bio} [M/T] is the zero order reaction rate associated with the biological degradation loss mechanism, and λ_{hydr} [T^{-1}] is the first order reaction rate associated with hydraulic recovery.

$\frac{dM_{cont}}{dt}$ can be estimated as $\frac{\Delta M_{cont}}{\Delta t}$ and ΔM_{cont} can be expanded as $M_{cont}^{i+1} - M_{cont}^{i}$. Also $M_{cont}^{i+1/2}$ can be expanded as $\frac{M_{cont}^{i+1}+M_{cont}^{i}}{2}$ resulting in Equation A11-7.

$$\lambda_{vol} + f_{cont} * \lambda_{bio} + \lambda_{hydr} * \frac{M_{cont}^{i+1}+M_{cont}^{i}}{2} = \frac{M_{cont}^{i+1}-M_{cont}^{i}}{-\Delta t} \quad \text{[Eq. A11-7]}$$

$$-\Delta t * (\lambda_{vol} + f_{cont} * \lambda_{bio}) - \Delta t * \lambda_{hydr} * \frac{M_{cont}^{i+1}}{2} - \Delta t * \lambda_{hydr} * \frac{M_{cont}^{i}}{2} = M_{cont}^{i+1} - M_{cont}^{i}$$

$$-M_{cont}^{i+1} - \Delta t * \lambda_{hydr} * \frac{M_{cont}^{i+1}}{2} = \Delta t * \lambda_{hydr} * \frac{M_{cont}^{i}}{2} - M_{cont}^{i} + \Delta t * (\lambda_{vol} + f_{cont} * \lambda_{bio})$$

$$-M_{cont}^{i+1} * \left(1 + \frac{\Delta t * \lambda_{hydr}}{2}\right) = M_{cont}^{i} * \left(\frac{\Delta t * \lambda_{hydr}}{2} - 1\right) + \Delta t * (\lambda_{vol} + f_{cont} * \lambda_{bio})$$

$$M_{cont}^{i+1} = \frac{M_{cont}^{i} * \left(1 - \frac{\Delta t * \lambda_{hydr}}{2}\right) - \Delta t * (\lambda_{vol} + f_{cont} * \lambda_{bio})}{\left(1 + \frac{\Delta t * \lambda_{hydr}}{2}\right)} \quad \text{[Eq. 12]}$$

12. APPENDIX E

Linear Best Fit Analysis of Volatilization and Dissolution Data for Base Case Experiment

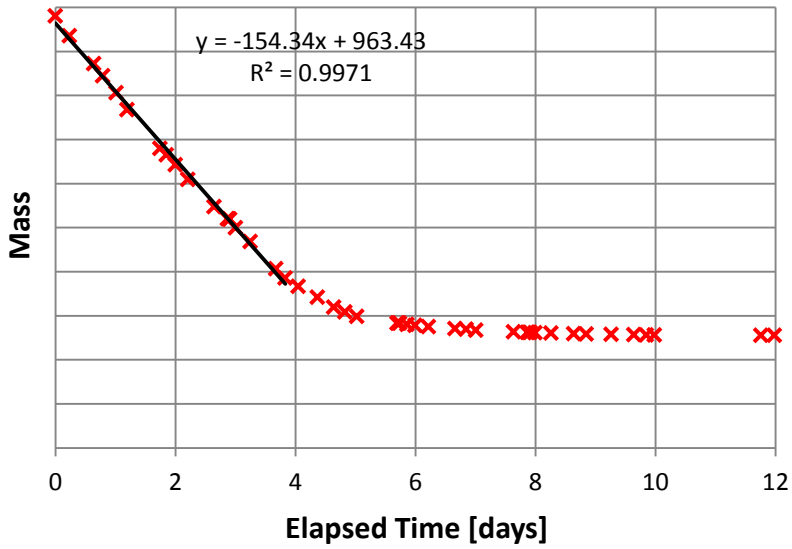

Figure 29 – Linear regression of volatilized mass to estimate volatilization reaction rate for Base Case simulation, values of mass are not shown because they became arbitrary once dissolution and volatilization data were separated

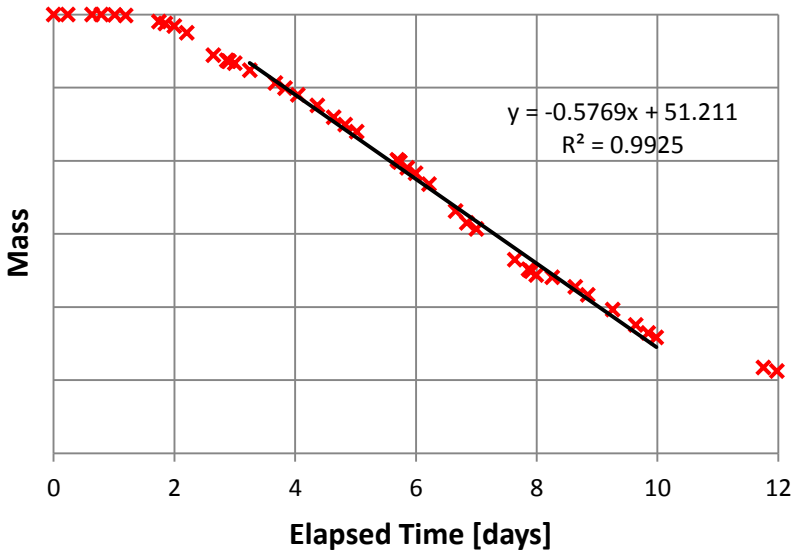

Figure 30 – Linear regression of dissolved mass to estimate dissolution reaction rate for Base Case simulation, values of mass are not shown because they became arbitrary once dissolution and volatilization data were separated